

POLITECNICO
MILANO 1863

SCUOLA DI INGEGNERIA INDUSTRIALE
E DELL'INFORMAZIONE

Battery Electric Bus: a technical and economic simulation framework for battery aging assessment

Tesi di Laurea Magistrale in
Mobility Engineering - Ingegneria della mobilità

Author: **Giorgio Isacco**

Student ID: 252767
Advisor: Prof. Fabio Borghetti
Co-advisors: Prof. Stefano Rossi, Eng. Paolo Rapinesi
Academic Year: 2024-25

Abstract

The transition from internal combustion engine vehicles to zero-emission vehicles represents one of the main strategies for reducing greenhouse gas emissions and local pollutants generated by the transport sector, which pose a serious threat to both the environment and human health. In this context, the increasing deployment of battery electric buses (BEBs) in public transport services introduces new operational and economic challenges, particularly related to battery management and charging strategies. This study analyses the main mathematical models used to estimate the State of Health (SoH) of lithium-ion batteries and proposes a methodological approach aimed at making them applicable to real-world operational contexts. For this purpose, a Python-based simulation environment is developed, allowing the modeling of battery aging in BEBs as a function of operational conditions, environmental factors, and adopted charging strategies, and enabling the estimation of battery useful life. The work also includes the development of an optimization algorithm for charging scheduling, which is used to assess the feasibility of the proposed strategies and to analyze their impact on energy costs and charging infrastructure requirements. The application of the model to a real fleet of BEBs operated by Autoguidovie S.p.A shows that charging strategies oriented towards reducing battery degradation can lead to a reduction in the vehicles' Life Cycle Cost (LCC) exceeding 20% with respect to the initial operating conditions. However, the results also highlight that extending battery lifetime represents only one component of a broader economic framework, in which energy costs and charging infrastructure play a decisive role.

Keywords: battery aging, battery degradation, electric buses, charging scheduling, electric mobility, fleet management

Abstract in lingua italiana

La transizione dai veicoli a combustione interna ai veicoli a zero emissioni rappresenta una delle principali strategie per ridurre le emissioni di gas serra e gli inquinanti locali generati dal settore dei trasporti, che costituiscono una seria minaccia sia per l'ambiente sia per la salute umana. In questo contesto, la crescente diffusione degli autobus elettrici a batteria (BEBs) nei servizi di trasporto pubblico introduce nuove sfide operative ed economiche, in particolare legate alla gestione delle batterie e alle strategie di ricarica. Questo studio analizza i principali modelli matematici utilizzati per la stima dello stato di salute (SoH) delle batterie agli ioni di litio e propone un approccio metodologico finalizzato a renderli applicabili a contesti operativi reali. A tal fine, viene sviluppato un ambiente di simulazione implementato in Python, che consente di modellare l'invecchiamento delle batterie dei BEBs in funzione delle condizioni operative, dei fattori ambientali e delle strategie di ricarica adottate, permettendo di stimarne la vita utile. Il lavoro include inoltre lo sviluppo di un algoritmo di ottimizzazione per la pianificazione delle ricariche, utilizzato per valutare la fattibilità delle strategie proposte e per analizzarne l'impatto sui costi energetici e sui requisiti infrastrutturali di ricarica. L'applicazione del modello a una flotta reale di BEBs operata da Autoguidovie S.p.A. mostra come strategie di ricarica orientate alla riduzione del degrado delle batterie possano portare a una riduzione del costo del ciclo di vita (LCC) dei veicoli superiore al 20% rispetto alle condizioni operative iniziali. Tuttavia, i risultati evidenziano anche che l'estensione della vita utile delle batterie rappresenta solo una componente di un quadro economico più ampio, nel quale i costi dell'energia e delle infrastrutture di ricarica svolgono un ruolo determinante.

Parole chiave: invecchiamento delle batterie, degrado delle batterie, autobus elettrici, pianificazione delle ricariche, mobilità elettrica, gestione della flotta

Contents

Abstract **i**

Abstract in lingua italiana **iii**

Contents **v**

1 Introduction **1**
1.1 Pollution and climate change 1
1.2 EU emission reduction strategy 5
1.3 Motivation of the work 7
1.4 Aims and objectives 8

2 State of the art and literature review **11**
2.1 Battery types 11
2.2 Battery aging and wear factors 15
2.3 Cell imbalance and balancing techniques in Li-ion battery packs 21
2.4 Battery aging models 25
2.5 Battery aging model integration in the electric bus scheduling problem . . 29
2.6 Electricity market 36
2.6.1 The Italian case 38
2.7 Key insights and research gaps from the literature review 42

3 Model presentation **45**
3.1 SoH Estimation Model 46
3.1.1 Model calibration 47
3.1.2 Model application and simulation results 50
3.2 Battery Optimization Model 55
3.2.1 A simulation-based approach for realistic battery management . . . 56
3.3 Charging Optimization Model 63

3.4 Economic Evaluation Model 69

4 Practical application and results **75**
4.1 Case study 75
4.2 Application of the Battery Optimization Model 80
4.3 Application of the Charging Optimization Model 87
4.4 Application of the Economic Evaluation Model 91

5 Conclusions and future developments **99**
5.1 Future developments 100

Bibliography **101**

A Appendix – Python functions **111**
A.1 run_alternating_turns 111
A.2 charging_optimization 117
A.3 calculate_LCC_scenario 123

B Appendix – Charging schedules under non-school period operation **127**

List of Figures **131**

List of Tables **135**

Acknowledgements **137**

1 | Introduction

1.1. Pollution and climate change

In Europe, one in every eight deaths is linked to pollution [1]. This shocking statistic alone should be enough to highlight the urgency of reducing pollution and developing environmentally friendly solutions to accelerate the transition toward a more sustainable future.

Pollution is one of the main drivers of biodiversity loss, not only because of the release of harmful chemicals into the soil, air, and water, but also due to its significant contribution to global warming. Global mean temperatures have increased significantly (Figure 1.1) since the pre-industrial period, around 1850, due to the intensification of greenhouse gas (GHG) emissions. The greenhouse effect is the process by which certain gases, such as carbon dioxide, methane, nitrous oxide, and water vapor, trap heat from the Sun. This trapped heat helps keep the planet warm enough to support life; however, excessive concentrations of these GHGs can lead to abnormal warming, contributing to climate change.

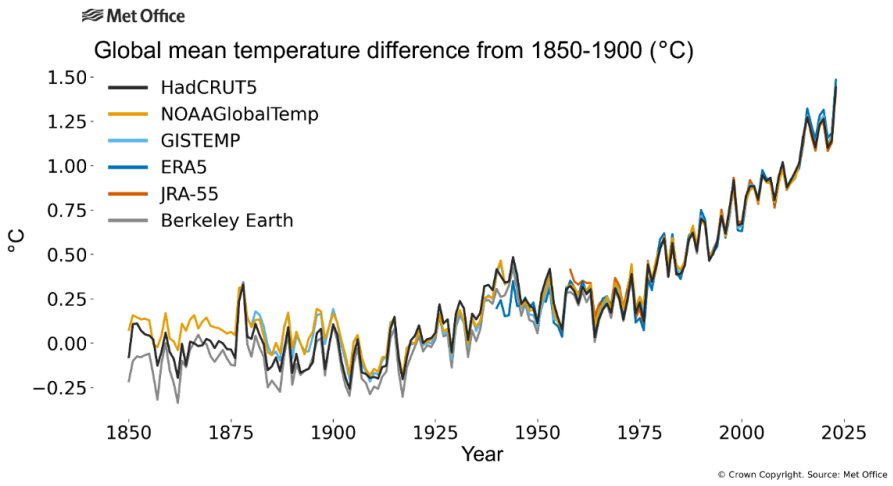


Figure 1.1: Global mean surface temperature anomaly relative to the pre-industrial period (1850–1900), estimated from multiple independent datasets [2].

Different greenhouse gases have varying abilities to trap heat in the atmosphere. To compare their impacts, it is necessary to consider their Global Warming Potential (GWP). Since carbon dioxide is the most significant GHG in terms of cumulative emissions, other greenhouse gases are commonly expressed as carbon dioxide equivalents (CO_2 eq). This allows the warming impacts of all GHGs to be aggregated into a single measure of total greenhouse gas emissions. Figure 1.2 illustrates the CO_2 eq trends from 1850 to the present.

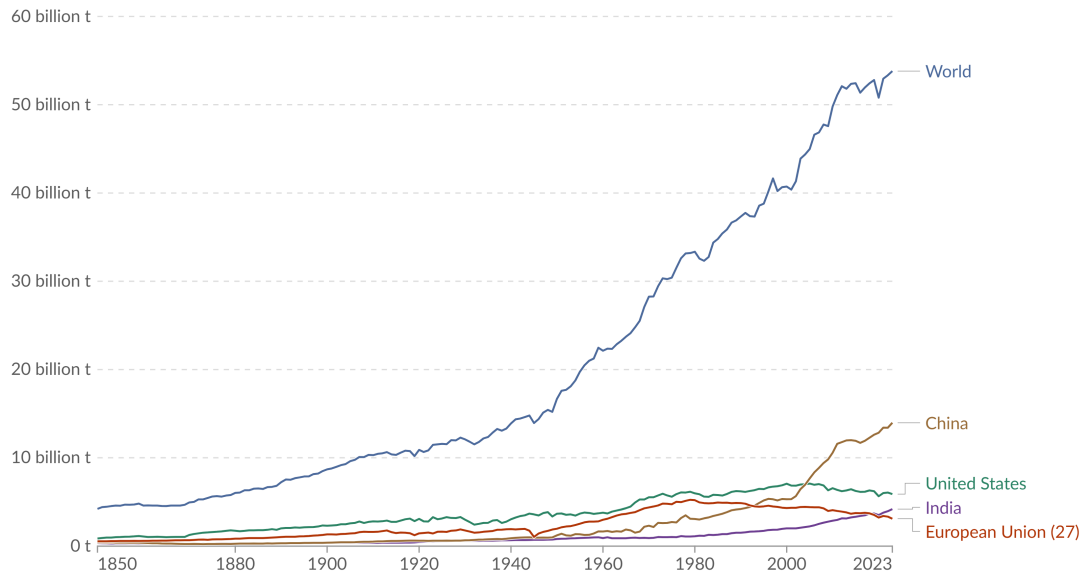


Figure 1.2: Greenhouse gas emissions from all sources, expressed in tonnes of CO_2 eq [3].

Rising global temperatures are causing glacier melting, sea level rise, and profound changes in fragile marine ecosystems. For instance, coral reefs, are extremely sensitive to temperature variations; when ocean temperatures increase, corals undergo a process known as coral bleaching, which results in the loss of the symbiotic algae responsible for their color and nutrition, ultimately leading to coral death. Although coral reefs cover less than 0.1% of the ocean floor, they are home to more than 25% of all marine species [4]. The loss of coral reefs exemplifies the broader consequences of global warming on biodiversity and ecosystem stability, underscoring the urgent need for sustainable energy and transport solutions.

The transport sector is the second-largest contributor to GHG emissions (Figure 1.3) making it a key area of intervention to reduce global emissions and mitigate global warming. For this reason, in recent years, a major technological transition has begun. The European Union has promoted a shift from conventional Internal Combustion Engine (ICE) vehicles, powered by fossil fuels, to vehicles powered by cleaner energy sources.

Among these, Electric Vehicles (EVs) have been identified as one of the most promising solutions to achieve this goal.

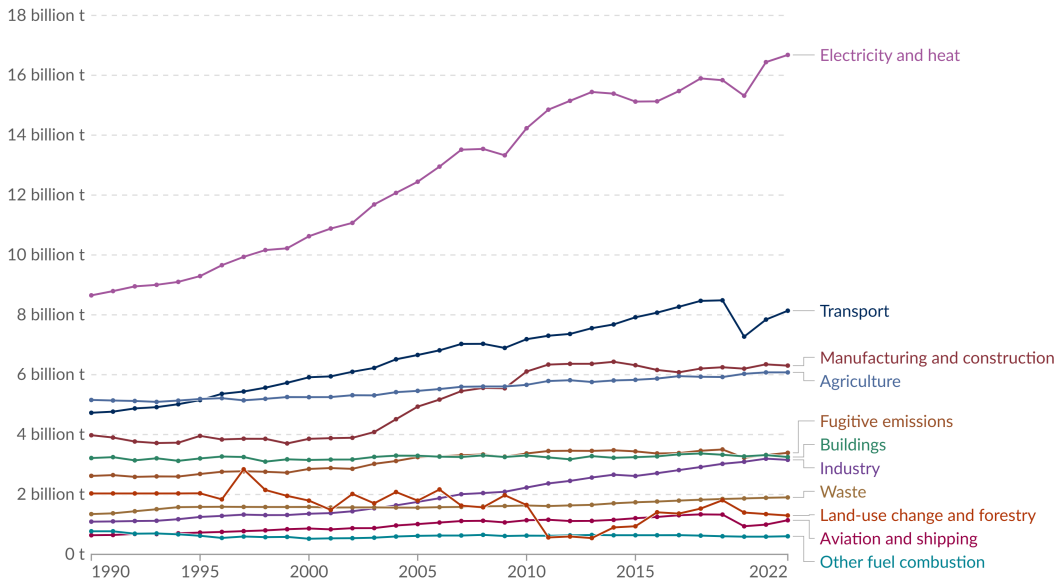


Figure 1.3: Global greenhouse gas emissions by sector, expressed in tonnes of CO_2 eq [5].

However, since the largest share of GHG emissions originates from electricity and heat production, it is evident that the transition of the transport sector must proceed in parallel with the decarbonization of the energy generation system, otherwise, the overall impact of this shift will remain limited. In this context, Figure 1.4 shows that the European electricity market was largely dominated by fossil fuel sources, such as oil, natural gas, and coal, until a few years ago. Only in recent years the share of renewable energy has increased rapidly, eventually becoming the dominant component of the EU electricity mix.

This transition has been driven by substantial investments in renewable energy technologies, including wind, solar, and hydroelectric power, which have progressively reduced the carbon intensity of electricity generation.

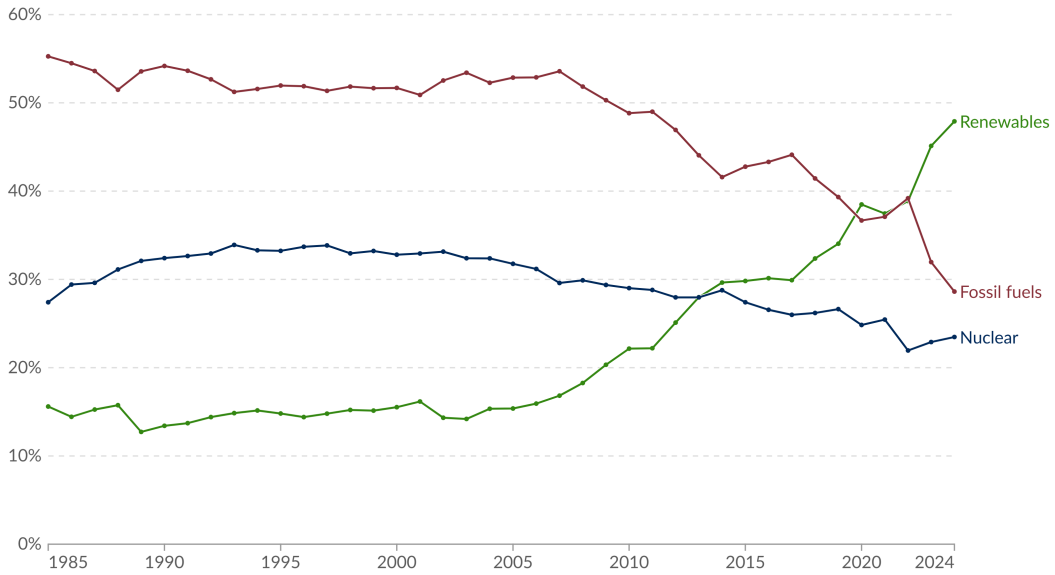


Figure 1.4: Share of electricity generation from fossil fuels, renewables, and nuclear sources in the EU [6].

There are two main groups of emissions: global emissions and local emissions. Global emissions have effects that extend far beyond their point of release; this category includes substances that contribute to ozone layer depletion as well as the well-known greenhouse gases. Local emissions, on the other hand, affect only the immediate area where they are released. These include particulate matter (PM), nitrogen oxides (NO_x), carbon monoxide (CO), and unburned hydrocarbons (HC). Local pollutants directly impact air quality and human health. In 2022 in the EU, an estimated 250,000 premature deaths, caused by a variety of conditions including stroke, cancer, ischemic heart disease, diabetes, and respiratory diseases, were attributable to air pollution [7].

EVs do not burn hydrocarbons. Although their global emissions depend on the source of the electricity used for charging, EVs have the significant advantage of producing no tailpipe emissions. As a result, they can almost completely eliminate local emissions from vehicles, with the only remaining contributions coming from component wear, such as tires.

Considering that the transport sector is a major source of local pollutants (Table 1.1), the electrification of transport represents a significant opportunity to improve urban air quality, reduce health risks, and enhance life expectancy and quality for city residents.

	Produced impact	Industrial	Transport
CO	Poisoning, cardiovascular diseases	$< 10\%$	$> 80\%$
HC	Photochemical smog,physiological harms	$< 10\%$	$> 80\%$
PM	Lung damages, physiological harms	30%	30%
NO_x	Smog, acid rain, toxic chemicals	50%	40%

Table 1.1: Local pollutants, their impacts, and contributions from industry and transport [8]

1.2. EU emission reduction strategy

The European Union is strongly committed to addressing climate change through a progressive reduction of emissions. In recent years, under the presidency of Ursula von der Leyen, the European Commission (EC) has introduced several major policy initiatives to concretely advance this objective. In 2019, the Commission presented the European Green Deal (EGD), an ambitious policy framework designed to make the EU the first climate-neutral continent by 2050. At the core of the EGD lies the goal of achieving climate neutrality by 2050, with an intermediate target of reducing net greenhouse gas emissions, compared to 1990 levels, by at least 55% by 2030. To achieve this, in 2021 the EC launched the Fit for 55 package, a comprehensive set of legislative proposals aimed at aligning EU policies with the 2030 emissions-reduction target and maintaining a steady trajectory toward carbon neutrality by 2050. Among its measures, the package includes a provision stating that all new cars and vans sold after 2035 must produce zero CO_2 emissions at the tailpipe. However, this measure has sparked considerable debate: some stakeholders have raised concerns regarding the technological readiness and economic implications of a full transition to zero-emission vehicles by that date. Consequently, it is possible that, in the coming years, if the European Commission assesses that the technological maturity required for such a transition has not yet been fully achieved, the EC may reconsider the 2035 deadline or introduce limited exemptions, such as allowing certain hybrid technologies or biofuels.

Despite these ongoing discussions, the target remains formally embedded in EU law and continues to guide the trajectory of regulatory and industrial planning, and it is present in the last European Environmental Agency (EEA) report, published on 29 September 2025.

These doubts about the feasibility of a complete transition from ICE vehicles to zero-

emission vehicles stem primarily from two major challenges.

The first concerns the potential economic impact of EV adoption: European car manufacturers are technologically less advanced compared to their Chinese counterparts, who began their electrification process years earlier. If they are unable to close this gap, there is a concrete risk of losing a significant market share in Europe. This, combined with the expected loss of market share abroad due to global electrification trends, could result in European manufacturers losing up to € 7 billion in annual profits by 2030, with substantial repercussions for the European economy, particularly in automotive-dependent countries such as Germany, Slovakia and the Czech Republic [9].

The second critical issue relates to the inadequacy of Europe's current charging infrastructure. A significant gap remains to enable the widespread adoption of zero-emission vehicles across the continent. By the end of 2023, the European Union had just over 600 000 public charging points, with an annual increase of around 153 000 new installations. However, the European Commission estimates that approximately 3.5 million public charging points will be required by 2030 to achieve the electrification targets set in the Fit for 55 package. Other projections, such as those from the European Automobile Manufacturers' Association (ACEA), the organization representing major European car manufacturers before EU institutions, suggest that at least 8.8 million charging points will be needed by 2030 [10]. Both estimates underscore that is necessary a massive acceleration in infrastructure deployment, making this target particularly ambitious and challenging.

This complex transition does not only concern the private transport sector but also public transport. Although diesel buses still dominate the market, with 89.2% of the buses in European fleets in 2023 powered by diesel and only 2.5% being Battery Electric Buses (BEBs) [11], the trend is rapidly changing. In fact, the share of newly registered BEBs has grown significantly in recent years: while in 2018 they accounted for only 1.84% of new bus registrations, by 2025 this figure has risen to 21.74% (Figure 1.5). This sharp increase highlights the growing importance of electric mobility within the public transport sector.

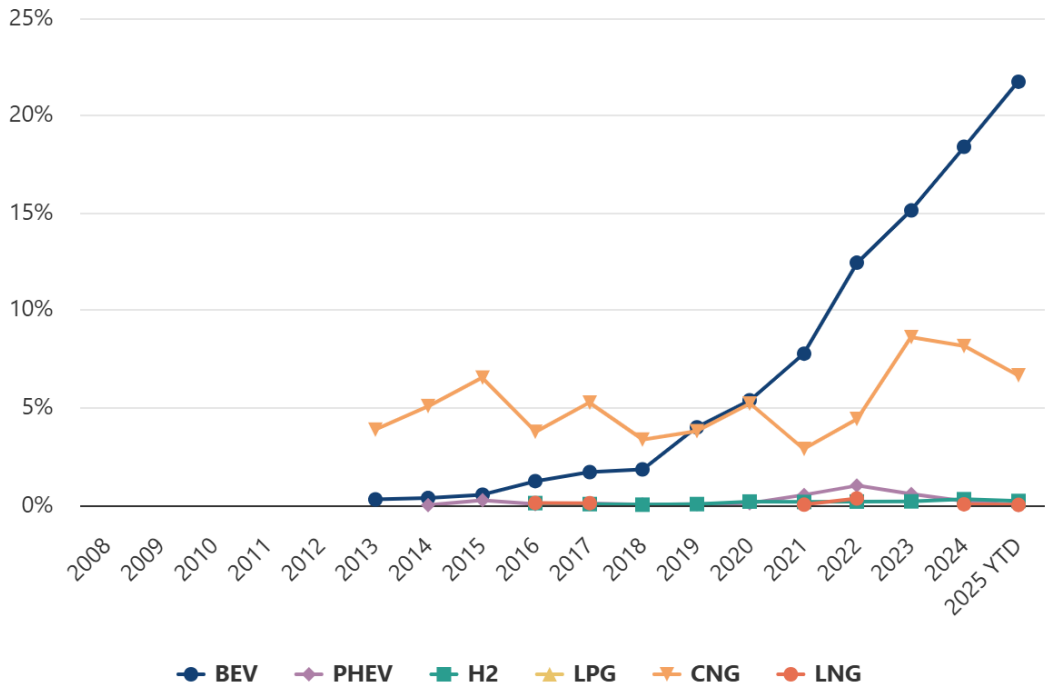


Figure 1.5: Share of newly registered alternative fuelled buses as a percentage of total registrations in the EU [12]

The purchase price of a Battery Electric Bus is generally higher than that of a conventional diesel bus; however, this gap is gradually narrowing, mainly due to the steady decline in battery prices observed over the past years. On the other hand, the maintenance costs of electric buses are significantly lower than those of traditional vehicles. Several studies have shown that, thanks to their mechanical simplicity and reduced component wear, BEBs can enable Public Transport Operators (PTOs) to save up to 30% in maintenance expenditures [13], making their adoption increasingly attractive for public transport fleets.

1.3. Motivation of the work

The increasing presence of BEBs in public transport fleets introduces new and complex problems for PTOs. The first of these is the charging scheduling problem, which arises from the fact that, while refuelling conventional buses takes only a few minutes, BEBs require significantly more time to recharge. Therefore, it is necessary to plan charging activities carefully in order to ensure both an efficient use of resources and an effective delivery of service. This problem is also affected by the limited driving range of BEBs; however, thanks to the rapid evolution of technology, particularly improvements in battery capacity, this limitation is becoming less critical. Indeed, modern BEBs can now

cover many more kilometres on a single charge compared to just a few years ago.

Another major difference between diesel buses and BEBs lies in the impact of the refuelling or charging strategy on the vehicle's lifetime. In the case of diesel buses, this impact is essentially irrelevant, since the energy source is stored in a simple tank: regardless of how much or how quickly fuel is added, the tank itself does not degrade as a result. In contrast, for BEBs the energy carrier is electricity, which is stored in a battery, a component that is far more complex than a fuel tank and whose condition is strongly affected by how much energy is stored and how it is managed. This fundamental difference gives rise to a second challenge: how to properly treat a battery, specifically, which charging strategies can extend its useful life and how to estimate its State of Health (SoH).

These aspects, including both the scheduling of charging activities and the proper management of battery degradation, represent the key issues addressed in this thesis.

1.4. Aims and objectives

The main objective of this work is to provide a tool to help PTOs better understand the impact of their charging choices on the useful life of their buses.

The tool aims to support PTOs in identifying the most cost-effective charging strategies, not only by extending battery life but also by considering the influence of their decisions on infrastructure requirements and energy costs. Ultimately, this allows operators to gain a clear overview of the implications of their choices and to achieve significant economic benefits.

The idea underlying this objective originated from the direct observation of real-world operational practices within a Public Transport Operator. In particular, it emerged from the awareness that real-life operating conditions differ substantially from the simplified assumptions typically adopted in theoretical frameworks. As a consequence, much of the existing theoretical knowledge and, as will be discussed in the next chapter, several mathematical models are not directly applicable to real operational contexts without significant adaptations.

For this reason, the core motivation of this thesis is to bridge the gap between the theoretical and the practical domains. The proposed tool is conceived as a reference methodological framework, designed to be applicable to different operational contexts

and adaptable to future developments in theoretical and mathematical modeling.

The present thesis was developed in collaboration with Autoguidovie S.p.A., an Italian PTO founded in 1908 by Enrico Laviosa and active in Northern Italy. The company directly manages a fleet of approximately 800 vehicles, in addition to several hundred buses operated through its subsidiaries (Società Trasporti Novaresi, Dolomiti Bus, Cavourese, Girobus, Addabus, and Venetiana) and its affiliate Mobilità di Marca. Its services include both urban and suburban routes in Lombardy and Emilia-Romagna, as well as operations in Piedmont and Veneto through affiliated companies.

The fleet is still predominantly composed of conventional diesel buses, but the share of electric vehicles is steadily increasing as part of the company's ongoing electrification strategy. In recent years, Autoguidovie has actively promoted the transition toward sustainable mobility by introducing Battery Electric Buses into its fleets and developing its own charging infrastructure. This transition, however, is still in its early stages, and the company aims to further expand its zero-emission fleet in the coming years. As the proportion of electric vehicles grows, Autoguidovie has recognized the need to optimize charging operations, monitor operational data to improve energy efficiency, and analyze how operational choices influence battery degradation and lifespan.

The collaboration with Autoguidovie therefore represented not only a valuable opportunity to apply the concepts learned during the academic program at Politecnico di Milano, but also a meaningful chance to contribute directly to the company's electrification efforts and gain first-hand experience in the evolving field of sustainable public transport.

2 | State of the art and literature review

2.1. Battery types

Lithium-ion (Li-ion) batteries have become the standard energy storage technology for EVs due to their superior performance compared to alternative chemistries such as nickel-metal hydride (NiMH) and lead-acid batteries. Their key advantages include high energy density, high efficiency, low self-discharge, fast charge and discharge rates, and long cycle life. A schematic illustration of the working principle of Li-ion batteries is shown in Figure 2.1

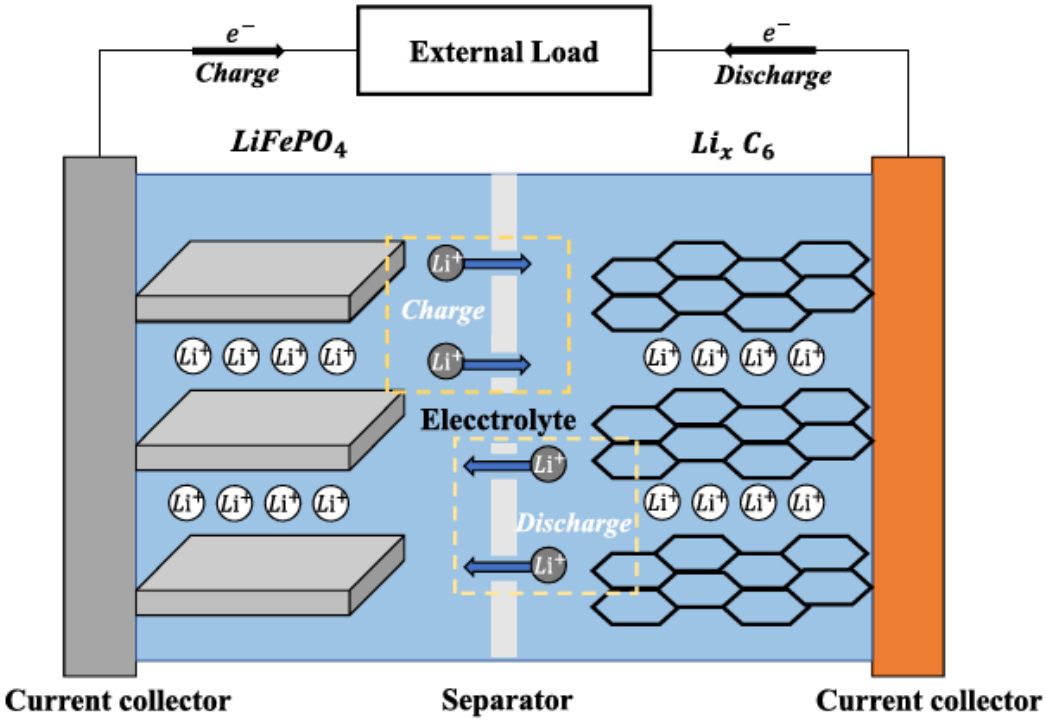


Figure 2.1: Schematic illustration of Li-ion working principle in charging and discharging modes [14].

There are different kind of Li-ion batteries, the most common Li-ion chemistries adopted in the EVs sector are:

- **Nickel Manganese Cobalt oxide (NMC)**: NMC batteries present a cathode made of lithium nickel manganese cobalt oxide ($LiNi_xMn_yCo_zO_2$), where nickel (Ni), manganese (Mn), and cobalt (Co) are present in specific proportions. By adjusting the ratio of these elements, it is possible to modify the overall performance characteristics of the battery, since each metal contributes differently: nickel increases the energy density, manganese enhances structural stability, and cobalt improves electrical conductivity and cycle life. The stoichiometric ratio of these three metals is typically indicated by the numbers following the NMC abbreviation. For example, NMC622 corresponds to a composition with 60% nickel, 20% manganese, and 20% cobalt.

  NMC batteries are among the most widely used chemistries in electric mobility, as they offer a well-balanced combination of energy density, power capability, thermal stability, and cycle life.

  In recent years, the market for passenger vehicles has been progressively moving towards high-nickel compositions, such as NMC811, to further increase the specific energy and vehicle range. However, in the electric bus sector, manufacturers generally prefer lower-nickel variants, such as NMC532, as safety, thermal stability, and longevity are more critical than maximum energy density. Nevertheless, even in this sector, there is a gradual shift toward higher-nickel formulations, driven by the need to extend range without compromising operational reliability. Therefore, this transition must be accompanied by technological innovations aimed at improving stability and safety, such as the development of solid-state electrolytes and advanced thermal management systems.

- **Nickel Cobalt Aluminium oxide (NCA)**: NCA batteries feature a cathode composed of lithium nickel cobalt aluminium oxide ($LiNi_xCo_yAl_zO_2$), where nickel (Ni), cobalt (Co), and aluminium (Al) are present in specific proportions. This chemistry offers very high specific energy, making it particularly suitable for long-range and high-power electric vehicles.

  However, NCA batteries are more sensitive to high temperatures and prone to accelerated aging; therefore, this chemistry requires advanced Battery Management Systems (BMS) to ensure safety and long-term reliability. Despite their high energy

density, NCA batteries have limited applications in the electric bus sector, mainly due to their thermal instability and the requirement for complex and costly BMS solutions. Nevertheless, they have found a strong presence in other segments of the electric mobility market, with Tesla being the primary user of this chemistry.

- **Lithium Iron Phosphate (LFP)**: LFP batteries use a cathode made of lithium iron phosphate ($LiFePO_4$). Unlike NMC and NCA chemistries, they do not contain nickel or cobalt; instead, they use iron and phosphate, inexpensive materials that are abundant on Earth, resulting in lower production costs. These batteries offer excellent thermal and chemical stability, long cycle life, and outstanding safety characteristics, particularly under high-stress operating conditions. Their main drawback lies in their lower energy density compared to NMC and NCA cells; however, recent advances in cell design have significantly improved their performance, making LFP a competitive and attractive alternative to nickel- and cobalt-based chemistries.

  LFP technology is especially popular in low-cost electric vehicles, urban transport applications, and increasingly in electric buses, where safety, longevity, and cost-effectiveness are often more important than achieving the highest possible energy density. The LFP market is currently dominated by China, which has long recognized the potential of this chemistry and heavily invested in its development. As a result, the Chinese electromobility market is now largely based on LFP technology (Figure 2.2). Although NMC batteries still dominate in Europe and in the United States, this balance is shifting, with LFP expected to take the lead in the coming years. Chinese companies hold eight of the top ten positions among global LFP battery manufacturers, with CATL and BYD playing particularly significant roles in the electric bus sector.

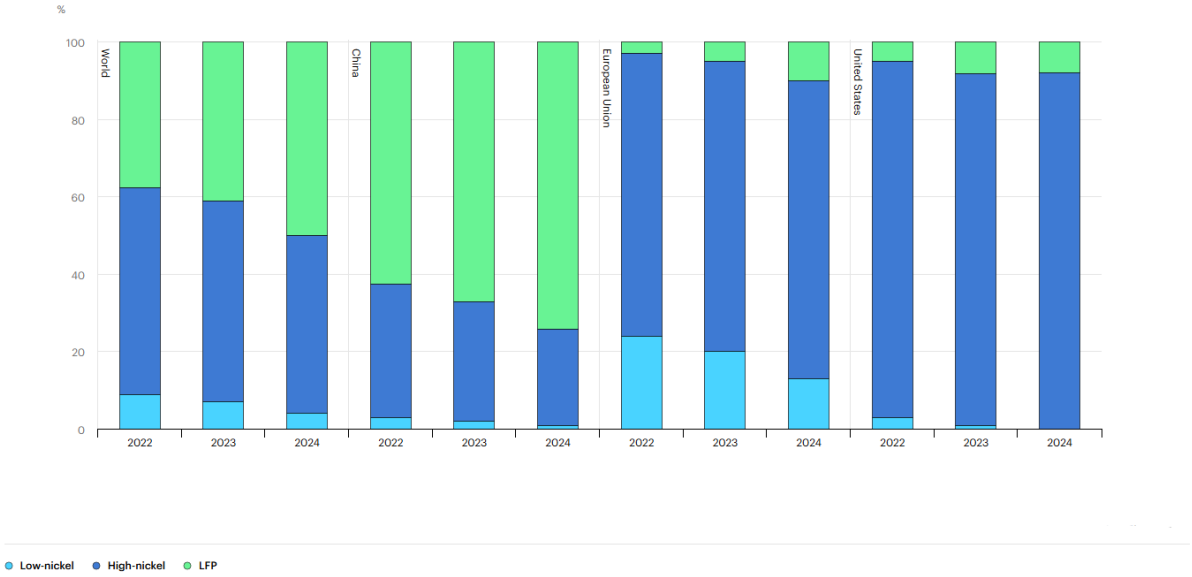


Figure 2.2: EV battery market share by chemistry and region [15].

Nickel and cobalt are considered critical materials from an environmental perspective, not only during extraction and processing but also at the disposal stage. In particular, cobalt has raised increasing concern in recent years, not only for its environmental impact but also for the severe social and humanitarian issues associated with its extraction. Approximately 70% of global cobalt production originates from the Democratic Republic of the Congo (DRC), a country that has faced decades of political instability, armed conflicts, and widespread child labor exploitation. According to numerous international reports, many Congolese mines operate under unsafe and unsustainable conditions, with inadequate safety regulations, workers constantly exposed to toxic dust, and thousands of children involved in mining activities. Moreover, cobalt extraction has been linked to the fuelling of armed conflicts and further destabilization in several regions of the DRC. For these reasons, the United States has included cobalt in its list of "conflict minerals", resources whose control can trigger wars and whose production is often associated with severe environmental damage, pollution, and human rights violations [16].

In addition to the lithium-ion technologies that currently dominate the electric mobility sector, several companies are developing next-generation battery systems based on fundamentally different principles. Among these emerging technologies, solid-state batteries and sodium-ion batteries stand out as two of the most promising candidates for future large-scale adoption.

- **Solid-state battery (SSB)**: SSBs use a solid electrolyte to transport ions between the cathode and the anode, whereas conventional lithium-ion batteries rely on a liquid organic electrolyte. This fundamental change offers several advantages, including improved safety, higher energy density, longer cycle life, and the potential for faster charging. In principle, these characteristics could enable electric vehicles to achieve significantly greater driving range while reducing thermal runaway risks. However, despite their potential, SSBs still face major technical challenges that currently prevent widespread commercialization. One of the most critical issues concerns the degradation of lithium-metal anodes and high-nickel cathodes, which can undergo microstructural changes and develop lithium dendrites during cycling. These phenomena reduce performance and compromise safety. Ongoing research aims to overcome these limitations by improving the understanding of the electrode-electrolyte interface and by optimizing the microstructure and composition of both solid electrolytes and active materials. Studies have shown, for example, that tailoring the cathode microstructure can significantly mitigate these degradation mechanisms [17].
- **Sodium-ion battery (SIB)**: SIBs use sodium ions (Na^+) instead of lithium as charge carriers. Sodium has chemical properties similar to lithium, but it is far more abundant in the Earth's crust and its extraction is generally less environmentally intrusive. For these reasons, SIBs are considered a more sustainable and cost-effective alternative to lithium-based chemistries. Another notable advantage is their high thermal stability and excellent performance at low temperatures, which makes them particularly suitable for use in cold regions where conventional Li-ion batteries often suffer from reduced efficiency. Despite these strengths, the energy density of sodium-ion batteries remains significantly lower than that of current Li-ion technologies. As a result, substantial technological improvements are still required before SIBs can become competitive in applications demanding high autonomy, such as long-haul transportation. Further research is essential to enhance their efficiency and overall electrochemical performance [18].

2.2. Battery aging and wear factors

Although the basic operating principle of a Li-ion battery can be considered relatively simple, the situation becomes far more complex when analyzing how different operating conditions and external factors affect the battery. It is well known that Li-ion batteries undergo aging processes that, through various chemical and electrochemical mechanisms,

gradually reduce their reliability and can ultimately lead to failure.

These degradation phenomena are mainly expressed through changes in two key parameters: capacity and internal resistance. Over its lifetime, a battery typically experiences capacity fade and an increase in internal resistance, which in turn leads to power fade. Capacity fade refers to the gradual decrease in the battery's ability to store and deliver energy, resulting in a reduction of the usable energy content. Power fade, on the other hand, denotes the progressive decline in the battery's ability to meet high power demands or to sustain heavy loads, often leading to pronounced voltage drops under such conditions. Understanding the factors influencing these two parameters is therefore essential to extending battery lifetime and minimizing the occurrence of faults.

Two main aging mechanisms can be distinguished: calendar aging and cycling aging. The impact of these two mechanisms is strongly influenced by operating conditions, and they occur simultaneously throughout the lifecycle of an electric vehicle. Moreover, the authors in [19] showed that these processes are not independent, but influence each other in a complex way, making them particularly difficult to model.

- **Calendar aging** refers to the degradation processes that occur over time when the vehicle, and therefore its battery, is not in active use. This mechanism becomes relevant when the battery is kept at a certain State of Charge (SoC) without undergoing charge and discharge cycles. Calendar aging is particularly important in applications where batteries spend long periods in standby. The public transport sector, and more generally the entire automotive sector, is a clear example, since EVs remain parked for many hours each day. Importantly, this aging mechanism does not occur only during very long inactive periods such as weeks or months, but also during daily rest phases, for example during overnight parking, when the battery remains at a given SOC without cycling. The authors in [20] report that an electric car typically spends about 80% of its lifetime in standby, therefore, despite being a slow mechanism, the impact of calendar aging cannot be underestimated. Even more strikingly, the authors in [21] suggest that standby time may reach 90% or more, and that for electric cars the contribution of calendar aging is so significant that cycling aging can be considered negligible. Electric buses also spend a considerable amount of time in standby, generally less than the 80%-90% reported for electric cars, but still substantial. For this reason, calendar aging is highly relevant in public transport applications and may even be the dominant aging mechanism, although completely neglecting cycling aging would be inappropriate.

- **Cycling aging** refers to the degradation processes that occur over time when a battery is subjected to repeated charge and discharge cycles. This mechanism is particularly relevant in applications involving frequent and intensive battery use, such as electric buses in public transport.
  It is interesting to note that a commonly cited practical guideline for mitigating cycling aging in lithium-ion batteries is the "20/80 rule", which suggests keeping the SoC between roughly 20% and 80% to reduce battery wear. Although this rule is a simplification and does not capture all the complexities of battery aging, it illustrates how cycling-related degradation is widely recognized and can be managed in everyday applications, from electric vehicles to portable electronics.

Taken together, calendar aging and cycling aging contribute to the various degradation processes that ultimately manifest as capacity fade and power fade. These two metrics result from multiple underlying mechanisms, each influenced by operating conditions and aging factors. Figure 2.3 provides an overview of these mechanisms, illustrating their causes and the associated degradation modes.

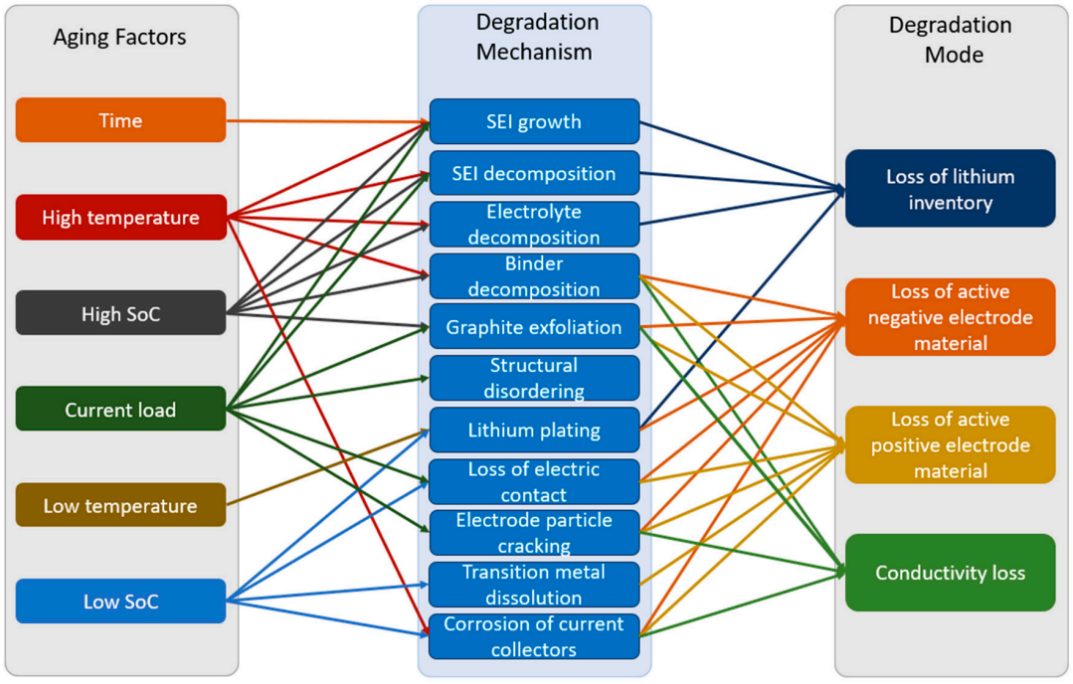


Figure 2.3: Factors affecting aging, chemical and physical mechanisms, and the effects they cause [22].

According to the authors in [23], among these various degradation mechanisms, the growth of Solid Electrolyte Interphase (SEI) is widely recognized as the primary contributor to

capacity loss and internal resistance increase in Li-ion batteries under normal usage conditions.

SEI is a thin solid layer that forms on the surface of the battery's anode, which is typically made of graphite. SEI is composed of both organic and inorganic compounds that originate from the reduction and decomposition of the liquid electrolyte and subsequently accumulate on the graphite surface. During the battery's lifetime, this layer continues to grow over time, this growth increases interfacial resistance and consumes active lithium by incorporating Li^+ into stable inorganic compounds; as a result, the amount of cyclable lithium decreases, leading to a gradual loss of capacity.

As shown in Figure 2.3, common aging factors include temperature, C-rate, and SoC. Another important factor is the Depth of Discharge (DoD), that is a measure of how much energy has been drawn from a battery relative to its total capacity. Although DoD is not explicitly represented in Figure 2.3, it has been identified in several studies as a major contributor to battery degradation. For example, the authors in [24] report that for many Li-ion battery chemistries, deep cycles cause more severe degradation than shallow ones, leading batteries to reach their End of Life (EoL) more quickly when subjected to high-DoD cycling. Although all these parameters influence battery aging, this thesis places particular emphasis on the minimum and maximum SoC values, as well as on the DoD. Unlike aging factors such as temperature or time, SoC and DoD can be directly influenced through optimal fleet management strategies, making them key variables in the context of this study.

Many studies described the relevant factors that affect battery life, among these the most discussed are SoC, DoD, temperature and C-rate; the effect of each of these factors is analyzed below.

- **SoC** contributes to both calendar and cycling aging. Regarding calendar aging, the authors in [25] observed that batteries stored at high SoC experience greater capacity fade than those stored at lower SoC. As for cycling aging, operating batteries within high SoC ranges (ΔSoC) similarly accelerates degradation. This behavior is explained by the fact that elevated SoC levels, and consequently high terminal voltage, promote mechanisms such as electrolyte oxidation, SEI growth and decomposition, graphite exfoliation, and binder deterioration. Although low SoC levels are generally beneficial from a calendar aging perspective, prolonged cycling at very low SoC can instead trigger lithium plating, transition-metal dissolution, and current-

collector corrosion, all of which negatively affect battery lifetime and safety. For these reasons, cycling within a moderate ΔSoC window and storing the battery at low SoC levels are widely considered good practices for limiting Li-ion battery degradation.

- **DoD** strongly affects cycling aging. In particular, the authors in [26] highlight a non-linear relationship between the lifespan of a Li-ion battery and the DoD of the cycles to which it is subjected. As DoD increases, the maximum number of cycles the battery can undergo before reaching EoL decreases. Higher DoD values impose more intense mechanical and chemical stress on the electrode materials, primarily causing loss of active material, which contributes to capacity fade. The relationship between DoD and cycle life is illustrated in Figure 2.4.

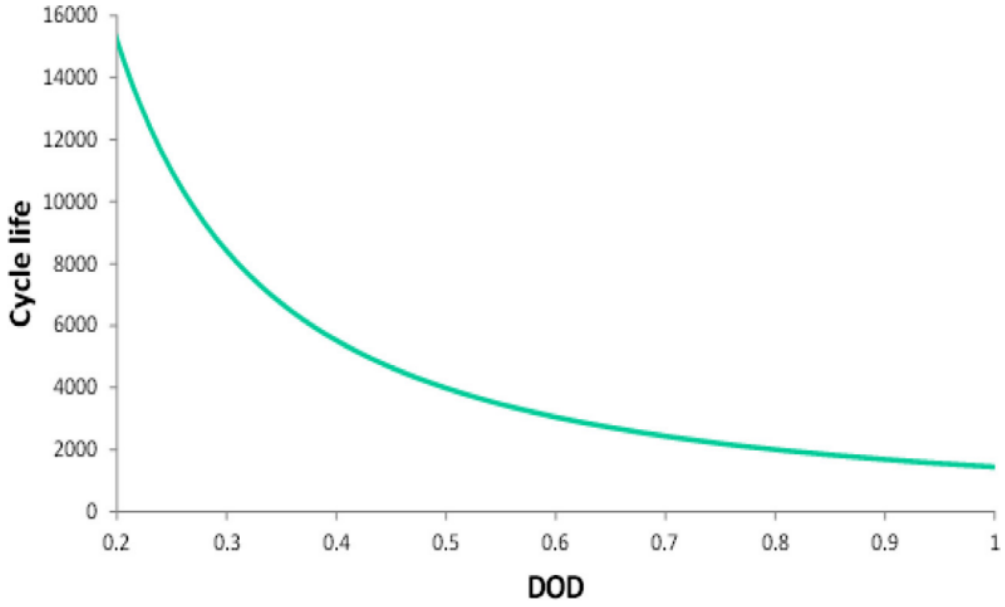


Figure 2.4: relationship between the number of achievable cycles and DOD [26].

- **C-rate** is defined as the ratio between the charge or discharge current and the nominal capacity of the battery. A rate of "1C" corresponds to the current required to fully charge or discharge the battery in one hour. The C-rate can therefore be interpreted as the speed at which the battery is charged or discharged. Numerous studies indicate that high C-rates are associated with accelerated aging. In particular, elevated C-rates can induce structural damage such as SEI decomposition, graphite exfoliation, and electrode particle cracking. The authors in [27] experimentally demonstrated this relationship by conducting cycling tests on Li-ion batteries under different C-rate conditions. Their results are reported in Figure 2.5.

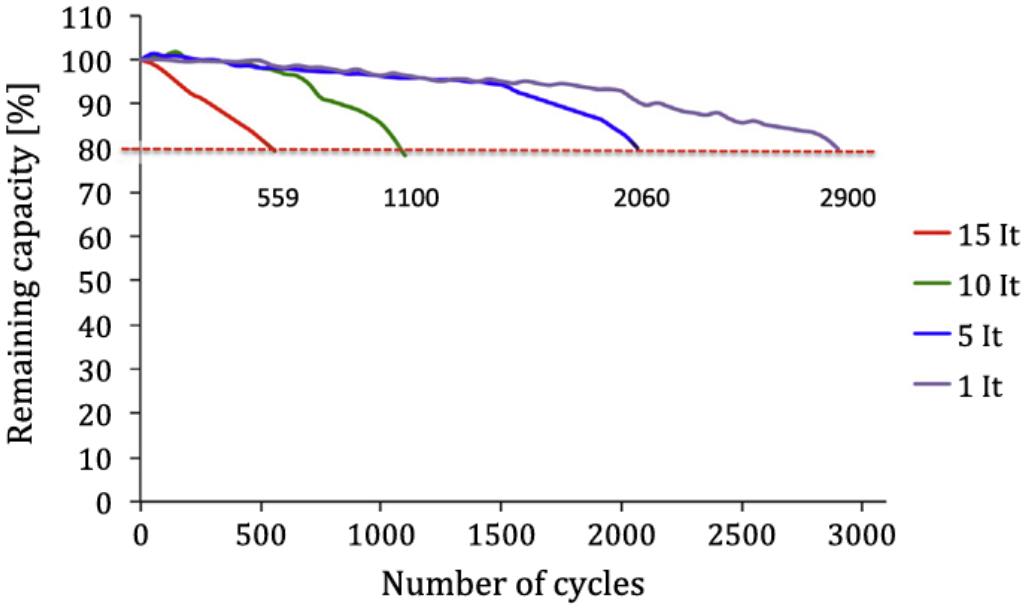


Figure 2.5: Evolution of remaining capacity versus cycle life at different current rate [27].

- **Temperature** affects battery aging during both cycling and resting periods. High temperatures are known to be harmful for battery health and safety, as they accelerate degradation mechanisms such as SEI growth, SEI decomposition, and electrolyte degradation. Conversely, very low temperatures also contribute to battery damage. For example, the authors in [28] showed that, at low temperatures, lithium plating becomes the dominant degradation mechanism. Temperature is a critical aging factor, as it not only contributes to capacity and power fade, but must also be continuously monitored by the BMS to prevent overheating. Excessive temperatures can lead to thermal runaway, an extremely dangerous condition in which heat generation triggers a series of exothermic reactions that further increase the temperature, causing an uncontrolled escalation. This process can ultimately result in smoke, fire, or even explosion. The authors in [29] investigate and describe the thermal runaway mechanism in Li-ion batteries for EV applications, identifying it as one of the key scientific challenges in contemporary battery safety research.

The aging factors discussed above affect calendar and cycling aging differently depending on the lithium-ion battery chemistry. Table 2.1 provides a brief overview of how these factors influence different chemistries.

	NMC	NCA	LFP
Low SoC	•	•	•
Medium SoC	•	•	•
High SoC	•••	•••	••
Low C-rate	•	•	•
Medium C-rate	••	•	•
High C-rate	••••	•••	••
Low Temperature	••	•	••
Medium Temperature	••	•	•
High Temperature	••••	•••	••

Table 2.1: Effect of stress factors on aging for cell chemistries for both aging modes. (••••: highest impact,•••: high impact,••: medium impact,•: low impact) [22].

2.3. Cell imbalance and balancing techniques in Li-ion battery packs

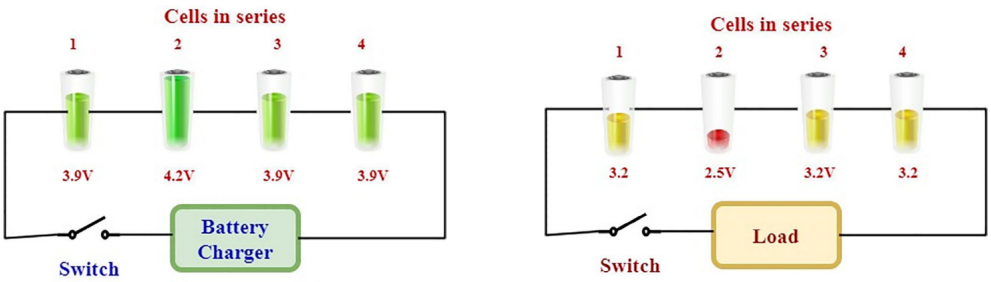
After introducing the main aging mechanisms and wear factors that affect battery life, it is also necessary to examine another important aspect for effective battery management. The following section addresses cell imbalance and the corresponding cell balancing techniques, with a focus on both the underlying technical principles and the insights emerging from the literature.

Li-ion battery packs are composed of a given number of individual cells arranged in series and parallel configurations to achieve the desired electrical characteristics. Connecting cells in parallel increases the pack capacity, as the total capacity corresponds to the sum of the capacities of the parallel-connected cells. Conversely, connecting cells in series increases the overall pack voltage, which is equal to the sum of the voltages of the individual cells. Cells within a battery pack are theoretically identical, and series-connected cells are therefore expected to operate at the same voltage. However, small variations in internal cell composition, initial capacity, and manufacturing tolerances, as well as external factors such as non-uniform temperature distribution, inevitably cause cells to charge and discharge at slightly different rates [30]. Over time, these differences lead to unequal cell voltages and SoC, a phenomenon known as cell imbalance. Several studies have demonstrated the inevitability of cell imbalance. For example, the authors in [31] reported a noticeable divergence in the SoC among the cells of an EV battery pack

after approximately 5000 km of operation.

Cell imbalance is an undesirable phenomenon because it reduces the overall usable capacity of the battery, accelerates aging, and may also pose safety risks. As highlighted by the authors in [32], cell balancing is essential to mitigate performance degradation and extend the operational lifespan of battery packs affected by imbalance. In addition, they state that proper balancing ensures safe operation, since cell imbalance can cause some cells to reach the upper voltage limit earlier than others. If charging continues, these overstressed cells may become overcharged, which can lead to instability and potentially trigger thermal runaway or cell rupture, representing a serious hazard.

The BMS not only continuously monitors all the relevant parameters of each cell, preventing individual cells from becoming overcharged or overdischarged, but also implements cell balancing techniques to ensure that all cells within the pack maintain uniform voltage levels. This is essential to guarantee safe and efficient operation and to prevent undesired events such as early charge (Figure 2.6a) or discharge (Figure 2.6b) termination.



(a) Early charge termination. (b) Early discharge termination.

Figure 2.6: Illustration of early charge and early discharge termination events [33]

.

In the literature, the various balancing techniques are typically classified into two main approaches: passive balancing and active balancing.

Passive balancing relies on dissipating excess charge from higher-voltage cells through resistors, bringing their voltage in line with that of the lower-voltage cells. This method is simple, cost-effective, and easy to integrate, which explains its widespread adoption in the EV industry. However, its main limitation lies in the inefficient use of energy, as the surplus charge is wasted as heat. Two main schemes are commonly employed in passive balancing systems:

- Top balancing aims to equalize cell voltages at the end of the charging phase, when the SoC is close to 100% and cell voltages increase rapidly. In this approach, cells are charged independently until one reaches its upper voltage threshold. At that point, excess charge in the higher-voltage cells is dissipated through resistors until all cells are aligned at the top of the voltage range.
- Bottom balancing aims to equalize cell voltages at the end of the charging phase, when the SoC is close to 0% and cell voltage drop significantly. The authors in [34] reported that bottom balancing requires more time, but consumes less energy than top balancing. However, its effectiveness depends on the battery being deeply discharged before balancing, which is difficult to achieve in practice due to range anxiety. Moreover, as discussed in the previous sections, repeatedly reaching very low SoC levels can severely harm Li-ion batteries.

From a circuit-design perspective, passive balancing can be implemented using the following configurations:

- Fixed shunt resistor method: in this approach, each cell is connected to a resistor that continuously dissipates excess energy as heat, as shown in Figure 2.7. The resistor value is sized to limit the balancing current and constrain cell voltage. Although simple and low-cost, the resistors operate continuously, even when no balancing is required, causing constant energy losses and unnecessary heating. Furthermore, because the discharge path cannot be disabled, if cell capacities are mismatched, some cells may reach full charge earlier and risk overcharging. For these reasons, this method is mainly used for lead-acid and nickel-based batteries and is generally unsuitable for Li-ion chemistries [31].

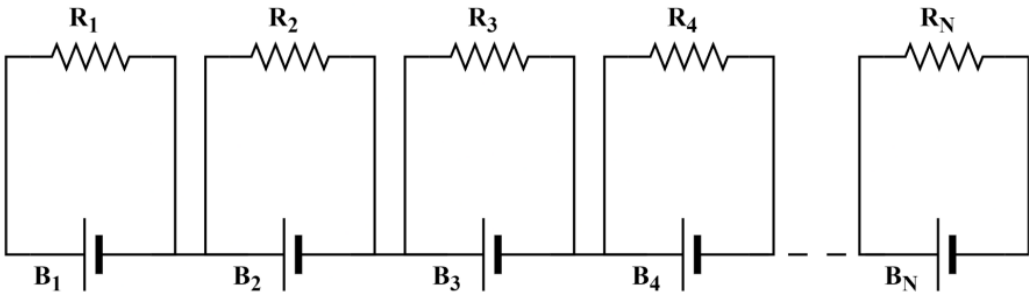


Figure 2.7: Fixed shunt resistor passive balancing [32].

- Switched shunt resistor method: in this configuration, resistors are selectively connected in parallel with individual cells through controllable switches, as shown in Figure 2.8. Unlike fixed shunt balancing, the discharge path is activated only when

a cell exceeds a predefined voltage threshold. The BMS monitors cell voltages and selectively dissipates energy from higher-voltage cells to reduce imbalance. This method offers better efficiency and thermal control, as balancing occurs only when needed. Although energy is still dissipated as heat, its controlled operation and improved reliability make it suitable for Li-ion batteries. Nevertheless, the method requires additional circuitry and may generate localized heat during high-current balancing, making thermal management an important design consideration. Overall, the switched shunt technique provides a compromise between simplicity and performance and is widely adopted in applications where cost constraints are relevant.

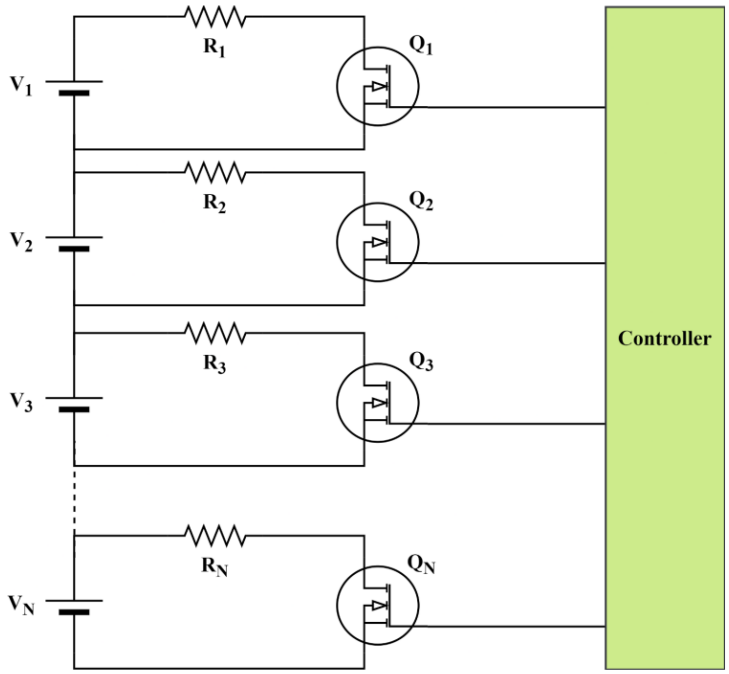


Figure 2.8: Switched shunt resistor passive balancing [32].

Active balancing, in contrast, redistributes energy from higher-voltage cells to lower-voltage ones using inductive, capacitive, or DC-DC converter-based circuits. This approach significantly improves energy efficiency and can enhance both driving range and battery lifespan. However, active balancing is more complex and costly, requiring sophisticated control algorithms and specialized hardware, which can limit its applicability in cost-sensitive systems.

From a circuit-design perspective, active balancing can be implemented using several architectures. The authors in [35] provide an exhaustive review of active balancing prin-

ciples and circuit configurations. For completeness, this work presents a brief overview of the main topologies; however, since active balancing is not implemented in the subsequent developments, the following description is limited to a general outline:

- Capacitor-based charge transfer methods: these methods use one or more capacitors that alternately connect to different cells. When connected to a high-voltage cell, the capacitor charges to that cell's voltage; when switched to a lower-voltage cell, it discharges into it. Over repeated cycles, capacitors transfer charge from higher-voltage to lower-voltage cells. These systems are simple and effective, but they generally require long equalization times.
- Inductor-based charge transfer methods: they are similar in principle to capacitor-based designs, these methods use inductors, often as part of a buck-boost converter, as intermediate energy-storage elements. Compared with capacitor-based methods, inductor-based balancing typically offers higher efficiency and faster balancing, while being cheaper, more compact, and easier to design and implement. However, these systems may experience higher current ripple and require careful duty-cycle control to ensure stable operation.
- Transformer-based charge transfer methods: These approaches employ isolated DC-DC converters incorporating transformers to transfer energy between cells. Galvanic isolation allows the management of large voltage differences safely and efficiently. Although highly flexible and effective, transformer-based systems are typically more expensive, larger, and more complex than capacitor-based or inductor-based designs, which limits their use to applications where performance and safety outweigh cost and size considerations.

In the EV sector, passive balancing remains the most widely adopted solution due to its simplicity and low cost. Active balancing, on the other hand, is attracting increasing attention as a promising alternative, particularly for high-performance or long-range applications, although cost and system complexity continue to limit its widespread adoption. In the context of electric buses, the passive top-balancing technique, typically implemented through a switched shunt resistor circuit, is commonly used.

2.4. Battery aging models

The following section presents and critically analyses some of the battery aging models available in the literature. The objective is to identify how an aging model should be constructed, drawing on previous work to understand the underlying assumptions, assess

the strengths of existing approaches, and highlight their limitations. This review provides the foundation for developing an appropriate modeling framework for the purposes of this study.

A battery aging model is a predictive tool that, based on operating conditions and key system parameters, estimates the degradation of a battery over time. By quantifying how usage patterns, environmental factors, and control strategies influence aging, such a model enables the prediction of when a battery will reach its EoL. This allows determining the appropriate moment for its replacement in the EV application and assessing whether it can be repurposed for less demanding uses, such as stationary energy storage.

For EV applications, the EoL of a battery is typically defined as the point at which its usable capacity has decreased to 80% of the initial value or when its internal resistance has doubled. According to the literature, capacity fade is generally the dominant aging mechanism limiting the lifetime of Li-ion batteries. For this reason, capacity is the primary parameter used to track degradation, and the EoL is commonly identified as the moment when the battery's SoH, defined as the ratio between the current capacity and the initial nominal capacity, drops to 80%.

Battery aging models available in the literature are generally derived from experimental observations. In these studies, a set of batteries is subjected to specific cycling profiles and/or resting periods under controlled conditions, with the aim of assessing the impact of the selected parameters on battery SoH. The resulting experimental data are then used to formulate mathematical models capable of describing and reproducing the observed degradation behavior.

The authors in [24] conducted tests on Li-ion NMC pouch cells with a nominal capacity of 20 Ah, manufactured by EIG. Cycle aging was assumed to be influenced by four stress factors: operating temperature, DoD, mean SoC, and the number of full equivalent cycles (FECs). For calendar aging, the considered stress factors were storage temperature, storage SoC, and storage time. A total of 116 cells were tested under 36 different cycle aging conditions, each with varying combinations of stress factors, while 30 additional cells were assigned to 10 distinct calendar aging test conditions. Notably, the cycle-aging model was validated using driving profiles representative of real EV operating conditions. Although the resulting mathematical formulation is relatively complex to analyze or to use directly as a basis for the model developed in this study, it provides highly accurate predictions, as demonstrated by the validation results under real-world operating scenarios.

Another aging model, presented by the authors in [36], is based on tests conducted on more than 60 Li-ion NMC round cells with a nominal capacity of 2.15 Ah, manufactured by Sanyo. Cycle aging was assumed to be driven by three stress factors: DoD, mean voltage, and cumulative charge throughput. These factors were combined to define 22 different cycling conditions for testing. For calendar aging, the selected stress factors were storage temperature, storage voltage, and storage time, resulting in 14 distinct aging conditions. The main strength of this work lies in the authors' ability to formulate a clear and compact equation that enables direct estimation of the SoH under both cycling and calendar aging modes.

The authors in [37] conducted tests on Li-ion LFP cells with a nominal capacity of 1.1 Ah, manufactured by A123 Systems. In this study, only cycling aging was considered, as the calendar aging component was deemed negligible by the authors. The cells were tested in a controlled environment, where each cell was continuously cycled using a specific current profile for ten weeks. The stress factors considered included operating temperature, average SoC, SoC deviation (accounting for DoD), and cumulative charge throughput. Notably, the authors also analyzed the impact of discharge C-rate on battery aging, but decided not to include it in the SoH mathematical formulation, as the experiments demonstrated that different discharge C-rates around room temperature did not contribute significantly to additional capacity fade. This finding, which contrasts with other literature, was justified by the fact that batteries in EV applications typically operate at C-rates well below their maximum specifications. The model provides a clear equation to estimate SoH; however, its main limitation is the neglect of the calendar aging component, which, as demonstrated by more recent studies such as those in [19] and [38], is highly relevant and should not be neglected.

Another relevant contribution is provided by the studies in [39] and [40]. The authors acknowledge the importance of considering both calendar and cycling aging to achieve accurate SoH estimation. In [39], several Li-ion LFP cells with a nominal capacity of 2.3 Ah were tested in a temperature-controlled environment. Each cell was stored under different combinations of resting SoC and temperature to develop a predictive model for calendar lifetime. In [40], using the same cell type and environmental conditions as in the previous study, the authors focused on cycling aging, analyzing the impact of DoD and C-rate variations on battery lifetime to develop a cycle aging model. The broader objective of these two studies is to establish a unified lifetime prognosis methodology that incorporates both calendar and cycling aging effects, covering a wide range of operational

conditions. The authors also recognize the limitations of their work, emphasizing the need for further research to bridge existing gaps. In particular, they highlight the importance of developing models capable of capturing more complex operational profiles, such as combinations of cycling patterns, rest periods at different SoC levels, and partial-charging conditions.

The studies discussed above represent only a small portion of the broad and heterogeneous landscape of battery aging models, each characterized by specific assumptions and modeling choices. In the literature, numerous models have been proposed, often relying on different sets of stress factors and sometimes leading to contradictory conclusions, as reflected in the varying emphasis placed on calendar aging relative to cycling aging. Moreover, the mathematical formulations adopted across studies are far from uniform, with stress factors typically related to SoH through either linear or exponential functions.

Despite this diversity, one common and well-established element across most aging models is the formulation that describes the relationship between temperature and capacity fade. Multiple studies have shown that capacity loss during storage follows the Arrhenius law, which links temperature to the rate of chemical reactions. This relationship forms the basis for modeling calendar aging and is widely employed in predictive aging formulations. The authors in [22] provide a commonly adopted mathematical expression:

$$Q_{\text{loss}} = A \cdot e^{\left(-\frac{E_a}{R \cdot T}\right)} \cdot t^z \tag{2.1}$$

In Equation 2.1 , A is the pre-exponential factor, E_a is the activation energy associated with the degradation reaction, R is the universal gas constant, T is the absolute temperature, and t is the storage time.

To capture the influence of the storage SoC on calendar aging, several experimental studies have introduced the SoC dependency directly into the Arrhenius pre-exponential factor. This leads to a modified formulation (Equation 2.2) for estimating calendar-related capacity fade:

$$Q_{\text{loss}} = A(SoC) \cdot e^{\left(-\frac{E_a}{R \cdot T}\right)} \cdot t^z \tag{2.2}$$

As can be observed, some models consider SoC as a stress factor, while others use voltage instead. On this point, it is necessary to provide a clarification and better describe the

relationship between these two parameters, in order to show that both assumptions are reasonable, as they ultimately account for the same aging mechanism. In fact, voltage and SoC are linked by a mathematical relationship that depends primarily on the battery chemistry; however, variations may also arise between manufacturers and cell models. For each specific battery, this relationship can be described through an OCV–SoC curve, a diagram that shows how the open-circuit voltage varies as a function of the SoC. The open-circuit voltage corresponds to the cell voltage when no current is flowing.

For Li-ion batteries, the OCV–SoC curve is generally nonlinear, with flatter regions in the mid-SoC range and steeper slopes at low and high SoC. The authors in [41] reported an OCV–SoC curve for an NMC Li-ion cell, which is reproduced in Figure 2.9.

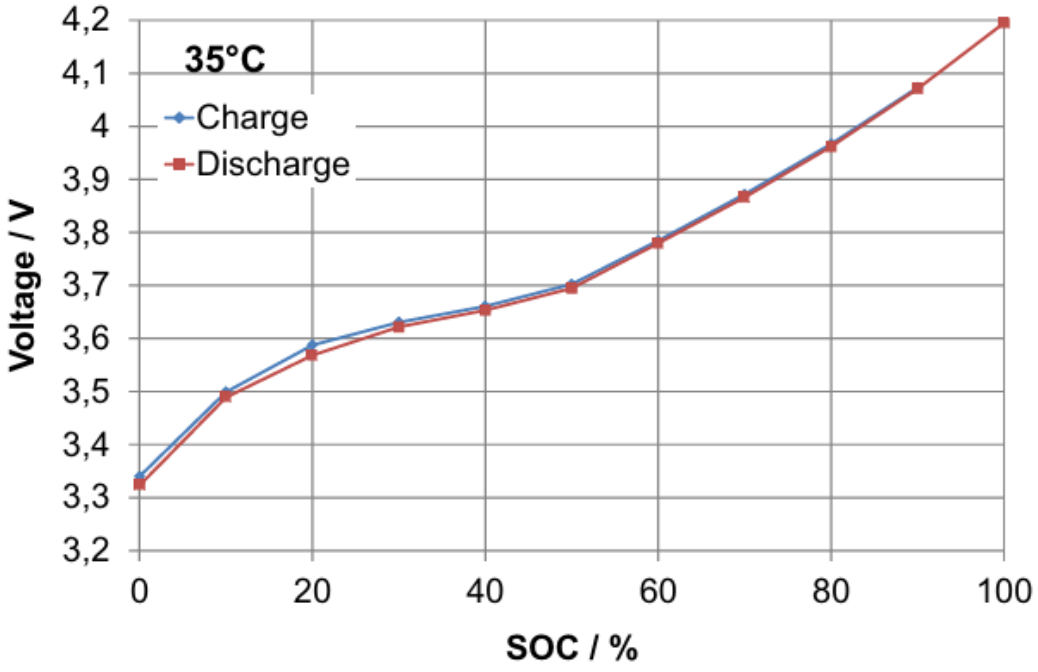


Figure 2.9: Open circuit voltage over State of Charge [41].

2.5. Battery aging model integration in the electric bus scheduling problem

In the following section, several studies from the literature addressing the Electric Bus Scheduling Problem (EBSP) are reviewed, with particular attention to how they incorporate battery aging considerations. The focus is on the operational and charging strategies proposed to mitigate degradation and extend battery lifespan.

The Vehicle Scheduling Problem (VSP) is a well-known optimization problem in the operational planning of public transportation systems. It aims to generate efficient and reliable schedules by assigning a set of predefined trips, with fixed departure times, origins, and destinations, to a fleet of vehicles operating from one or more depots. The primary objective is to minimize operating costs and fleet size while ensuring high service quality and passenger satisfaction [42].

In recent years, the rapid increase in the share of battery electric buses within public transport fleets has introduced new challenges, leading to the formulation of the EBSP. The EBSP is a specialized extension of the VSP that incorporates the technical constraints of electric buses, most notably their limited driving range and, even more critically, the time required for battery charging. These additional constraints significantly affect scheduling feasibility and require the integration of charging operations within vehicle blocks, making the EBSP considerably more complex than the traditional VSP.

The authors in [43] developed an optimization model aimed at determining the optimal charger deployment, on-board battery capacity, and charging schedule for a BEB system. The objective was to minimize the overall system cost by considering both investment and operational charging expenses. Investment costs included the cost of on-board batteries and charging infrastructure, while charging costs encompassed energy consumption and demand charges, the latter representing the fees imposed by the transmission system operator for the peak power drawn during each billing period. The authors highlighted the importance of incorporating charging costs into the EBSP framework and reported that their model can reduce total system cost by 19.5% compared to existing methods. They also acknowledged a limitation of their work, noting that the residual value of infrastructure and equipment was not considered, which may lead to a biased estimation of total system cost. Regarding battery aging, the model included lower and upper limits for the battery SoC, set at 20% and 90% respectively, to avoid the detrimental effects of overcharging and overdischarging on battery health. However, the authors did not explicitly model the impact of charging strategies on battery aging or on the resulting system cost. Instead, they assumed a fixed battery lifetime of six years, independent of the operational and charging conditions experienced by the battery. Finally, another limitation arises from the strong assumption that each bus operates on a single fixed route. In real-world operations, buses commonly rotate among multiple routes to maximize fleet utilisation, ensure more uniform vehicle wear, and comply with the mileage constraints typically imposed by the PTO. This limitation was addressed by the same authors in a

subsequent study. In [44], they developed an improved optimization model that again aimed at minimizing the overall BEB system cost, but without imposing a fixed route assignment. Instead, the algorithm was allowed to determine how to allocate the available buses to the required trips. The resulting BEB schedule and the corresponding battery SoC profiles are shown in Figure 2.10.

The enhanced model provides valuable insights and represents a step forward compared to the previous formulation. However, despite overcoming the single-route assignment constraint, the remaining shortcomings of the original model, most notably the simplified treatment of battery aging, remain unaddressed.

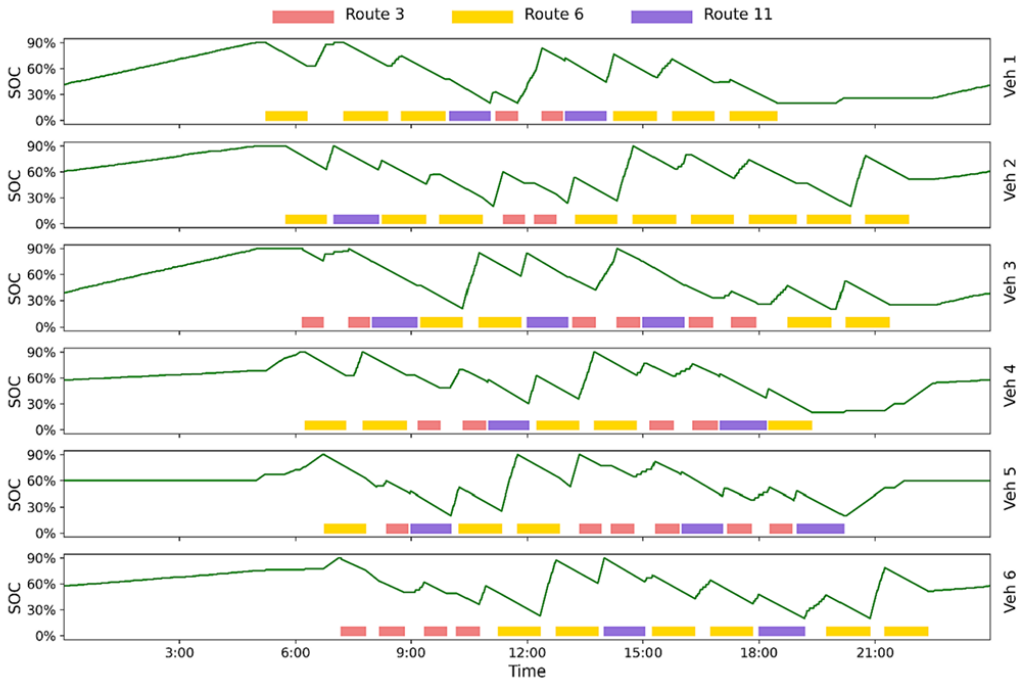


Figure 2.10: Electric bus schedule and battery SOC profile [44].

The authors in [45] developed an optimization model for charger placement and fleet configuration aimed at reducing the total BEB system cost, including charging infrastructure investment, bus purchase costs, energy consumption, and battery degradation. The explicit inclusion of battery degradation costs represents a notable improvement over previous studies that overlooked this component, making the model more realistic and comprehensive. The proposed model was applied to a real-world case study in Oslo, Norway, yielding promising results. According to the authors, their approach can achieve a 21.27% reduction in total annualized costs compared to conventional models that rely on a single BEB type and ignore the impact of SoC variations on battery degradation.

The authors also acknowledge several limitations of their work. First, the model assumes that BEBs are always charged whenever they reach a stop equipped with a charger and that buses must reach a predefined upper SOC limit upon arrival at the central terminal. A more flexible strategy would allow partial or opportunistic charging, enabling buses to decide whether or not to charge at intermediate stops. Second, the model assumes a linear relationship between energy consumption and driving distance, without accounting for route-specific characteristics such as elevation, traffic, or passenger load.

Further limitations relate to the simplified battery degradation model, which accounts only for SoC variations while neglecting other relevant stress factors such as temperature and charge throughput. Most importantly, the model captures only cycling aging and does not include any contribution from calendar aging. Moreover, the absence of residual value considerations leads to an incomplete representation of battery degradation, since the model does not link degradation to potential battery replacement events.

In [46], the authors addressed a different challenge within the EBSP framework by developing a vehicle scheduling model for BEB routes that accounts for stochastic variations in both trip travel time and energy consumption. An interesting aspect of this study is the recognition that charging strategies influence not only the number of buses available for deployment but also the battery cycle life. Building on the findings presented by the authors in [47], they noted that mitigating battery degradation requires operating the battery around medium SoC levels, approximately 50%. Nevertheless, due to energy consumption considerations, they opted for a slightly higher SoC window. As shown in Figure 2.11, the 60%-80% SoC range was identified as the most suitable solution for the case study conducted on a bus route in Meihekou City, China.

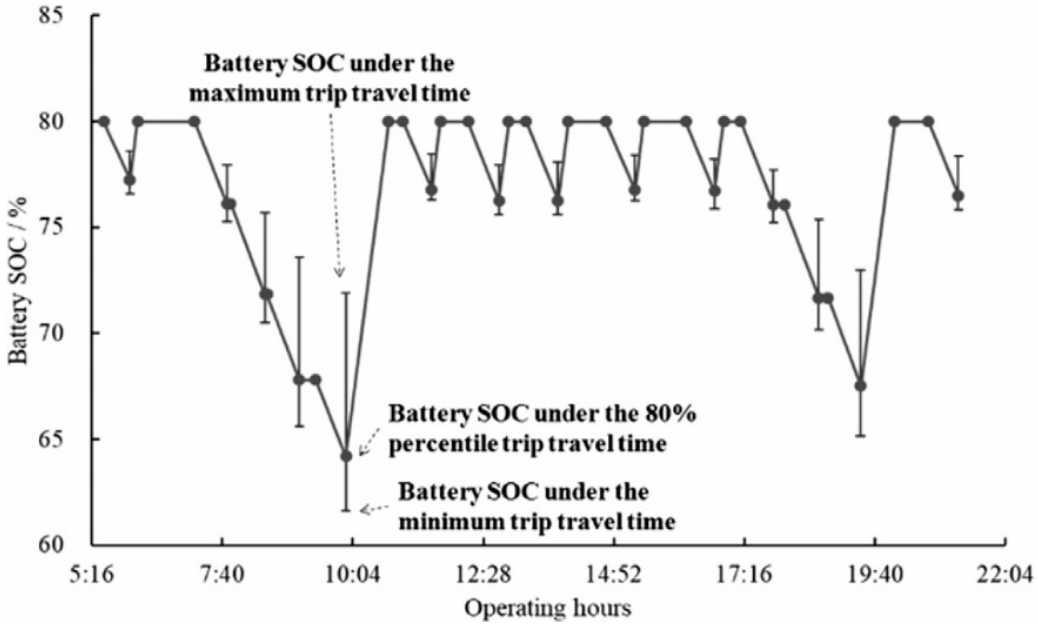


Figure 2.11: Battery State of Charge variation curve [46].

The authors in [48] developed a model aimed at reducing the total cost of operating a fleet of electric freight vehicles used for goods delivery. Although formulated for freight transport, the authors noted that the model can be applied to any electric vehicle routing including those involving electric bus operations. Initially, the cost function considered only charging costs. Subsequently, drawing on the model presented in [49] to translate cyclic aging into monetary terms, they incorporated battery degradation costs into the objective function, thus capturing the impact of cycle aging on the overall system cost.

Recognizing that calendar aging also contributes significantly to battery degradation and therefore to total system cost, the authors examined the findings presented in [50] and observed that degradation during storage increases with the State of Charge. They concluded that substantial lifetime improvements can be achieved by charging vehicles as close as possible to their departure times, thereby avoiding extended periods spent at high SoC.

To account for both aging mechanisms, the authors adopted a two-phase strategy. In the first phase, they minimized energy costs and cycle related degradation costs. In the second phase, they aimed to minimize the sum of periodic SoC variables while constraining the total cost, or its individual components, to remain equal to the values obtained in the first phase or within an acceptable deviation. This approach encourages the model

to avoid maintaining batteries at high SoC for long periods whenever this is not strictly necessary.

The resulting framework is relatively comprehensive. Although calendar aging is not fully embedded in the cost function, the proposed strategy effectively limits the rest period spent at high SoC and therefore significantly mitigates battery degradation associated with calendar aging, leading to an overall improvement in battery longevity.

Another relevant contribution is presented in [51]. The authors proposed a methodological approach to manage the overnight charging of an electric bus fleet, with the goal of identifying an optimal charging strategy that minimizes battery aging costs. They recognized the importance of calendar aging in the EV sector, noting that it can become the dominant aging mechanism in applications characterized by shallow cycling and low current rates. For this reason, they designed a charging strategy specifically aimed at reducing the impact of calendar aging.

The proposed strategy was compared with three typical approaches: a greedy baseline, in which batteries are charged at maximum power as soon as charging becomes available; a medium baseline, where charging is performed at an intermediate power over the entire available charging window; and a postponed baseline, in which charging is delayed until just before the next operation. The corresponding SoC and power profiles for these strategies are shown in Figure 2.12.

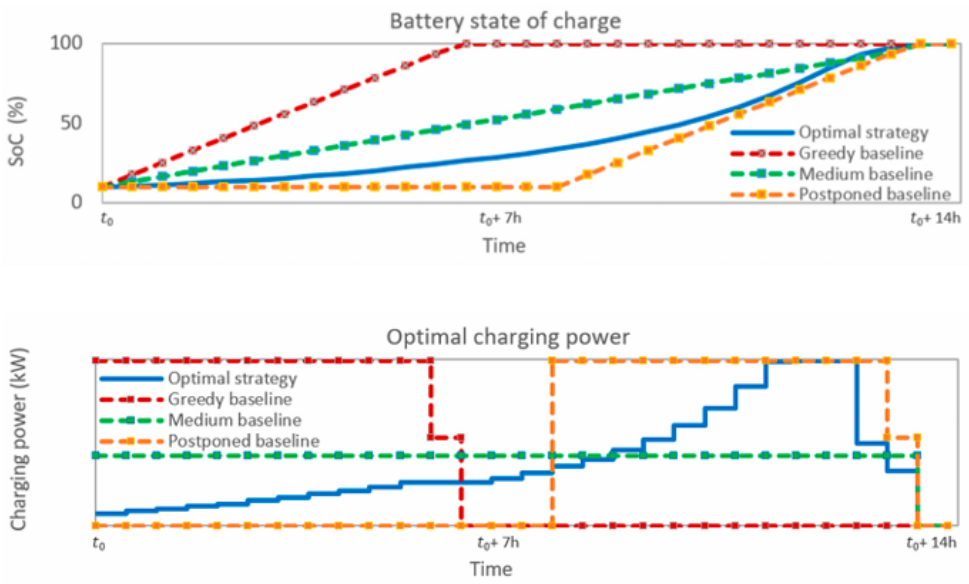


Figure 2.12: Optimal charging schedules compared with three typical charging strategies [51].

Figure 2.13 reports the simulation results obtained in the study, illustrating the battery capacity loss after ten years of operation. The authors concluded that their proposed strategy can nearly double battery lifetime compared with the greedy baseline. This study offers a valuable contribution to the EBSP framework, though its main limitation lies in the exclusive focus on battery aging costs, without taking into account other relevant cost components. As highlighted in previous research, battery degradation costs are substantial, but charging costs are typically even higher and therefore cannot be neglected.

Nevertheless, the analysis clearly shows how battery aging can be significantly reduced simply by avoiding greedy charging behavior. The medium and postponed baselines already achieve markedly better results and remain close to the optimal solution, despite being simpler to implement.

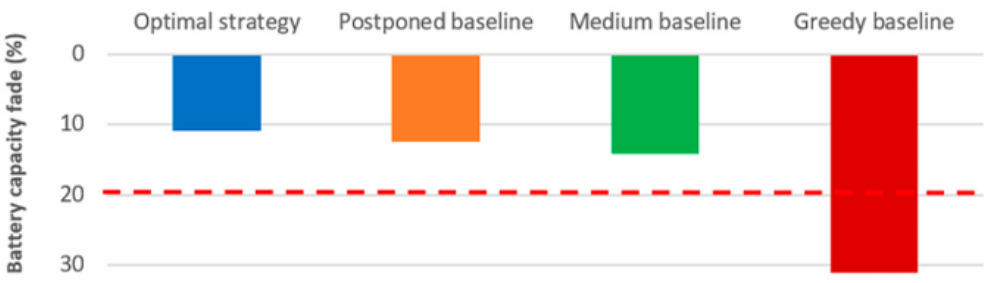


Figure 2.13: Battery capacity loss after 10 years of operation [51].

2.6. Electricity market

As shown in the previous sections, charging costs represent a key component of the total cost of a BEB system. It is therefore necessary to analyze and discuss the structure of the European and Italian electricity markets in order to understand the factors that influence electricity prices. Such knowledge is essential for a PTO wishing to implement charging strategies that can yield economic benefits.

In Europe, the electricity market is structured into two main markets: the wholesale market and the retail market. The wholesale market is the core of the electricity system, where energy is traded among generators, aggregators, traders and suppliers. The retail market, on the other hand, concerns the sale of electricity from suppliers to end customers, such as households and businesses.

Prices in the wholesale market are established through auction mechanisms that reflect aggregate supply and demand conditions. This is a competitive environment where the wholesale price forms the basis upon which retail electricity providers design customized offers for final customers. A key concept within the wholesale market is the clearing price, defined as the uniform price paid to all accepted generators in a given market session. This price is determined through auctions by matching supply and demand curves. Generator offers are ranked in ascending order according to the merit order and progressively accepted until the expected demand is fully met. The price of the last accepted offer, corresponding to the most expensive unit required to satisfy demand, sets the clearing price. All accepted generators receive this uniform price, regardless of their individual bids.

Transmission System Operators (TSOs) are responsible for maintaining grid reliability by ensuring that power plants are dispatched according to the merit order while respecting network constraints. Renewable energy sources are typically dispatched first due to their near-zero marginal costs, followed by nuclear, coal, gas and oil-fired power plants, depending on availability and bid prices. An illustration of the merit order mechanism is reported in Figure 2.14.

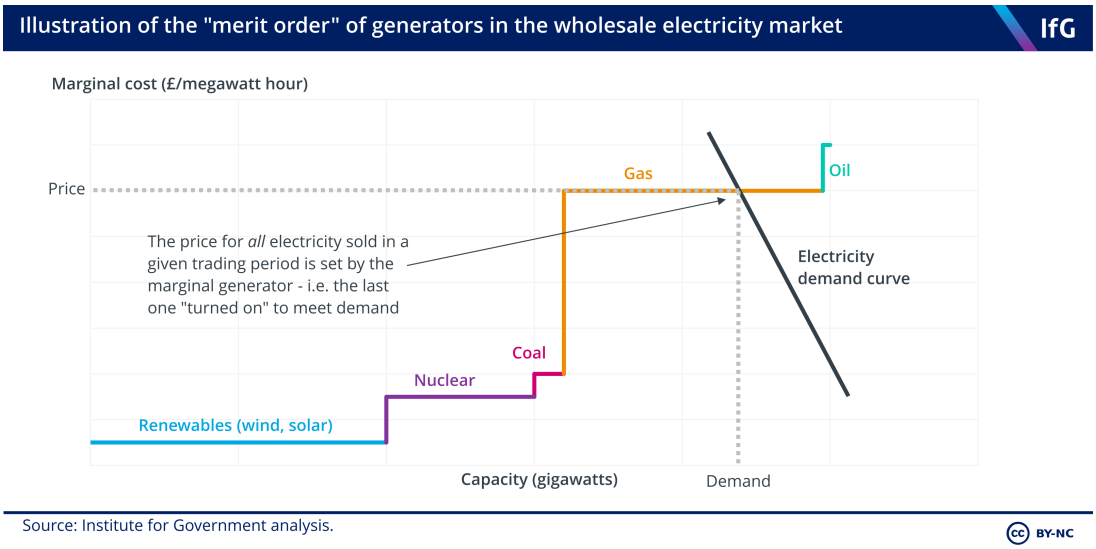


Figure 2.14: Merit order illustration [52].

It is important to note that the clearing price is not uniform across Europe. Instead, it is determined independently within each bidding zone. A bidding zone is defined as the largest geographical area in which bids and offers can be matched without the need to allocate cross-zonal transmission capacity. In Europe, bidding zones generally coincide with national borders [53].

Electricity trading in the wholesale market occurs primarily through two structured stages: the Day-Ahead Market (DAM) and the Intraday Market (IDM). In the Day-Ahead Market, participants submit bids for electricity delivery on the following day. While bids were historically based on hourly trading intervals, since 30 September 2025 the DAM has transitioned to 15-minute intervals to better reflect expected generation and demand patterns. Prices are fixed 24 hours in advance. In the DAM, generators specify the amount of electricity they can produce and the minimum price they are willing to accept, while buyers indicate the quantity they wish to purchase and their maximum acceptable price. The market operator then matches supply and demand, determining the clearing price for each trading period of the next day.

To mitigate discrepancies between forecasted and actual conditions, the Intraday Market allows participants to adjust their positions closer to real time. Such discrepancies may arise from unexpected changes in supply, for example due to weather-driven variations in renewable generation, or fluctuations in demand. The IDM comprises both discrete auction sessions and continuous trading, allowing a more accurate alignment between scheduled production and real-time system needs. This enhances system flexibility and

reduces the need for costly balancing interventions by the TSO.

Beyond the DAM and IDM, the Balancing Market plays a crucial role in maintaining real-time equilibrium between electricity supply and demand. This market enables the TSO to procure additional flexibility resources necessary to address unforeseen deviations and ensure system security. Complementing these is the Ancillary Services Market, which is essential for guaranteeing the stable and reliable operation of the power grid. Coordinated by national TSOs, this market procures services such as frequency regulation, voltage control, congestion management and operating reserves. These services are provided by generation units and, increasingly, by demand-side resources and storage systems that meet specific technical and operational requirements.

2.6.1. The Italian case

In Italy, the electricity market framework relies on two key entities: Terna and the Gestore dei Mercati Energetici (GME).

Terna, the national Transmission System Operator, is responsible for the secure and reliable operation of the electrical grid. It manages electricity flows, system balancing, and power plant dispatching while ensuring compliance with technical and safety constraints. Terna also oversees the Ancillary Services Market, which procures frequency regulation, voltage control, congestion management and reserve capacity to ensure system stability.

GME operates the electricity markets where energy is traded, including the Day-Ahead Market, the Intraday Market and the Balancing Market. It manages market platforms, clearing operations and ensures transparent and efficient price formation through auctions and continuous trading.

Unlike most European countries, which typically operate under a single bidding zone, Italy is divided into seven bidding zones. This structure reflects the country's geographical complexity and the need to differentiate electricity prices based on the local balance between generation and demand. Bidding zones are not static and may evolve over time. In Italy, the current configuration entered into force on 1 January 2021, following a multi-year review that led to the transition from six to seven zones (Figure 2.15).

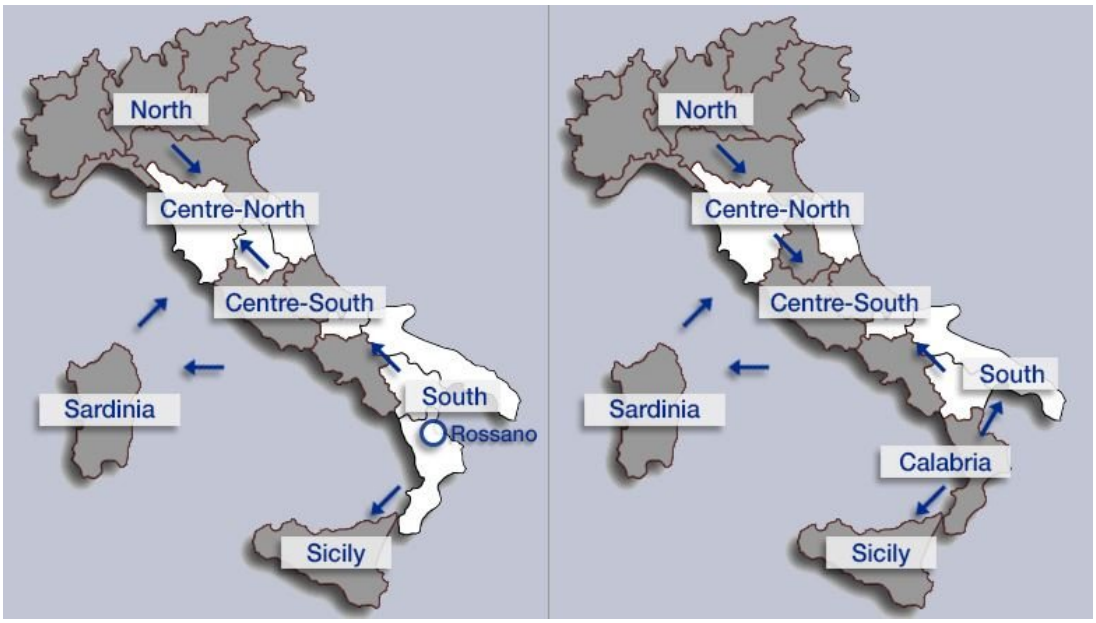


Figure 2.15: Evolution of the Italian electricity market bidding zone configuration, showing the transition from six to seven zones [54].

Each bidding zone has its own clearing price used to compensate generators. However, end users pay a uniform national electricity price known as the Prezzo Unico Nazionale (PUN). The PUN is calculated as the weighted average of the zonal clearing prices, where the weights correspond to the volumes of electricity purchased in each zone.

The PUN exhibits notable variability across both the day and the year, reflecting fluctuations in supply and demand. During daytime hours, electricity demand, and consequently the PUN, is typically higher due to the activity of commercial, office and industrial facilities. At night (and during weekends), demand decreases significantly.

From the supply side, photovoltaic generation reaches its peak around midday. Since solar energy has near-zero marginal cost, its presence tends to lower the clearing price, and therefore the PUN, during these hours. The interaction between demand patterns and renewable generation shapes the characteristic daily PUN profile, as shown in Figure 2.16.

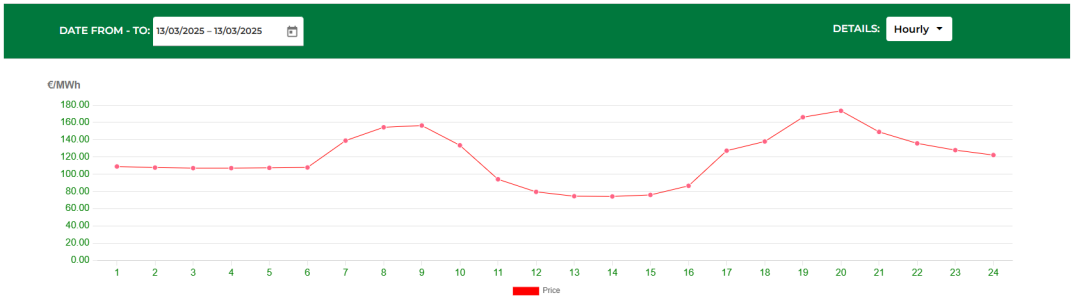


Figure 2.16: Typical daily fluctuation of the Italian PUN [55].

Seasonal fluctuations are also evident. Electricity demand generally increases during summer and winter due to air conditioning and heating needs, while spring and autumn typically exhibit lower and more stable consumption levels.

Seasonality influences not only demand but also supply. In spring and especially in summer, longer daylight hours and stronger solar radiation enhance photovoltaic production, contributing to lower PUN values. Conversely, reduced solar availability in autumn and winter increases reliance on more expensive generation sources, resulting in higher prices. The combined effect of supply and demand fluctuations typically results in two annual price peaks: one in winter and one in summer. The winter peak is generally higher, as electricity demand is elevated and supply often depends on costlier generation sources. A typical monthly trend is illustrated in Figure 2.17.

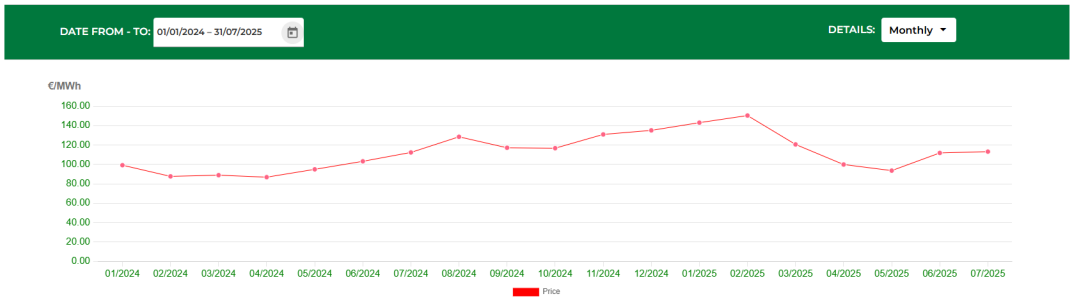


Figure 2.17: Typical monthly trend of the Italian PUN [55].

The PUN is strongly influenced by the price of primary energy sources, particularly natural gas. Natural gas often acts as the marginal price setter in the electricity market, since gas-fired power plants are typically the last units dispatched to meet demand. In the second half of 2021, Europe faced an energy crisis marked by a sharp rise in natural gas prices, which in turn caused a substantial increase in electricity prices. This surge

was driven by a rapid rebound in global energy demand following the post-COVID-19 economic recovery, combined with supply constraints that were unable to keep pace with the growing demand [56].

The situation further deteriorated in February 2022, when Russia, Europe's main supplier of natural gas, launched its military invasion of Ukraine. This geopolitical shock exacerbated the ongoing energy crisis, triggering an even more pronounced escalation in energy prices. As a consequence, the PUN reached an unprecedented monthly average of over 500 €/MWh in August 2022. Throughout the first year of the conflict, the annual average PUN remained above 300 €/MWh, a value nearly eight times higher than the average recorded in 2020 (Figure 2.18).

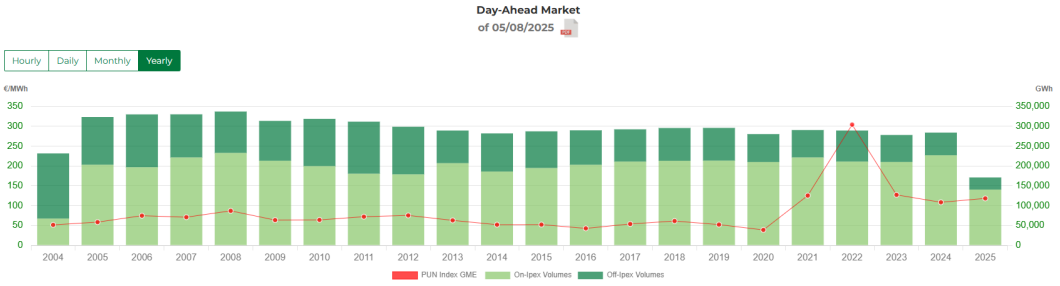


Figure 2.18: Historical trend of the Italian PUN, 2004-2025 [55].

As previously noted, the PUN serves as the reference price in the wholesale electricity market; however, it also has a significant impact on the retail market, where many supply contracts are indexed to it either directly or through time-of-use tariffs. In Italy, supply contracts for small enterprises are typically structured according to the three time bands defined by ARERA (Autorità di Regolazione per Energia Reti e Ambiente):

- **F1**: Monday to Friday, from 8:00 AM to 7:00 PM, excluding national holidays.
- **F2**: Monday to Friday, from 7:00 AM to 8:00 AM and from 7:00 PM to 11:00 PM, excluding national holidays; Saturday from 7:00 AM to 11:00 PM, excluding national holidays.
- **F3**: Monday to Saturday, from 12:00 AM to 7:00 AM and from 11:00 PM to 12:00 AM; all hours on Sundays and national holidays.

These time bands reflect typical patterns of electricity demand and are designed to incentivize shifting consumption toward less critical periods for the electrical system, thereby improving overall efficiency and helping maintain grid stability. In a typical supply con-

tract based on these time bands, the customer pays according to the amount of energy consumed in each band, with the price for each band indexed to the monthly average PUN published by GME. In addition to the energy component, the contract between the supplier and the customer includes several regulated charges that apply uniformly across all supply agreements. These include transmission and metering costs, system charges, and taxes, all defined by ARERA [57].

2.7. Key insights and research gaps from the literature review

In the previous sections of Chapter 2, the state of the art in battery management modeling has been presented, with a focus on both technical aspects and practical implementation in real-world applications. In addition to topics directly related to battery aging modeling, the discussion also addressed electricity markets and battery balancing systems, in order to provide a comprehensive overview of all relevant components of this complex framework. This thorough analysis establishes the necessary background to identify existing research gaps and to justify the relevance of the present thesis. Based on this review, several important considerations can be drawn.

The first consideration that emerges from the analyzed literature is that an accurate battery aging model must account for both cycling aging and calendar aging. Neglecting either component leads to incomplete and potentially inaccurate results, limiting the model's applicability to real BEB systems, where batteries undergo frequent cycling during operation and prolonged resting periods, particularly overnight while parked in the depot. Indeed, not all reviewed aging models include calendar aging; however, those that do provide strong justification for its inclusion, supported by technical references and relevant studies that highlight its significant contribution to overall battery degradation.

Another important consideration is that, when analyzing an electric bus scheduling problem, the primary objective should be the reduction of total system costs. These costs should include charging costs, namely the expenses associated with energy consumption during charging, and battery aging costs, which account for the degradation of the battery over time. It is also appropriate to include capital expenditures, such as those related to buses and charging infrastructure, whenever the evaluated charging strategies influence the required number or type of assets. Finally, the system boundaries should consider the residual value of the equipment, including batteries, since this value can be significantly

affected by how the assets are used and managed throughout their lifetime.

A further issue observed in many battery aging models and their applications is the intrinsic limitation of representing situations in which an electric vehicle does not follow a constant charging-discharging pattern. This makes several models purely theoretical and unsuitable for real-life scenarios. In a BEB system, a vehicle typically operates on multiple routes over its lifetime, each characterized by different DoD levels, SoC ranges, and subsequent resting periods. Therefore, a battery aging model should be able to account for a combination of cycling patterns, rest periods at different SoC levels, and partial-charging conditions. Incorporating these aspects is essential to bridge the gap between theoretical models and practical, real-world applications.

Finally, an interesting insight emerging from the literature review is that, although many relevant studies describe how cell balancing should be performed and emphasize its importance in preventing battery failures, extending battery lifetime, and ensuring safe operation, the battery aging models found in the literature and their applications in the EBSP framework generally do not account for cell-balancing constraints. In some cases, they even propose charging strategies that are incompatible with the balancing requirements of BEBs. For example, several studies suggest limiting the SoC range without considering that the passive balancing systems adopted in many electric vehicles cannot be activated if charging is consistently interrupted before reaching high SoC levels. For this reason, the model developed in this thesis also aims to address this limitation by incorporating periodic balancing events into the operational charging scheme.

3 | Model presentation

As discussed in Chapter 2, numerous models have been proposed in the literature to estimate the SoH evolution of Li-ion batteries under different operating conditions. Since battery degradation is strongly affected by operating conditions, and different chemistries respond differently to these conditions, each chemistry requires a tailored modeling approach. In particular, this thesis focuses on NMC chemistry, as it is currently the technology adopted by many European bus manufacturers for the electric buses available on the market. The aim of this thesis is not to develop an entirely new aging model from scratch, as doing so would require a dedicated battery testing campaign on a representative set of cells. Instead, the focus lies on the practical application of existing aging models under real operating conditions. For this reason, an established model from the literature was selected as a starting point, calibrated to better reflect current battery technologies, and subsequently developed into a practical tool suitable for real-world operations typically observed in Public Transport Operator services. This tool was developed in parallel with a charging scheduling tool. Together, these two components provide the necessary inputs for an economic evaluation, enabling the assessment of the financial implications of various battery management and charging strategies. The overall workflow and interactions among the models implemented in this work are illustrated in Figure 3.1.

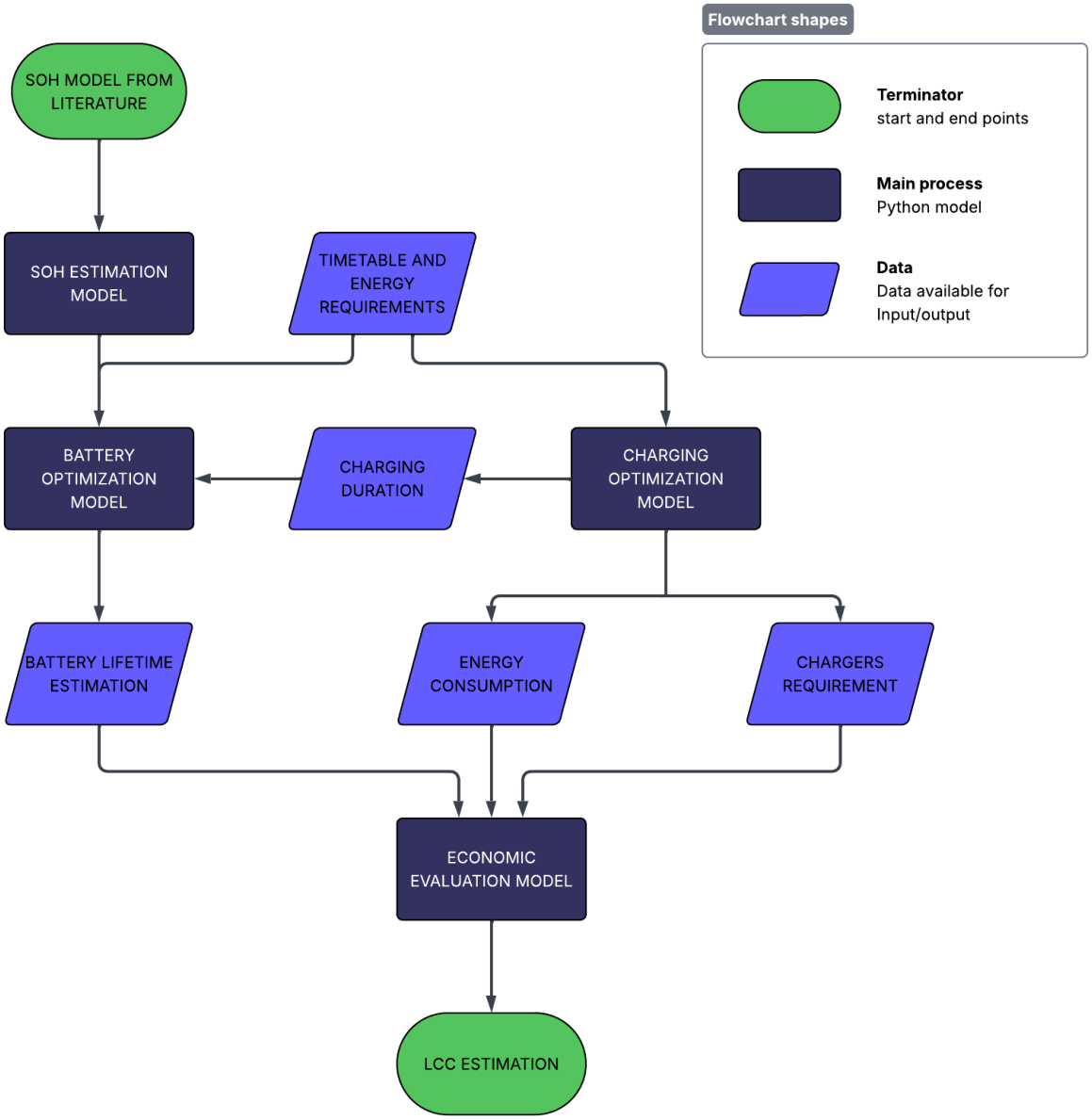


Figure 3.1: Workflow of the models implemented in this thesis.

3.1. SoH Estimation Model

Among the various aging models available in the literature, a well-established one for NMC Li-ion batteries is the holistic aging model proposed in [36], which accounts for both cycling and calendar aging. The model explicitly incorporates dependencies on temperature, average voltage, and DoD, and is based on empirical fitting of extensive accelerated aging tests conducted on commercial NMC 18650 cells. In this model, the total aging function is obtained by superimposing the calendar and cycling aging components.

This results in a formulation capable of computing the capacity evolution over time, and therefore the battery SoH, under fixed cycling and resting conditions. The mathematical formulation is reported in Equation 3.1.

$$C = 1 - \alpha_{\text{cap}} \cdot t^{0.75} - \beta_{\text{cap}} \cdot \sqrt{Q} \tag{3.1}$$

In Equation 3.1, the calendar component is expressed through the Arrhenius law, with α_{cap} being the calendar aging coefficient defined as reported in Equation 3.2:

$$\alpha_{\text{cap}} = (7.534 \cdot V - 23.75) \cdot 10^6 \, e^{-\frac{6976}{T}} \tag{3.2}$$

where V is the storage voltage and T is the absolute temperature in Kelvin. The cumulative resting time is denoted by t, expressed in days.

The cycling component is based on a square root function, with β_{cap} being the cycling aging coefficient, which depends on the mean voltage during cycling $\overline{V}$ and the DoD for each cycle, as defined in Equation 3.3:

$$\beta_{\text{cap}} = 7.348 \cdot 10^{-3} \cdot (\overline{V} - 3.667)^2 - 7.600 \cdot 10^{-4} + 4.081 \cdot 10^{-3} \cdot \text{DoD} \tag{3.3}$$

The cumulative charge throughput Q, expressed in ampere-hours, represents the total amount of charge that has flowed through the battery over its lifetime and can be related to the number of Full Equivalent Cycles and the cell nominal capacity C_{cell}, as defined in Equation 3.4:

$$Q = \text{FEC} \cdot C_{\text{cell}} \tag{3.4}$$

However, since the model was originally developed for small cylindrical NMC cells, which differ from the battery technology currently used in electric buses, it needs to be recalibrated to better represent the state of the art of current NMC battery technology, both in terms of capacity and expected lifespan.

3.1.1. Model calibration

As mentioned in the previous section, it is important to note that the original aging model was developed for small cylindrical NMC cells with a nominal capacity of 2.15 Ah, whereas

modern electric buses typically employ large-format pouch cells with capacities ranging approximately from 50 Ah to 70 Ah. Without proper calibration, applying the original model to these larger cells would lead to misleading results, as the charge throughput of a single cycle would be overweighted.

To address this issue, a capacity calibration coefficient, c_{cal} , has been introduced. This coefficient is defined as the ratio between the nominal capacity of the reference cell used in the original model and the capacity of the target cell, as shown in Equation 3.5:

$$c_{\text{cal}} = \frac{2.15\,\text{Ah}}{C_{\text{cell}}} \tag{3.5}$$

By applying this empirical correction, the contribution of one FEC is normalized across cells of different capacities. This enables the original model to be reliably adapted for larger cells currently used in electric buses, preserving the consistency of degradation predictions while maintaining the underlying structure of the original formulation. A second calibration step is required because the model was originally developed using an earlier generation of cells, which were capable of sustaining only a limited number of cycles before reaching their EoL. Owing to the technological advances achieved in recent years, modern Li-ion batteries exhibit a substantially higher lifetime expectancy. Without this additional calibration, the lifetime predicted by the model would be significantly underestimated when compared with the actual performance of current battery technologies. To perform this calibration, a representative battery pack must be selected as a benchmark. In this work, the ZEN 42 battery pack produced by Forsee Power has been chosen (Figure 3.2), as it reflects the state of the art for NMC battery systems employed in electric buses. The ZEN 42 pack consists of multiple NMC pouch cells with a nominal capacity of 66 Ah each, providing a total energy capacity of 42.5 kWh per pack. According to the manufacturer, the nominal useful life of the ZEN 42 pack is eight years.



Figure 3.2: ZEN 42 battery pack [58].

For the purposes of modeling battery aging, however, it is more meaningful to express battery lifetime in terms of Full Equivalent Cycles rather than calendar years. Since the manufacturer does not disclose detailed operational data, such as the expected annual cycling profile or typical DoD, reasonable assumptions are adopted to convert the nominal eight-year lifetime into an equivalent number of FECs. Specifically, it is assumed that the battery undergoes 300 cycles per year at an 80% DoD, which is representative of typical operating conditions for electric buses in daily service.

Additionally, a daily inactive period of 12 hours is considered, during which the battery is maintained at an average State of Charge of 50% and a temperature of 298 K. To account for rest days, maintenance stops, and other non-operational periods, an additional 65 full idle days per year are included under the same conditions.

Following widespread practice in both scientific literature and industry standards, a battery is considered to have reached its EoL when its SoH decreases to 80%, corresponding to a remaining usable capacity equal to 80% of its nominal value. This threshold is adopted in the present work as the reference criterion for EoL determination.

Under the assumptions outlined above, the total number of Full Equivalent Cycles required to reach EoL can be estimated using Equation 3.6:

$$\mathrm{FEC}_{\mathrm{EoL}} = N_{\mathrm{cycles,year}} \cdot N_{\mathrm{years}} \cdot \mathrm{DoD} \tag{3.6}$$

Applying this formula, the ZEN 42 battery pack is estimated to reach its EoL after approximately 1920 Full Equivalent Cycles. Starting from Equation 3.1, it is therefore possible to compute the calibration factor required to ensure that the model predicts an EoL at exactly 1920 FECs under the assumed operating conditions. For simplicity, in the next sections the ZEN 42 pack is considered representative of the current technological state of the art, leading to a fixed calibration factor of γ=0.589. This fixed value provides a practical coefficient that can be applied to different batteries without requiring repeated recalibration.

Nevertheless, if a more tailored estimation is required for a specific battery system, the user may compute the coefficient using the following Equation 3.7:

$$\gamma = \frac{1 - \mathrm{SoH_{EoL}}}{\beta_{\mathrm{cap}}(\overline{V}, \mathrm{DoD}) \cdot \sqrt{c_{\mathrm{cal}} \cdot \mathrm{FEC_{EoL}} \cdot C_{\mathrm{cell}}} + \alpha_{\mathrm{cap}}(V, T) \cdot t^{0.75}} \tag{3.7}$$

In Equation 3.7, t denotes the cumulative resting time, including both the idle periods between cycles and the additional inactive days associated with maintenance or other operational interruptions.

By applying both the capacity calibration coefficient c_{cal} and the scaling factor γ to the mathematical formulation of the original model (reported in Equation 3.1), an updated and fully calibrated degradation model is obtained. This revised formulation enables the simulation of capacity fade under various cycling conditions for modern NMC batteries. The resulting expression is given in Equation 3.8:

$$C = 1 - \gamma \left(\alpha_{\mathrm{cap}} \cdot t^{0.75} + \beta_{\mathrm{cap}} \cdot \sqrt{c_{\mathrm{cal}} \cdot Q} \right) \tag{3.8}$$

This calibrated model retains the original parametric structure and physical dependencies, while being adapted to accurately reflect the aging behavior of modern NMC batteries with different capacities. It enables consistent and realistic estimation of battery degradation across a wide range of operational scenarios.

3.1.2. Model application and simulation results

To further explore the implications of the calibration model, a Python-based simulation environment has been developed. The cycling and calendar aging components have been analyzed independently in order to better understand and visualize their respective ef-

fects on battery health. This approach allows a clear separation of the mechanisms driving degradation, enabling targeted analysis and interpretation of the results.

In the first set of simulations, the cycling component was examined while the calendar aging contribution was neglected. Different combinations of DoD and average SoC were simulated. For each scenario, the evolution of the SoH was computed as a function of FEC, and the results were visualized through degradation curves. These plots provide a clear and intuitive representation of how usage patterns affect the battery's usable life.

In each graph, the point at which the SoH reaches the EoL threshold, defined as 80% of the nominal capacity, is automatically identified and marked. The corresponding FEC value is displayed in a label box to enhance readability and facilitate comparisons. This graphical approach highlights how battery lifetime responds to variations in both DoD and average SoC.

The cycling aging simulation results are shown in Figures 3.3 - 3.4 - 3.5, which report the degradation curves for DoD values of 80% (Figure 3.3), 60% (Figure 3.4), and 40% (Figure 3.5). Each plot includes multiple curves corresponding to different average SoC values.

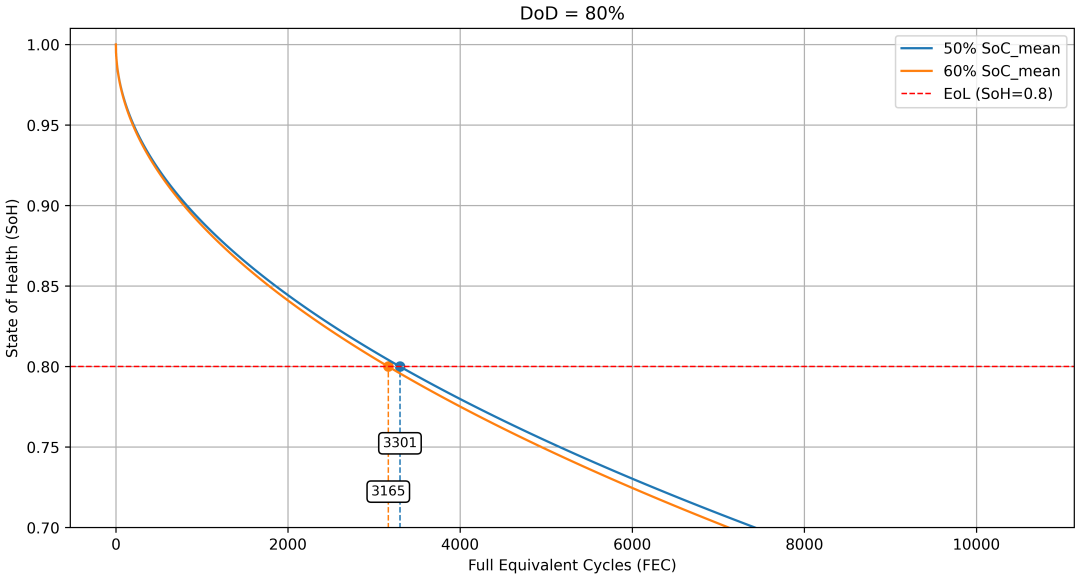


Figure 3.3: Capacity degradation curves due to cycling aging, as predicted by the calibrated aging model, for different mean SoC values under an 80% DoD cycling condition.

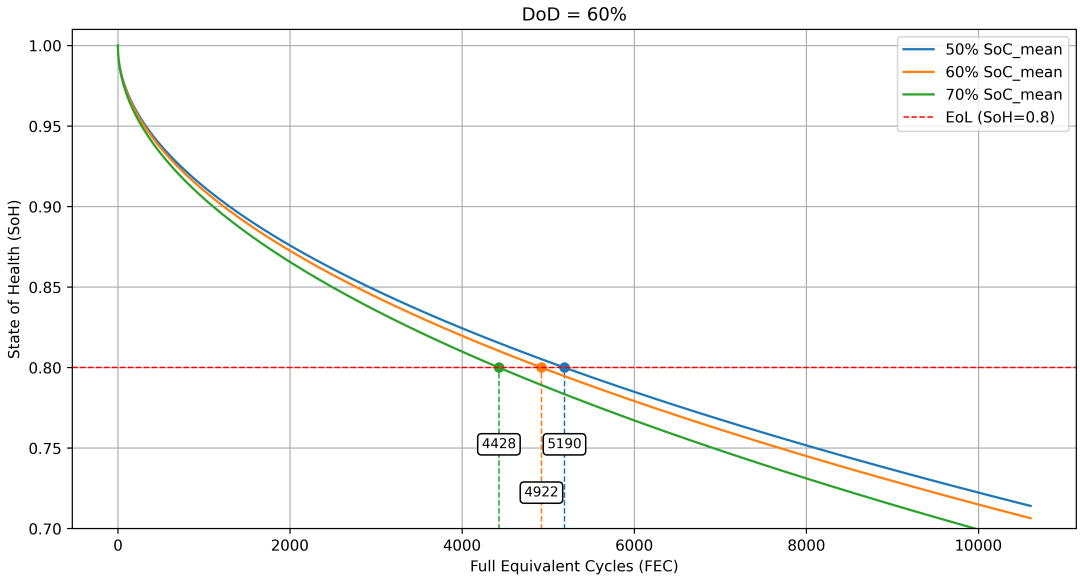


Figure 3.4: Capacity degradation curves due to cycling aging, as predicted by the calibrated aging model, for different mean SoC values under an 60% DoD cycling condition.

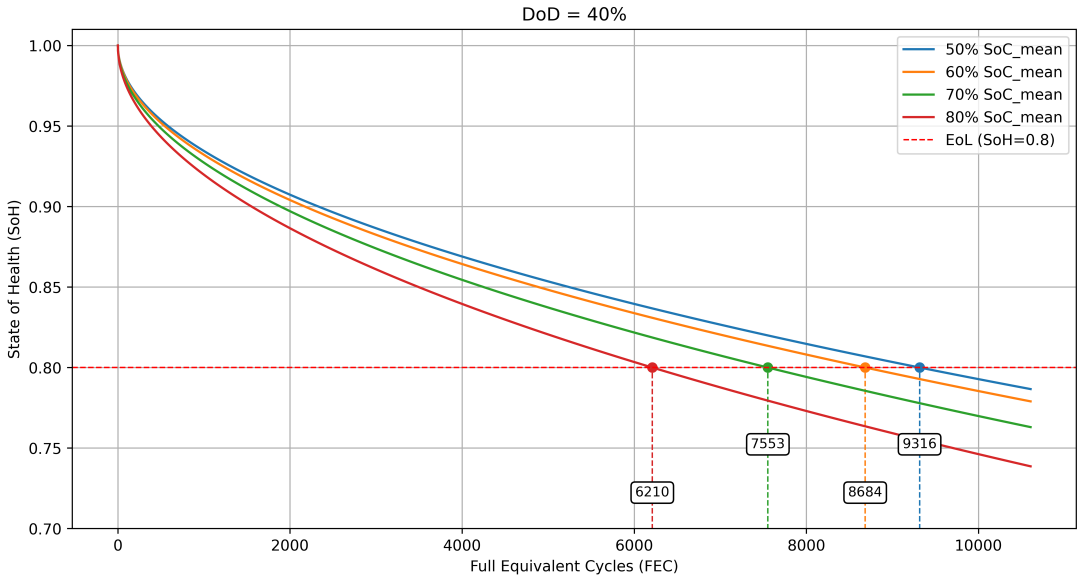


Figure 3.5: Capacity degradation curves due to cycling aging, as predicted by the calibrated aging model, for different mean SoC values under an 40% DoD cycling condition.

By analyzing the obtained plots, the following observations can be made:

- Figure 3.3 (DoD = 80%): degradation proceeds rapidly, with the EoL typically reached around 3000 FEC, consistent across all simulated profiles.
- Figure 3.4 (DoD = 60%): degradation is slower, resulting in a noticeable increase in lifetime across all curves.
- Figure 3.5 (DoD = 40%): all profiles exhibit significantly extended lifespans, and the influence of average SoC becomes more prominent; the FEC required to reach the EoL ranges from 6210 (at 80% average SoC) to 9316 (at 50% average SoC).

These results highlight the critical influence of both DoD and average SoC on battery aging. The degradation curves clearly demonstrate how operational strategies directly affect battery longevity: by reducing the Depth of Discharge and maintaining moderate average SoC levels, the usable lifetime of NMC Li-ion batteries can be significantly extended.

In a second set of simulations, the calendar contribution to battery aging has been analyzed, with the effects of cycling degradation neglected. In the adopted model, calendar aging is driven primarily by two parameters: the storage temperature and the State of Charge at which the battery is stored. To better quantify their individual impact, these two factors were investigated separately.

In the first simulation, the storage SoC was fixed at 80%, and the effect of temperature was evaluated for values ranging from 15 °C to 35 °C. In the second simulation, the temperature was fixed at 25 °C, while the storage SoC was varied between 20% and 100%. The results of the two analyses are presented in Figure 3.6 and Figure 3.7, respectively. As in the previous section, each graph automatically identifies and marks the point at which the SoH reaches the EoL threshold, with the corresponding idle time (expressed in years) displayed in a label box to improve readability and facilitate direct comparisons across scenarios.

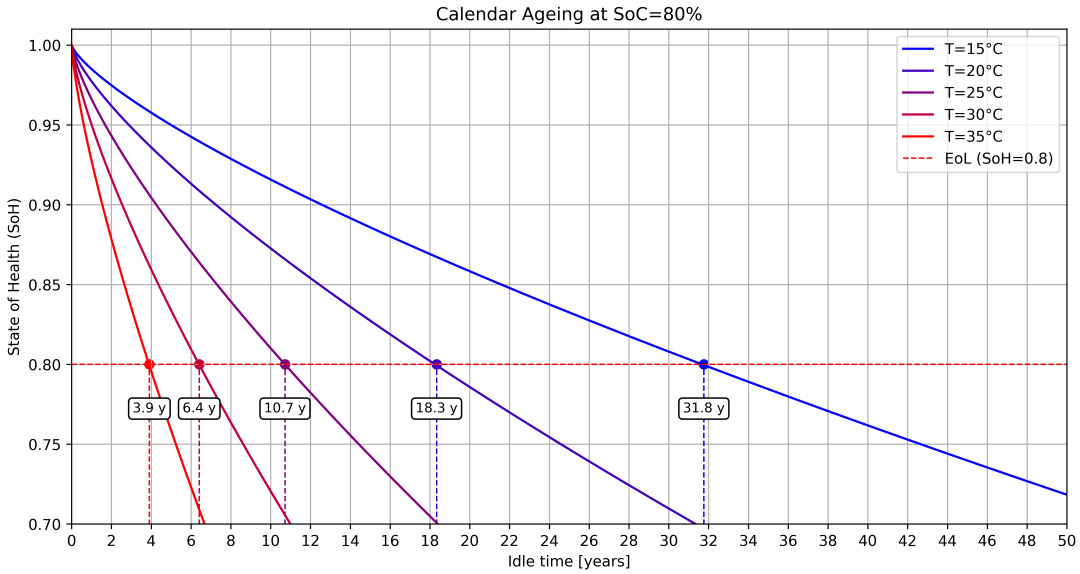


Figure 3.6: Capacity degradation curves due to calendar aging, as predicted by the calibrated aging model, for different storage temperatures at a fixed storage SoC of 80%.

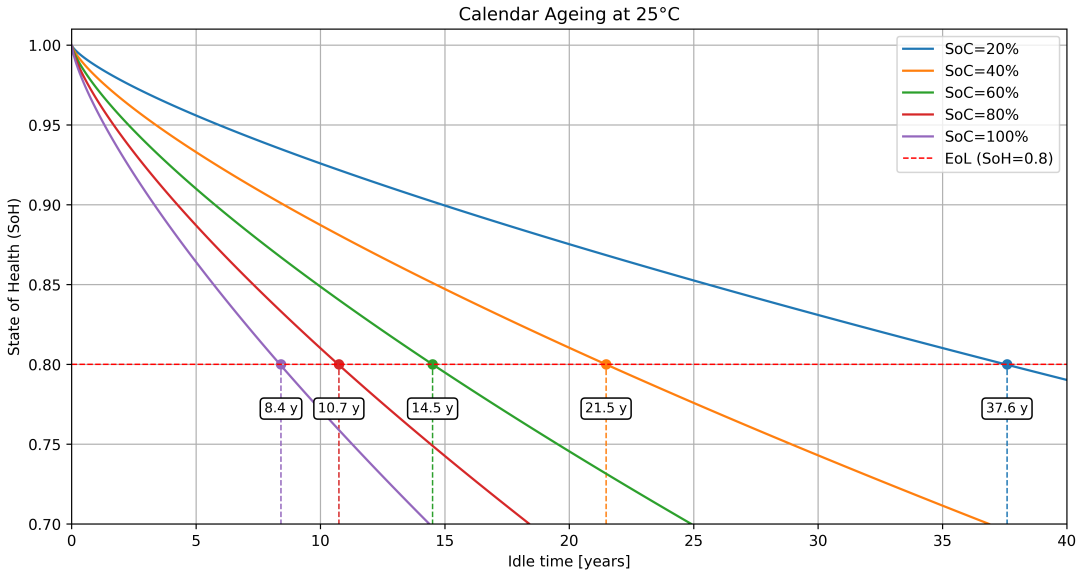


Figure 3.7: Capacity degradation curves due to calendar aging, as predicted by the calibrated aging model, for different storage SoC values at a fixed storage temperature of 25 °C.

The influence of storage temperature, shown in Figure 3.6, is particularly pronounced: even modest temperature increases lead to a significant acceleration of degradation. Batteries stored at 35 °C reach the EoL threshold more than eight times faster than those stored at 15 °C, confirming the strong thermal sensitivity of calendar aging mechanisms.

Figure 3.7 illustrates instead the effect of storage SoC. A clear trend emerges, with higher storage SoC levels resulting in substantially faster capacity loss. In particular, batteries stored at 100% SoC reach the EoL threshold more than four times faster than those maintained at 20% SoC, highlighting the detrimental impact of elevated voltage conditions during idle periods.

Overall, the results of the calendar aging simulations underscore the critical role of storage conditions in determining long-term battery durability. Reducing either the storage temperature or the storage SoC can extend the calendar life of NMC Li-ion batteries by several years. These findings highlight the importance of adopting optimized storage strategies, especially during prolonged inactivity or maintenance, in order to preserve battery health and maximize lifetime.

3.2. Battery Optimization Model

In the previous section, a model to estimate the SoH evolution of NMC batteries has been presented. The model has been developed starting from an existing aging formulation; in particular, the original model has been updated and calibrated to reflect current battery technologies. However, the presented model retains some of the limitations highlighted in Chapter 2.

The main limitation lies in its static nature. Once the degradation coefficients α (for calendar aging) and β (for cycling aging) are determined, the model can only generate a single SoH decay curve corresponding to the specific operating and resting conditions under which those coefficients have been computed. In other words, it implicitly assumes that the electric vehicle operates under constant charge–discharge cycling (with fixed DoD and average SoC) and that, during every idle period, the battery remains under identical resting conditions (same SoC and temperature) throughout its entire lifetime.

Such a static representation is unrealistic and does not adequately describe the complexity of real-world applications, such as electric bus operations, in which a battery is subjected to heterogeneous daily cycles characterized by varying energy demands and, when parked, experiences resting conditions that are far from constant.

This discrepancy between the mathematical model and real operating conditions highlights the need for a modeling approach capable of capturing dynamic and variable oper-

ating profiles.

3.2.1. A simulation-based approach for realistic battery management

In real-world applications, it is uncommon for a bus to follow the same daily schedule every day. Instead, buses typically alternate between different assigned routes (or "shifts") according to a repetitive sequence. For example, a bus may operate shift A on one day, shift B on the next one, and so on, cycling through a predefined set of shifts. Likewise, it is often possible to define a pool of buses that are rotated across a set of shifts, so that the workload is evenly distributed among all vehicles.

Each shift has its own characteristics in terms of energy consumption; consequently, the battery is subjected to different stress conditions, and the evolution of its SoH cannot be represented by a single degradation curve. Capturing this variability requires more than a static mathematical formulation. For this reason, a Python-based simulation tool has been developed.

This tool provides a ready-to-use platform that allows the user to estimate the expected battery lifetime of a bus operating under realistic cycling and resting profiles. It takes as input the shift-rotation schedule, along with the duration and energy demand of each shift, and returns as output not only the number of days until EoL, but also a graphical representation of the SoC profile and the evolution of the battery's SoH over time. In this way, the tool enables an accurate and flexible simulation of real operational conditions.

This tool is able to realistically reproduce operational conditions and simulate the SoH evolution over time, because it is not based solely on the continuous repetition of shifts and rest periods. Instead, it also incorporates periodic phenomena that commonly occur in real-life operations, such as rest days, annual maintenance downtime and battery-balancing events. With regard to battery balancing, the model explicitly accounts for the need to periodically equalize cell voltages to prevent the development of dangerous imbalances. If not properly managed, such imbalances may lead to accelerated degradation, sudden failures, or even unsafe operating conditions. To address this, the model enforces a mandatory full charge up to 100% SoC every 15 days. This periodic charging event enables passive cell balancing, ensuring a more uniform voltage distribution across the cells.

By integrating this mechanism, the model incorporates a crucial operational best practice that is often overlooked in theoretical studies and charging-optimization frameworks, thereby improving both the realism and reliability of the simulated battery behavior.

To represent the relationship between SoC and voltage, some assumptions were made based on the OCV–SoC curve presented by the authors in [30]. In particular, it was observed that the relationship between SoC and voltage cannot be considered strictly linear. However, the curve exhibits an approximately linear behavior in two distinct ranges: between 20% and 50% SoC, and between 50% and 100% SoC. Therefore, the overall OCV-SoC curve can be accurately approximated using two linear functions.

For the range between 20% and 50% SoC, the voltage can be computed using Equation 3.9:

$$V = 3.6 + \frac{1}{3}\,(\mathrm{SoC} - 0.2) \tag{3.9}$$

For the range between 50% and 100% SoC, the voltage can be computed using Formula 3.10:

$$V = 3.7 + 0.8\,(\mathrm{SoC} - 0.5) \tag{3.10}$$

The region between 0% and 20% SoC has not been modeled, as this range is considered a safety margin; the battery will not operate within 0%-20% SoC during the simulations. This piecewise linear approximation enables the model to capture the essential behavior of the cell voltage with sufficient accuracy while keeping the calculations simple and computationally efficient.

It should be noted that, due to its static nature, the SoH Estimation Model (Equation 3.8) is non-additive. Both t (cumulative idle time) and Q (cumulative charge throughput) accumulate over the battery's lifetime, and the non-linear dependencies in the model ($t^{0.75}$ and $\sqrt{Q}$) prevent simply summing daily degradation values. Consequently, the degradation occurring on any given day cannot be calculated independently and added to previous days; instead, each day's effect must be incorporated into the cumulative totals, as the SoH depends on the entire usage and idle history.

This intrinsic characteristic of the model makes it unsuitable for situations in which buses

are rotated across a set of assigned shifts with different operational characteristics, such as varying DoD and average SoC, rather than experiencing the same conditions every day (and thus the same α and β). If a bus completes a shift with different characteristics from the previous day, the α and β parameters change, meaning t and Q cannot simply be added to the cumulative values of the previous day. Doing so would be physically inconsistent and could even lead to unrealistic SoH fluctuations.

To overcome this issue and make the mathematical model suitable for real-life simulations, the Python-based simulation tool recalculates equivalent values of Q and t, referred to as $Q_{equivalent}$ and $t_{equivalent}$, whenever the α and/or β parameters change. These dummy values allow the simulation to continue from the same degradation state under the new parameters. In this way, each degradation phase starts from the SoH reached at the end of the previous phase, ensuring a physically consistent evolution of the battery's health.

To enable the analysis of different charging and operation strategies, the simulation tool offers flexible charging and operation settings. The user can decide whether charging is performed at the beginning or at the end of each resting period by simply adjusting a parameter. When the charging mode is set to "start", the vehicle is assumed to be charged immediately upon arrival at the depot. Conversely, when the mode is set to "end", charging is scheduled to be completed just before the start of the next operating shift.

In the latter case, charging time must be planned more carefully and conservatively, since in the "start" mode the bus often remains parked for several hours after charging is completed, whereas in the "end" mode the vehicle is used immediately after the designated charging slot. This difference can significantly influence the operational flexibility, as the timing of charging affects how readily buses are available for service.

Another parameter allows the user to define how the bus's daily shifts are handled in terms of charging. This parameter, a Boolean operator named *grouped* determines whether all shifts covered by a bus in a single day should be treated as a single, overall discharge cycle or considered independently. If *grouped* is set to True, all shifts are combined into a single daily cycle with a higher DoD, and charging is performed only at the end of the day, following an "overnight" charging strategy. Conversely, if *grouped* is set to False, each shift is treated individually, allowing multiple charging and discharging events within the same day. This approach reduces the DoD of each cycle and distributes the charging across multiple depot slots.

The Python-based simulation tool also includes a dedicated function to optimize the starting SoC for each shift, named optimize_soc_start. The aim of this function is to determine, for each cycle and the subsequent rest period, the optimal initial SoC that minimizes battery degradation due to both cycling and calendar aging. This is particularly relevant because, as demonstrated in Chapter 2, cycling degradation is minimized when the average SoC is around 50%, whereas lower SoC levels tend to prolong battery life from the perspective of calendar aging. Therefore, identifying the SoC profile that balances these two effects is not straightforward.

The function works by simulating the expected battery life for all possible starting SoC values permitted by the DoD of the considered cycle and selecting the value that maximizes the number of days until the battery reaches its EoL. A key feature of the function is the inclusion of a minimum SoC threshold, which can be set by the user. This threshold prevents the battery from reaching extremely low SoC levels, thereby bridging the gap between the theoretical model and real-life operation.

Indeed, while the mathematical model suggests that calendar aging is minimized at very low SoC values, potentially approaching 0%, such conditions are impractical and potentially dangerous in real-world operation. Extremely low SoC values increase the risk of irreversible damage due to self-discharge, which can cause the cell voltage to fall below the cut-off voltage. Moreover, setting the minimum SoC too low can lead to operational issues: if the actual energy demand during a cycle exceeds the planned consumption, the battery may not contain enough energy to complete the shift. For this reason, and to mitigate both safety risks and range anxiety, the default minimum SoC threshold is set to 20%, while still allowing the user to adjust it according to operational requirements.

In the Python script, five different simulation scenarios are implemented. The first scenario represents the reference case, which reflects a typical operational profile commonly adopted by transport operators without any form of optimization. The remaining four scenarios correspond to alternative charging strategies that could be implemented with varying levels of complexity and feasibility in real-world operations. The details of each scenario are reported below:

- **Base scenario**: in this scenario, the battery of each bus is fully recharged to 100% SoC at the end of every daily shift. As a result, the cycling profile is characterized by a high DoD and a high average SoC, while the calendar aging component is associated with resting periods at maximum SoC.

- **Start scenario**: in this scenario, the charging process is still performed at the end of the day, however, the battery is not fully recharged. Instead, it is charged only up to the optimal starting SoC computed by the SoC optimization algorithm for the following day. This strategy allows daily operation to begin from a SoC level that minimizes overall battery degradation. As a result, the cycling profile is characterized by a high DoD and a moderate average SoC, while the calendar aging component is associated with resting periods at the optimized starting SoC.
- **End scenario**: this scenario is similar to the previous one, with the only difference being that the charging process is postponed to finish just before the start of the following operational day. As a result, the cycling profile continues to be characterized by a high DoD and a moderate average SoC, but the calendar aging component is now associated with resting periods at low SoC.
- **Start-Split scenario**: in this scenario, the charging process is performed after each individual shift. During these depot periods, the battery is charged up to the SoC required for the next shift, as determined by the SoC optimization algorithm. As a result, the cycling profile is characterized by a lower DoD and a moderate average SoC. The calendar aging component is associated with resting periods at the optimized starting SoC, which are generally lower than those in the Start scenario, since the shifts are not grouped and the energy required for each is lower.
- **End-Split scenario**: this scenario is similar to the Start-Split scenario, with the only difference being that the charging process is postponed to finish just before the start of the subsequent shift. As a result, the cycling profile remains characterized by a low DoD and a moderate average SoC, but the calendar aging component is now associated with resting periods at low SoC.

These five scenarios provide a comprehensive framework to evaluate the impact of different charging strategies on both cycling and calendar aging. By progressively introducing charging time shifts and SoC optimization, they enable a direct comparison between a standard operational practices and more advanced approaches, allowing to quantify potential improvements in battery lifetime and overall system efficiency.

To summarize the main characteristics of each charging strategy, Table 3.1 provides an overview of the optimization elements implemented in each scenario. The three considered aspects are:

- **SoC optimization**: which refers to the application of the SoC optimization algorithm to determine the optimal SoC start.

- **DoD reduction**: which refers to the splitting of the required energy into multiple charging events.
- **Delayed charge**: which indicates that the charging process is postponed to finish just before the next operational period.

Scenario	SoC Optimization	DoD Reduction	Delayed Charge
BASE SCENARIO	×	×	×
START SCENARIO	✓	×	×
END SCENARIO	✓	×	✓
START-SPLIT SCENARIO	✓	✓	×
END-SPLIT SCENARIO	✓	✓	✓

Table 3.1: Overview of the charging strategy scenarios and enabled optimization features.

Several functions have been defined to power the Python-based battery optimization tool. Among them, one of the most important is the run_alternating_turns function. This function is used repeatedly and is essential for simulating each of the scenarios presented. Figure 3.8 shows the first section of the function, where input values, parameter definitions, and setup computations are performed. For completeness, the full implementation is provided in Appendix A.1.

```
def run_alternating_turns(DoD_turns_S, h_rest_S, h_charge_S, day_breaks_S, dur_turns_S, DoD_BASE_S, soc_rest_vals_S, soc_start_S,
                          DoD_turns_NS, h_rest_NS, h_charge_NS, day_breaks_NS, dur_turns_NS, DoD_BASE_NS, soc_rest_vals_NS, soc_start_NS,
                          plot_soc=False, soc_rest_mode="start"):

    S = preprocess_sequence(DoD_turns_S, h_rest_S, h_charge_S, day_breaks_S, dur_turns_S, DoD_BASE_S, soc_rest_vals_S, soc_start_S, T_rest_S)
    NS = preprocess_sequence(DoD_turns_NS, h_rest_NS, h_charge_NS, day_breaks_NS, dur_turns_NS, DoD_BASE_NS, soc_rest_vals_NS, soc_start_NS, T_rest_NS)
    # state variables
    SoH = 1.0
    Q_eq = 0.0
    t_eq = 0.0
    turn_idx = 0    # global turn counter
    day = 1         # calendar day count
    year_day_counter = 1  # calendar days since last annual downtime
    balance_counter = 1 # calendar days since last battery balancing
    balance= False
    current = S
    SoH_list = [SoH]  # initial SoH before any day

    def is_end_of_day(i):
        return (i in day_breaks_set) or (i == n_turns - 1)

    SOC=[]
    TIME=[]
```

Figure 3.8: Initial part of the Python function implementing the mathematical simulation of battery aging.

The main strength of the run_alternating_turns function lies in its high versatility. Thanks to the detailed specification and flexibility of its input parameters, the function can be used not only for the predefined scenarios, but also to simulate a wide range

of operating conditions that reflect user-defined constraints. In particular, the function requires the following input values:

- *DoD_turns*: an array describing the cumulative DoD between two consecutive recharges. If a recharge does not occur after a turn, the corresponding value in DoD_turns is set to zero, indicating the absence of a recharge cycle at that point. The value for the next turn then reflects the cumulative DoD since the last recharge, calculated by adding the DoD_base of consecutive turns without recharging. When a recharge occurs, the cumulative DoD is reset, and the next value starts from the DoD of the new turn, marking a new interval between two recharges.
- *h_rest*: an array containing the durations of inactivity periods between the end of one shift and the start of the next. Each element represents the time interval during which the vehicle is not in service and is either parked without operations or potentially available for charging.
- *h_charge*: an array specifying the duration of charging performed during the resting periods. Each element indicates the portion of the corresponding h_rest that is actually used for charging. If no charging occurs during a given resting period, the associated value is zero.
- *Day_breaks*: an array indicating after which shifts a day ends. This information is essential to accurately count the number of days from the start of the simulation to the battery's EoL.
- *Dur_turns*: an array containing the duration of each operational shift.
- *DoD_base*: an array specifying the DoD associated with each individual shift. Each element represents the battery's energy consumption during that single shift.
- *Soc_rest_vals*: an array containing the SoC at which the vehicle is left during its resting period.
- *Soc_start*: an array specifying the SoC at which the first shift of each day begins. For all subsequent shifts within the same day, the value is identical and corresponds to the SoC at the start of the first shift, regardless of the actual SoC at the beginning of each shift.
- *Plot_soc*: a Boolean variable indicating whether the SoC trend over time should be plotted. If set to True, the SoC curve is displayed; if False, no plot is generated.
- *Soc_rest_mode*: a string variable indicating when charging should be performed during resting periods. If set to start, charging begins at the start of each resting

period; if set to end, charging is postponed to finish just before the beginning of the next shift.

The function returns SoH_list as output, an array containing the evolution of the battery SoH under the specific scenario, from the beginning of operations until EoL. Within the function, the SoH is computed whenever a cycle or a resting period is completed, and at the end of each day, the SoH at that moment is added to SoH_list. Consequently, this array contains a large number of SoH values, one for each simulated day, making it particularly useful for graphical representation and further analysis.

The final output of the battery optimization tool is a graphical and numerical comparison of the expected battery life under the five scenarios. This enables the user to clearly understand the implications of adopting one charging strategy over another. As will be demonstrated in the case study application, the End-Split scenario consistently provides the best results by design. However, among the remaining scenarios, it cannot be assumed a priori which strategy is superior. The optimal choice strongly depends on the specific input conditions: for a given set of assigned shifts, factors such as DoD reduction or lower resting SoC can make the Start-Split scenario more effective than the End scenario, or vice versa. Therefore, a simulation is necessary to determine the most suitable charging strategy in each case.

3.3. Charging Optimization Model

In the Battery Optimization Model, five different charging strategies have been analyzed, with the sole objective of identifying the strategy that maximizes battery life and quantifying the difference, expressed in days until EoL, among the various scenarios. This assessment was carried out without considering the implications associated with adopting a specific charging strategy in terms of energy costs or charging-infrastructure requirements.

However, it is important to note that charging schedules must be carefully planned and managed, as the electric bus scheduling problem represents one of the most critical aspects of BEB operations. While extending battery lifespan is valuable, the ultimate motivation for a bus operator is to reduce the total costs incurred over the lifetime of the vehicle. Therefore, optimizing battery life alone, without assessing the impact on other cost components, would provide an incomplete analysis and would not capture the true economic benefits of a given charging strategy.

For these reasons, a dedicated Charging Optimization Model has been developed in parallel with the Battery Optimization Model. This model manages the charging schedule under realistic operational constraints and computes the relevant economic parameters associated with the assumed charging procedures. The information provided by this model will be crucial for the final stage of the study, which focuses on the economic analysis of the different charging strategies.

The model has been implemented in Python using the CP-SAT solver, which is included in the OR-Tools library. OR-Tools is an open-source software suite developed by Google for solving complex optimization problems such as vehicle routing, scheduling, integer and linear programming, and constraint programming [59]. OR-Tools provides several powerful solvers, and one of the most well-known is CP-SAT, a solver specialized in Constraint Programming (CP), a technique based on defining variables, constraints, and objectives.

Thanks to this powerful tool, it has been possible to develop an optimization algorithm that, by analyzing the scenario's input data, minimizes the number of chargers necessary to satisfy the energy demand while respecting the specific constraints imposed by the charging strategy adopted in the considered scenario. In addition, the algorithm generates a charging timetable in which the time slots assigned to each bus can be visualized.

The Charging Optimization Model includes several variables and parameters. To fully understand its purpose and functionality, it is first necessary to clearly describe the operational problem it aims to address.

The key challenge is to plan and schedule the charging operations of a fleet of buses. All recharging activities can only take place inside the depot, which is equipped with a limited number of chargers. Each charger has a fixed power capacity and is equipped with a specific number of plugs.

During the day, each bus returns to the depot one or more times for resting periods, referred to as blocks. In each block, the bus must recharge a certain amount of energy, namely, the energy needed to complete the shift or set of shifts between the end of the current charging block and the start of the next one. The only exception is the Base scenario, in which the bus must recharge the total amount of energy consumed since the previous charging event. The sequence of depot blocks for each bus, together with the corresponding energy to be recharged in each block, constitutes the only input data re-

quired by the optimization algorithm to produce an optimal charging schedule. Together with these input data, some parameters must be defined to properly configure the model output. In particular, it is necessary to specify the charging strategy (start or end) and to assign a title for the graphical representation of the results. Two additional binary parameters can also be defined: the first, named *detail*, can be set to True if all the information related to each charging slot has to be displayed in the output; the second, named *save*, can be set to True to save the generated charging schedule plot in JPEG format. If these two parameters are not explicitly defined in the input line, they are set to False by default.

To reduce the computational time of the algorithm, each depot block is divided into uniform time units, referred to as slots. To map actual times into this discrete structure, a simple utility function named time_to_slot (Figure 3.9) is implemented.

```
def time_to_slot(tstr, slot_minutes=5):

    hh, mm = map(int, tstr.split(":"))

    return (hh * 60 + mm) // slot_minutes
```

Figure 3.9: Python utility function for discretizing time into uniform simulation slots.

This function takes as input a time string in the format HH:MM and converts it into the corresponding slot index within the day. In the present study, each slot represents a 5-minute interval; however, this value can be freely adjusted. Shorter slot durations increase the temporal resolution of the simulation, thus improving accuracy, but also lead to higher computational effort.

The core of the Charging Optimization Model is implemented in the charging_optimization function, which contains the optimization algorithm described above. Figure 3.10 shows the first section of this function, highlighting the inputs and parameters previously discussed, as well as the specifications of the chargers.

The complete implementation of the function is reported in Appendix A.2.

```python
def charging_optimization(bus_blocks, charging_strategy="start", title="Charging_Plan", detail= False, save= False):

    # Slot definition
    slot_minutes = 5
    slots_per_day = 24 * 60 // slot_minutes
    slot_h = slot_minutes / 60.0

    # Charger parameters
    num_charger_upper = 5
    plugs_per_charger = 2 # Number of plugs per charger
    Power = 150 # Charger power in kW
    scale = 100 # Scaling factor for energy calculation
    slot_energy_single = int(round(Power * slot_h * scale)) # Energy per slot for single plug (scaled)
    slot_energy_double = int(round(Power/2 * slot_h * scale)) # Energy per slot per plug when two plugs are connected (scaled)
```

Figure 3.10: Initial part of the Python function implementing the charging optimization algorithm.

To ensure that the charging operations comply with real-world operational requirements, several conditions are defined within the model. The main constraints considered in the model are the following:

- Energy requirement per block: in each depot block, the bus must recharge exactly the predefined amount of energy associated with that block, as determined from the operational schedule and input data.
- Uninterrupted charging: once a charging session has started, it must continue without interruptions until the required energy has been fully delivered; therefore, only one charging session is allowed per block.
- Fixed charger and plug assignment: during a charging session, the bus must remain connected to the same plug and charger, with no switching permitted.
- Single connection per bus: each bus can be connected to only one plug, and therefore to a single charger, at any given time.
- Single bus per plug: each plug can serve only one bus simultaneously.
- Power sharing among buses: if multiple buses are connected to the same charger at the same time, the charger's maximum available power is equally distributed among all active charging sessions.
- Timing constraints based on strategy: if the charging strategy is set to start, the charging session must begin within the first three slots of the block. Conversely, if the strategy is set to end, the charging session must end within the last three slots of the block.

The objective function of the algorithm is designed with a two-level structure. Its primary objective is to minimize the number of chargers required to meet the total energy

demand of the fleet. The secondary objective is to maximize the total number of time slots allocated to charging operations. Different weighting factors are assigned to these two components, ensuring that the charger reduction always takes priority over slot maximization.

This secondary objective has been introduced to encourage lower-power charging whenever possible, rather than exploiting the maximum power capacity of the chargers. Although the battery degradation model adopted in this thesis does not explicitly account for the impact of charging power, several studies have shown that high-power charging negatively affects battery health and consequently reduces battery lifetime [60]. Therefore, by encouraging longer charging sessions at lower power, the model indirectly integrates this relevant degradation mechanism into the optimization framework.

Figure 3.11 shows the portion of the simulation function that contains the definition of the objective function, illustrating how the multi-level prioritization has been implemented.

```
# Multi-priority objective
MAX_SLOTS = slots_per_day * num_charger_upper
weight_charger = MAX_SLOTS
weight_slots = 1
# Minimize the number of charging columns used (primary priority) while maximizing the total charging duration (secondary priority)
model.Minimize(weight_charger * sum(charger_usage[c] for c in charger_range) - weight_slots * sum(L_var[bid] for bid in block_ids))
```

Figure 3.11: Excerpt of the Python function defining the two-level objective function of the charging optimization algorithm.

Starting from the provided input data, the CP-SAT solver systematically explores all feasible combinations of time slots that satisfy the imposed constraints and identifies the solution that best fulfils the objective function. Given the intrinsic computational complexity of the problem, characterized by a high number of binary decision variables and strongly interdependent constraints, specific strategies have been incorporated to significantly reduce the search space and improve computational efficiency.

One of the most effective techniques implemented is a symmetry-breaking constraint: if a charger with a higher index is used, all chargers with a lower index must also be activated. Although conceptually simple, this constraint removes a large number of equivalent symmetric solutions that would otherwise be evaluated by the solver, resulting in a substantial reduction in computation time without affecting optimality.

To ensure practical usability, a maximum solving time limit of 9,000 seconds has been imposed. If the solver proves optimality before reaching this limit, the process terminates early; otherwise, it stops when the time limit is reached and returns the best solution found up to that point. This approach maintains a balance between solution quality and computational feasibility, especially for large fleets or highly constrained operational scenarios.

At the end of the optimization process, the solver returns a status code, indicating the outcome of the search. The possible statuses are the following [61]:

- **UNKNOWN**: the solver did not find a feasible solution, and infeasibility has not been proven.
- **OPTIMAL**: an optimal solution has been found, and the solver established that no better solution exists.
- **FEASIBLE**: a valid solution has been found, but its optimality cannot be guaranteed within the time limit.
- **INFEASIBLE**: the solver has proven that no feasible solution exists under the given constraints.

If the solver finds a solution (either FEASIBLE or OPTIMAL), several key outputs are generated. These include the actual solver runtime, the final solver status, the minimum number of chargers required, the duration of each charging process, and the total amount of energy charged within each time band (F1, F2, F3). Additionally, the model produces a graphical representation of the overall charging schedule, allowing the user to immediately visualize the allocation of chargers, time slots, and power levels across the fleet.

If the *detail* parameter is set to True, the solver also provides a detailed breakdown of every individual charging operation. This includes the specific time slots assigned, the power delivered in each slot, the energy charged, and the associated charger and plug indices. An example of this detailed output is shown in Figure 3.12, which reports the scheduling and power allocation of a single charging block for a bus.

```
Bus 1 - Block 2 (window 19:10 - 07:00)
 -> Slot 230 (19:10), Charger 2, Plug 2, Power ~75.00 kW, Energy 6.2500 kWh
 -> Slot 231 (19:15), Charger 2, Plug 2, Power ~75.00 kW, Energy 6.2500 kWh
 -> Slot 232 (19:20), Charger 2, Plug 2, Power ~75.00 kW, Energy 6.2500 kWh
 -> Slot 233 (19:25), Charger 2, Plug 2, Power ~75.00 kW, Energy 6.2500 kWh
 -> Slot 234 (19:30), Charger 2, Plug 2, Power ~75.00 kW, Energy 6.2500 kWh
 -> Slot 235 (19:35), Charger 2, Plug 2, Power ~75.00 kW, Energy 6.2500 kWh
 -> Slot 236 (19:40), Charger 2, Plug 2, Power ~75.00 kW, Energy 6.2500 kWh
 -> Slot 237 (19:45), Charger 2, Plug 2, Power ~75.00 kW, Energy 6.2500 kWh
 -> Slot 238 (19:50), Charger 2, Plug 2, Power ~75.00 kW, Energy 6.2500 kWh
 -> Slot 239 (19:55), Charger 2, Plug 2, Power ~75.00 kW, Energy 6.2500 kWh
 -> Slot 240 (20:00), Charger 2, Plug 2, Power ~75.00 kW, Energy 6.2500 kWh
 -> Slot 241 (20:05), Charger 2, Plug 2, Power ~75.00 kW, Energy 6.2500 kWh
 -> Slot 242 (20:10), Charger 2, Plug 2, Power ~75.00 kW, Energy 6.2500 kWh
 -> Slot 243 (20:15), Charger 2, Plug 2, Power ~75.00 kW, Energy 6.2500 kWh
 -> Slot 244 (20:20), Charger 2, Plug 2, Power ~75.00 kW, Energy 6.2500 kWh
 -> Slot 245 (20:25), Charger 2, Plug 2, Power ~75.00 kW, Energy 6.2500 kWh
 -> Slot 246 (20:30), Charger 2, Plug 2, Power ~75.00 kW, Energy 6.2500 kWh
 -> Slot 247 (20:35), Charger 2, Plug 2, Power ~75.00 kW, Energy 6.2500 kWh
 -> Slot 248 (20:40), Charger 2, Plug 2, Power ~75.00 kW, Energy 6.2500 kWh
 -> Slot 249 (20:45), Charger 2, Plug 2, Power ~75.00 kW, Energy 6.2500 kWh
 -> Slot 250 (20:50), Charger 2, Plug 2, Power ~75.00 kW, Energy 6.2500 kWh
 -> Slot 251 (20:55), Charger 2, Plug 2, Power ~75.00 kW, Energy 6.2500 kWh
 -> Slot 252 (21:00), Charger 2, Plug 2, Power ~75.00 kW, Energy 6.2500 kWh
 -> Slot 253 (21:05), Charger 2, Plug 2, Power ~75.00 kW, Energy 6.2500 kWh
 -> Slot 254 (21:10), Charger 2, Plug 2, Power ~75.00 kW, Energy 6.2500 kWh
 -> Slot 255 (21:15), Charger 2, Plug 2, Power ~150.00 kW, Energy 12.5000 kWh
 -> Slot 256 (21:20), Charger 2, Plug 2, Power ~150.00 kW, Energy 12.5000 kWh
 -> Slot 257 (21:25), Charger 2, Plug 2, Power ~150.00 kW, Energy 12.5000 kWh
 -> Slot 258 (21:30), Charger 2, Plug 2, Power ~43.80 kW, Energy 3.6500 kWh
 ===> Total energy charged in block: 197.4000 kWh
```

Figure 3.12: Example of detailed scheduling and power allocation of a single charging block from the charging optimization algorithm.

All outputs generated for each simulation scenario are stored in a dedicated .pkl file so that they can be imported into the other models developed in this thesis. In particular, the charging duration computed by the optimization algorithm is used as an input for the Battery Optimization Model, while the minimum number of chargers and the daily energy distribution across the tariff bands constitute essential input parameters for the Economic Evaluation Model, where they are used to assess the operational and investment costs associated with each charging strategy.

3.4. Economic Evaluation Model

The Battery Optimization Model and the Charging Optimization Model provide all the key parameters required to compare the different scenarios from an economic perspective. To perform this comparison, a dedicated Python script has been developed. In this script, the SoH trends for each scenario are imported from the Battery Optimization Model, while the energy consumption for each scenario and time band, together with the corresponding number of chargers required, are imported from the Charging Optimization Model.

Additionally, the monthly average PUN for each time band during the simulation period must be provided as input. These values are used to calculate the average energy cost for each time band, according to the specific energy supply contract signed by the PTO.

To compare the different scenarios from an economic perspective, it is necessary to introduce an indicator capable of capturing all cost components arising over the lifetime of a bus. For this purpose, the Life Cycle Cost (LCC) is adopted as the reference metric.

To preserve the focus on the differences among scenarios, only cost items that vary depending on the adopted charging strategy or operational conditions are included in the analysis. Cost components that remain identical across all scenarios are deliberately excluded, as their inclusion would not affect the comparative results and would merely shift all outcomes by a constant amount. This assumption improves the readability of the results while preserving the validity of the comparison.

Accordingly, the LCC is defined as the discounted sum of the annual cash flows CF_t over the bus lifetime T_{life}, using a discount rate r, as expressed in Equation 3.11.

$$\text{LCC} = \sum_{t=0}^{T_{\text{life}}} \frac{CF_t}{(1+r)^t} \tag{3.11}$$

In this study, the cash flows considered include both capital and operational expenditures. The CAPEX components account for the purchase and installation of chargers, as well as the replacement of batteries throughout the vehicle's lifetime. The OPEX components include the costs associated with charger maintenance and electricity supply. Additionally, a residual value is considered for both chargers and batteries. For chargers, this value is only included at the end of the analysis period. For batteries, however, a residual value is assigned not only at the end of the analysis period, but also at each replacement event, reflecting the potential revenues from the sale of used batteries for second-life applications. A concise formulation of the CF_t computation is reported in Equation 3.12.

$$CF_t = \text{CAPEX}_t + \text{OPEX}_t - \text{Residual Value}_t \tag{3.12}$$

The length of the analysis period, which corresponds to the bus lifetime, can be a subject of discussion. In this study, the focus has been placed on optimizing the life of the bus

batteries, which are commonly regarded as the most critical component in terms of lifespan and thus often represent the limiting factor in estimating the overall bus lifetime. By enhancing battery life and considering the possibility of replacing them once they reach their EoL, the lifetime of the bus can be extended, but it ultimately depends on the durability of other components such as the chassis, motor, and mechanical parts. Moreover, the useful life of these components is strongly influenced by operational conditions, making it challenging to define a precise lifespan for an electric bus. Nevertheless, due to the relative simplicity of the electric powertrain, it is reasonable to assume that, excluding the batteries, an electric bus may sustain a longer operational life than a comparable diesel bus [62]. To account for the uncertainty in lifespan estimation, three different values have been considered in this study: 12 years, 16 years, and 20 years, representing pessimistic, moderate, and optimistic estimates of the electric bus's useful life, respectively.

When analyzing the concept of battery residual value, it is essential to clarify several aspects in order to properly justify the formulation adopted in this study. As discussed in previous sections, a battery used in electric vehicles is generally considered to have reached its EoL when its SoH falls below the commonly accepted threshold of 80%. Importantly, however, reaching this threshold does not imply that the battery is no longer functional or suitable for further use. Once removed from traction applications, it can still be repurposed for less demanding contexts, most notably stationary energy storage, where power requirements are lower and operational stresses are significantly reduced. For this reason, a battery dismissed from a BEB retains an economic value, as it may continue to provide useful service within a second-life application.

An additional consideration is that batteries are not always retired exactly at 80% SoH. Depending on operational practices or the timing of the vehicle's retirement, a battery may be removed from service while still exhibiting a higher SoH. In such cases, the residual value is naturally higher, since a battery with greater remaining capacity is capable of delivering a longer second-life operational period. For this reason, the residual value must be modeled as a function of the battery's actual SoH at the moment of retirement, rather than assuming a fixed residual value for every decommissioned battery regardless of its degradation state.

Before a used battery can be deployed as a Second-Life Battery (SLB), it must undergo a sequence of procedures, typically including diagnostic testing and refurbishment, to ensure that it meets safety and performance requirements suitable for stationary applications. This process, often referred to as revamping, entails a cost that is largely independent

of the battery's specific degradation level, as all units require the same standardized set of interventions to be safely redeployed. Consistent with the approach presented by the authors in [63], this study adopts a revamping cost of 45 $/kWh. This value represents the average cost reported in the literature for preparing EV batteries for second life applications and is applied uniformly across all batteries considered in the model. In Equation 3.13, the expression used to estimate the residual value of a battery at the end of its first-life service is reported. This formulation explicitly accounts for both the SoH at retirement and the revamping cost, and it includes a correction factor (γ_price=0.95) to provide a conservative estimate of the residual value:

$$\text{Battery Residual Value} = \gamma_{\text{price}} \cdot C_{\text{new}} \cdot \text{SoH} - C_{\text{revamping}} \tag{3.13}$$

In this study, the cost of a new NMC battery for automotive applications has been set at 139 $/kWh, in line with the average battery-pack prices reported for Europe in the most recent BloombergNEF report [64]. This value is used as the reference against which the residual value of a retired battery is computed.

Although determining the precise market price of a used battery is not the primary objective of this thesis, the adopted empirical approach yields results that are consistent with literature-based estimates and provides a realistic representation of current second-life market conditions.

To assess the consistency of the proposed methodology with literature estimates, Equation 3.13 was applied across a range of SoH values. For each SoH level, the corresponding residual value was calculated and expressed both in absolute terms and as a percentage of the initial battery value. This representation allows for a direct comparison with trends reported in the literature, highlighting the adequacy of the proposed model. The outcomes of this analysis are summarized in Table 3.2.

SoH	**Residual value [$/kWh]**	**Percentual of initial value**
0.95	80.5	58%
0.90	73.9	53%
0.85	67.2	48%
0.80	60.6	44%

Table 3.2: Battery residual value as a function of SoH, expressed in $/kWh and as a percentage of the initial value.

The core of the Economic Evaluation Model is the function calculate_LCC_scenario. This function generates a DataFrame that includes all the components necessary to compute the Life Cycle Cost for a given scenario, as well as the resulting LCC itself. In this way, it provides a comprehensive overview of the annual economic expenditures over the vehicle's entire lifetime.

The function requires, as inputs, a set of economic assumptions as well as the outputs obtained from the previously implemented Python scripts: the Battery Optimization Model and the Charging Optimization Model. An overview of the calculate_LCC_scenario function, including the required input parameters and the preliminary assumptions common to all scenarios, is presented in Figure 4.17. The complete function implementation is reported in Appendix A.3.

```
def calculate_LCC_scenario(scenario, df_results, num_chargers, SoH_12m, SoH_9m, energy_by_timeband_S, energy_by_timeband_NS,  bus_lifetime):

    # Common parameters for all scenarios
    discount_rate = 0.03
    charger_cost = 40000
    charger_opex = 0.05 # 5% of the charger cost
    num_buses_12m = 5
    num_buses_9m = 4
    cap_12m = 420  # kWh, battery capacity of a 12 m bus
    cap_9m = 294   # kWh, battery capacity of a 9 m bus
    battery_value_12m = battery_cost_per_kWh * num_buses_12m * cap_12m # value of new 12 m bus battery pack
    battery_value_9m  = battery_cost_per_kWh * num_buses_9m * cap_9m # value of new 9 m bus battery pack
    charger_lifetime = 24  # expected lifetime of a charger in years

    # Time horizon for the LCC analysis (years)
    years = range(2026, 2026+bus_lifetime)

    # Annual energy cost
    annual_energy_cost = (
        energy_by_timeband_S["F1"] * average_prices_S["F1 [€/kWh]"] +
        energy_by_timeband_S["F2"] * average_prices_S["F2 [€/kWh]"] +
        energy_by_timeband_S["F3"] * average_prices_S["F3 [€/kWh]"]
        ) * 225 + (
        energy_by_timeband_NS["F1"] * average_prices_NS["F1 [€/kWh]"] +
        energy_by_timeband_NS["F2"] * average_prices_NS["F2 [€/kWh]"] +
        energy_by_timeband_NS["F3"] * average_prices_NS["F3 [€/kWh]"]
        ) * 67
```

Figure 3.13: Initial part of the Python function used to compute the LCC for each scenario.

The Python script has been designed to apply the calculate_LCC_scenario function to the five battery management scenarios described in Section 3.2.1. For each scenario, the function is executed three times, to simulate all considered bus lifetime estimations. Subsequently, another function allows the aggregation and summarization of the resulting LCC DataFrames for each lifetime case. The aggregated results are then used to produce a bar chart, enabling a straightforward comparison of the LCC across the various scenarios, broken down into three main cost components: energy, chargers, and batteries.

4 | Practical application and results

In Chapter 3, the model has been presented in a parametric form in order to highlight its flexibility and wide range of applicability. In contrast, this chapter focuses on a real-world case study, selected to demonstrate the practical implementation of the proposed framework. The case study allows the model to be applied under realistic operating conditions, thereby assessing its effectiveness and robustness. Moreover, it enables a deeper understanding of the model's real-life applicability and provides the basis for a detailed discussion of the results and the insights that emerge from its application.

4.1. Case study

The analyzed case study concerns the application of the developed models to the electric bus fleet operated by Autoguidovie S.p.A. in the province of Cremona. The fleet consists of nine Iveco E-Way battery electric buses (Figure 4.1) equipped with lithium-ion NMC batteries, based on ZEN 42 battery modules produced by Forsee Power.



Figure 4.1: Iveco E-Way electric bus of the Autoguidovie S.p.A. fleet.

The fleet can be divided into two distinct groups, according to vehicle size and operational use. Five vehicles are 12-meter buses equipped with ten ZEN 42 battery modules each, providing a total installed energy capacity of 420 kWh. These buses are primarily deployed on interurban and suburban routes within the province (Figure 4.2), where higher daily energy demand and longer distances are required. The remaining four vehicles are 9-meter buses, each fitted with seven ZEN 42 battery modules for a total capacity of 294 kWh. These smaller buses are mainly employed on the urban network of the city of Crema (Figure 4.3), characterized by shorter routes and lower energy requirements.

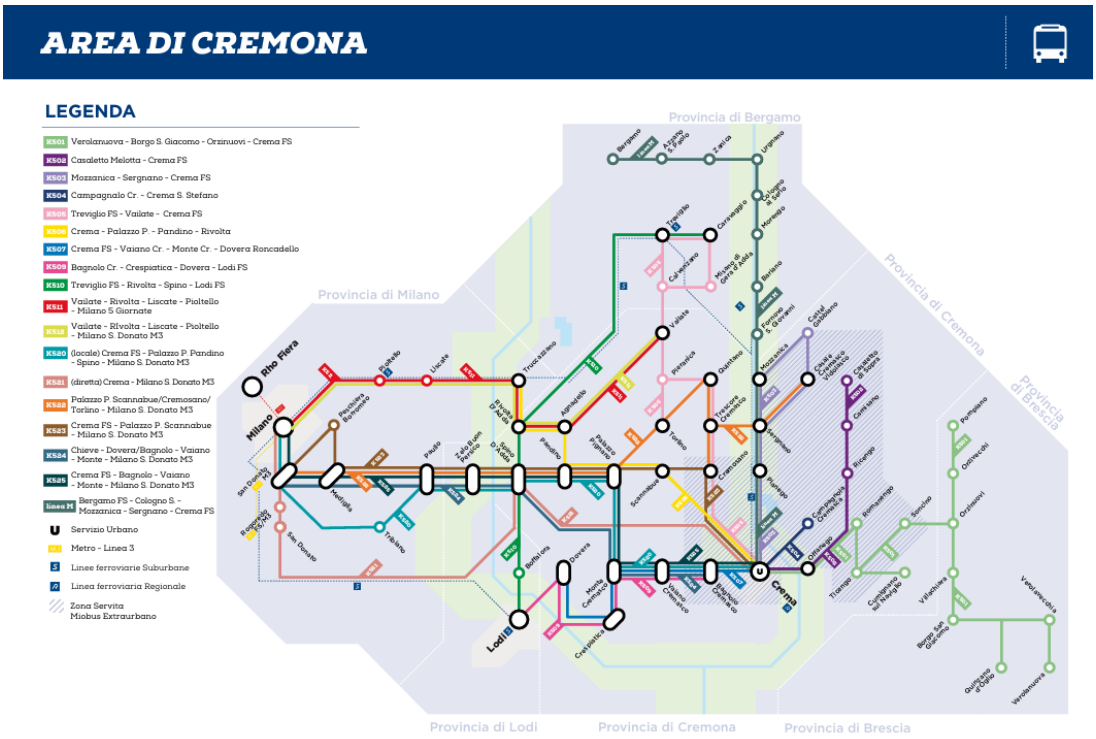


Figure 4.2: Interurban and suburban bus routes in the Cremona area.

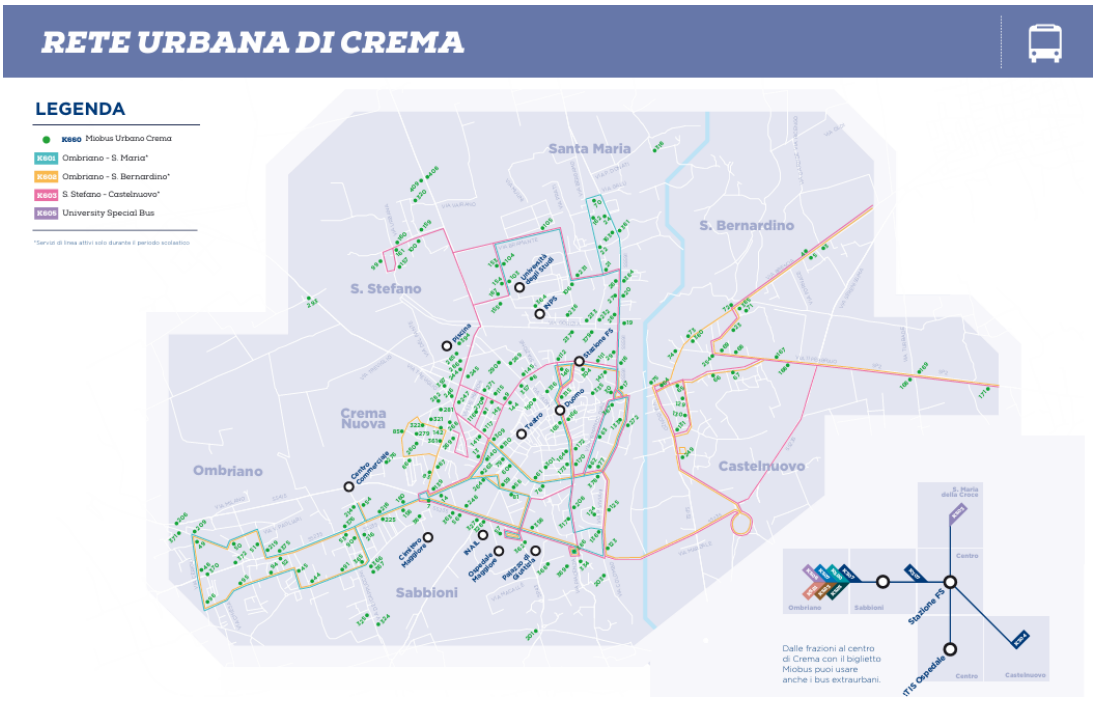


Figure 4.3: Urban bus routes within the city of Crema.

A summary of the main technical characteristics and configurations of the Iveco E-Way buses included in the fleet is provided in Table 4.1.

Model	Length [m]	Battery capacity [kWh]	Seat	Total passenger capacity
E-Way 12	12.06	420	37	80
E-Way 9	9.52	294	18	65

Table 4.1: Technical characteristics of the E-Way bus models considered in this study.

Each day, every bus is assigned to a specific bus block, defined as the sequence of trips and operational activities scheduled for that vehicle. A bus block typically includes service trips, layover times at terminals, deadhead movements, and resting periods spent at the depot. Bus blocks are not permanently assigned to the same vehicle, instead, they are rotated among the buses to ensure uniform wear and balanced utilization of the fleet.

The bus blocks analyzed in this study are real operational schedules provided directly by Autoguidovie S.p.A. and implemented by the company through Maior VSI. For the considered electric bus fleet, the operator defines two distinct sets of bus blocks: a first set

covering the period from September to June, corresponding to the school period service, and a second set adopted during the summer months to meet non-school period travel demand.

These bus blocks were further processed to remove unnecessary information and retain only the elements relevant for the purposes of this analysis, improving clarity and readability. In particular, each bus block was divided into several shifts, separated by breaks at the depot, during which buses may have the opportunity to recharge.

The energy demand of each shift was estimated through the analysis of real operational consumption data. Iveco's monitoring system enables the operator to track the daily profile of each electric bus in terms of State of Charge and odometer readings (Figure 4.4). For each bus block, multiple daily profiles, collected from different buses and over different days, were analyzed to derive an average profile representative of the energy required to operate the bus block and, more specifically, each individual shift.

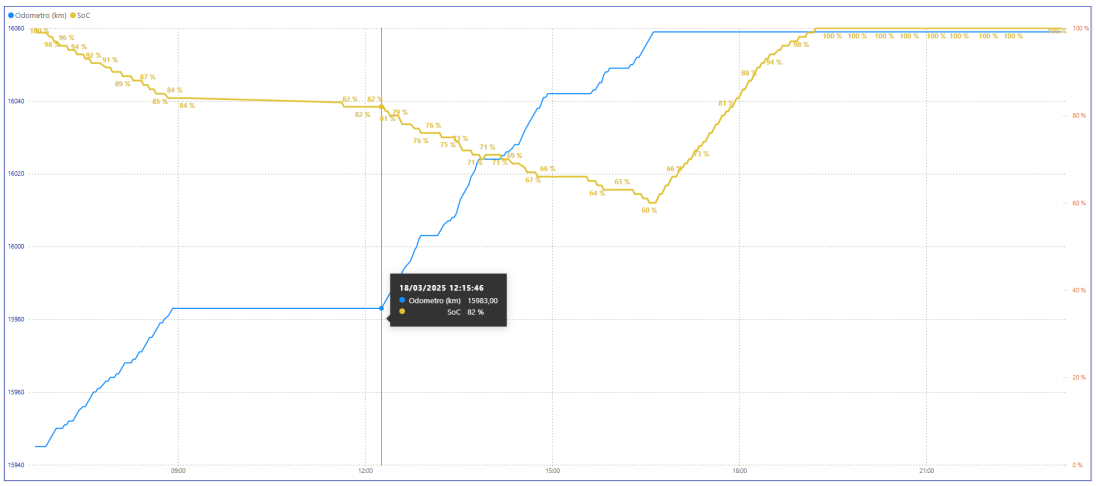


Figure 4.4: Example of daily profile data provided by Iveco's monitoring system.

With reference to the bus blocks operated by the 9-meter buses, some time slots are allocated to the so-called "Servizio a chiamata". During these periods, the bus operates on demand, responding to user requests submitted via a dedicated mobile application. As the distance traveled during these slots depends on user demand, the maximum energy consumption observed in Iveco's monitoring system was selected as the reference value. An additional 10% safety margin was then applied to account for variability and to ensure robustness of the energy demand estimation.

By combining the processed bus block schedules obtained from Maior VSI with the energy consumption estimates derived from Iveco's monitoring system, it is possible to obtain a clear and concise representation of each bus block in both temporal and energetic terms. Figure 4.5 shows a simplified representation of the scholastic bus blocks: light blue segments correspond to driving shifts, while orange segments indicate daytime break periods. For each driving shift, the associated energy demand is expressed in terms of State of Charge, representing the battery consumption required to complete that specific shift. A similar representation of the non-scholastic bus blocks is reported in Figure 4.6.

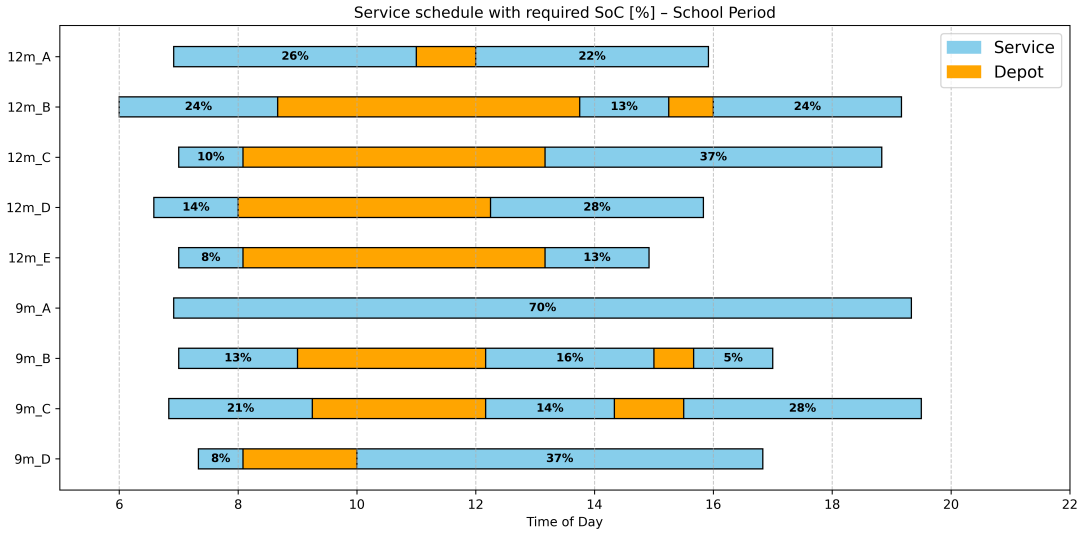


Figure 4.5: Bus blocks corresponding to the school period, showing the SoC [%] required for each shift.

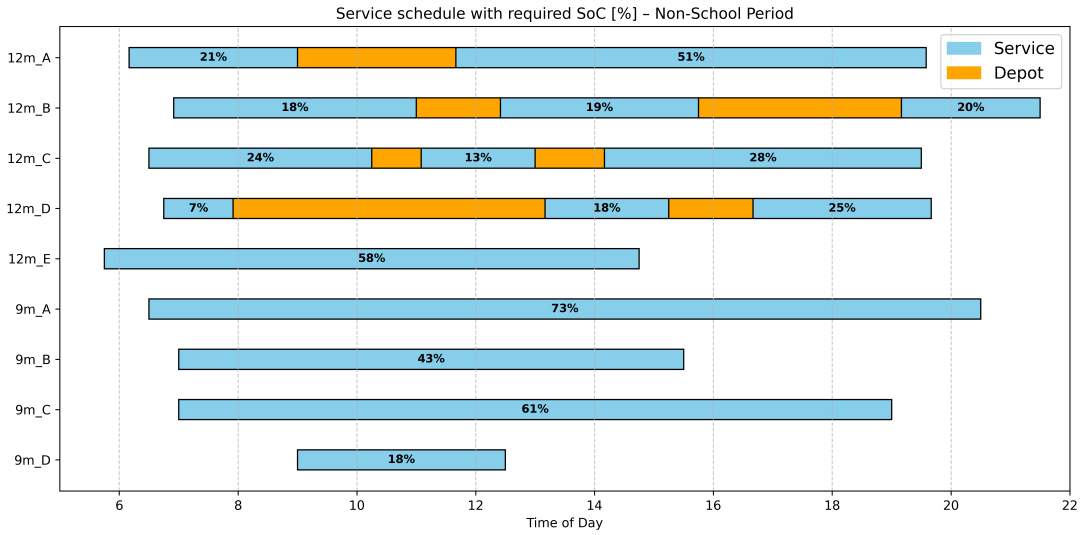


Figure 4.6: Bus blocks corresponding to the non-school period, showing the SoC [%] required for each shift.

4.2. Application of the Battery Optimization Model

The bus blocks described in the previous section have been used as input data to test and validate the Battery Optimization Model. By exploiting the detailed temporal and energetic information associated with each bus block, the model is able to reconstruct a realistic operating profile for the battery and, consequently, to generate a degradation curve from which the expected battery lifetime can be estimated. The capability of the model to reproduce the real-world battery aging behavior relies on the adoption of a set of assumptions and operational rules that closely reflect the actual operating conditions of the fleet and good practices.

First, bus blocks are rotated among vehicles belonging to the same group, namely 12-meter and 9-meter buses. This means that a bus assigned to a given bus block on one day will be assigned to a different bus block on the following day, according to a predefined rotation scheme. This approach avoids systematically assigning the same duty cycle to a single vehicle and ensures a more uniform distribution of energy demand, Depth of Discharge, and operating stress across the fleet.

Second, after completing five consecutive bus blocks, corresponding to five working days, each bus is assumed to have one rest day. During this day, the vehicle is not operated and remains parked at the depot for a full 24-hour period at a given SoC. These rest days are explicitly modeled, as resting periods at partial SoC contribute to calendar aging and

therefore affect the overall degradation curve of the battery.

In addition, every 15 days the battery is assumed to be charged up to 100% SoC. This operation is introduced to represent periodic full charges performed to ensure proper cell balancing and maintain the reliability of the battery management system.

With respect to seasonal operations, each bus is assumed to follow the school period service schedule for 270 days per year, after which it operates under the non-school schedule for the following 80 days. At the end of each yearly cycle, once both service periods have been completed, the bus is assumed to undergo an extended resting period of 15 consecutive days, during which it is not operated.

During the school period, the batteries are assumed to operate and rest at a temperature of 18 °C, corresponding to the average ambient temperature in Crema. In contrast, during the non-school period, the temperature is set to 35 °C, slightly above the city's average summer temperature, to account for additional heating effects from solar irradiation and direct sunlight, which cause the battery temperature to exceed the ambient level.

These temperature assumptions, combined with the defined operational schedules, resting periods, and balancing strategy, allow the model to reproduce a realistic annual operating pattern. Under this configuration, each bus completes 292 service days and 73 resting days per year. During the 292 service days, each vehicle covers approximately 50 000-55 000 km, which is consistent with the annual mileage declared by the operator and therefore confirms the goodness of the adopted assumptions.

The resting periods included in the model account not only for scheduled weekly rest days, but also implicitly for unplanned stops due to maintenance activities or unexpected failures. Specifically, 58 resting days are distributed throughout the year, reflecting the common condition of having at least one non-operational day per week, while the remaining 15 resting days are concentrated at the end of the year to represent a major maintenance stop or extended vehicle downtime. Although this representation constitutes a simplification of real-life operations, it provides a reasonable and effective compromise between model realism and computational tractability.

As discussed in the previous chapter, the model is capable of simulating five different scenarios, each characterized by a specific set of optimization elements, as summarized in Table 3.1. To facilitate the understanding of the adopted optimization elements, as well

as the operational rules described above, selected battery SoC profiles obtained from the simulations are presented and discussed in the following.

Figure 4.7 shows the SoC evolution of a 12-meter bus during the first ten days of the simulation under the Start scenario. During this initial period, the vehicle operates according to the school service schedule. In this scenario the parameter *grouped* is set to True, therefore no charging events are executed between shifts belonging to the same bus block; instead, charging occurs only between the last shift of a given bus block and the first shift of the subsequent one.

Moreover, as in this scenario the *Soc_rest_mode* parameter is set to start, all charging events are carried out immediately after the completion of the last shift of each bus block. As a result, the vehicle is recharged well before the beginning of the subsequent operating period.

It can be observed that the battery is recharged to different SoC levels at the end of each bus block. This behavior is the result of the optimize_soc_start function, which determines the optimal starting SoC for each bus block with the objective of minimizing overall battery degradation.

After the fifth day of operation, a resting day is clearly visible, during which the bus remains parked at the depot and no driving activities are performed.

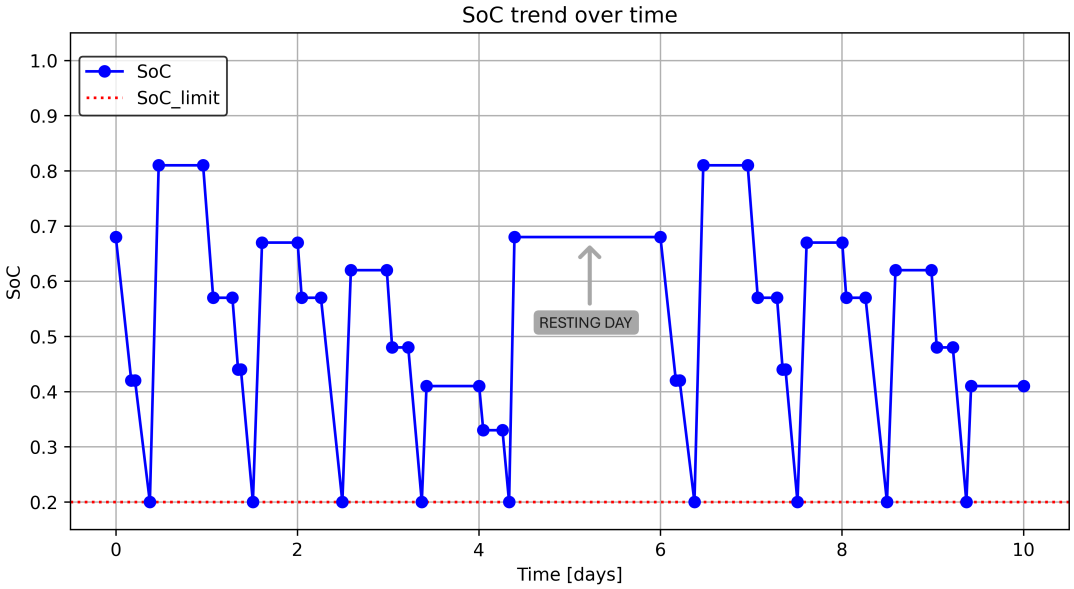


Figure 4.7: Excerpt of the SoC evolution over time for the Start scenario.

Figure 4.8 illustrates a section of the SoC evolution of a 12-meter bus operating under the non-school schedule in the End-Split scenario, a scenario that is conceptually opposite to the one previously presented. In this scenario, the parameter *grouped* is set to "False", implying that charging events are executed at the end of each individual shift rather than being aggregated. Additionally, the *Soc_rest_mode* parameter is set to end, which means that after each shift the bus undergoes the corresponding resting period, and the subsequent charging event is scheduled immediately before the start of the next shift.

Within the selected section, a periodic balancing event can be observed, during which the battery is deliberately charged up to 100% SoC to equalize the cell voltages. Correspondingly, subsequent charging events are adjusted to restore to the optimal SoC conditions.

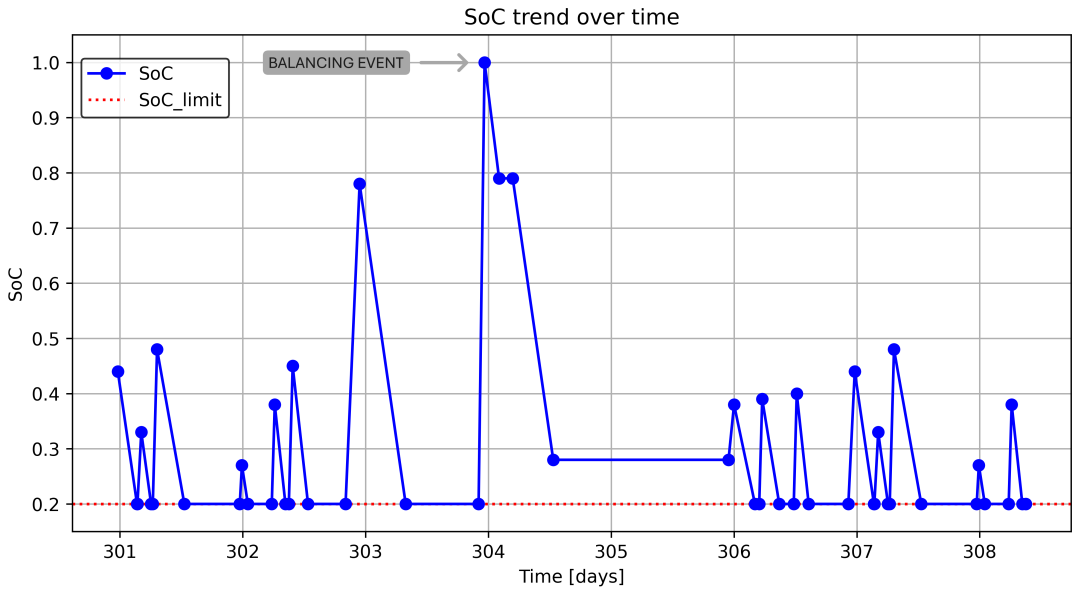


Figure 4.8: Excerpt of the SoC evolution over time for the End-Split scenario, showing a periodic cell-balancing event.

The final selected SoC profile is presented in Figure 4.9 and corresponds to a segment of the SoC evolution of a 12-meter bus operating under the Base scenario. In this scenario, no optimization strategies are implemented; consequently, the SoC trend is characterized by high Depths of Discharge, resting periods at elevated State of Charge, and charging events consistently reaching 100% SoC.

Unlike the previously presented profiles, which illustrate only few days of operation, the reported segment spans over more than one hundred days. This extended period allows the visualization of the transition from the school period schedule to the non-school

schedule, as well as the annual 15-day downtime.

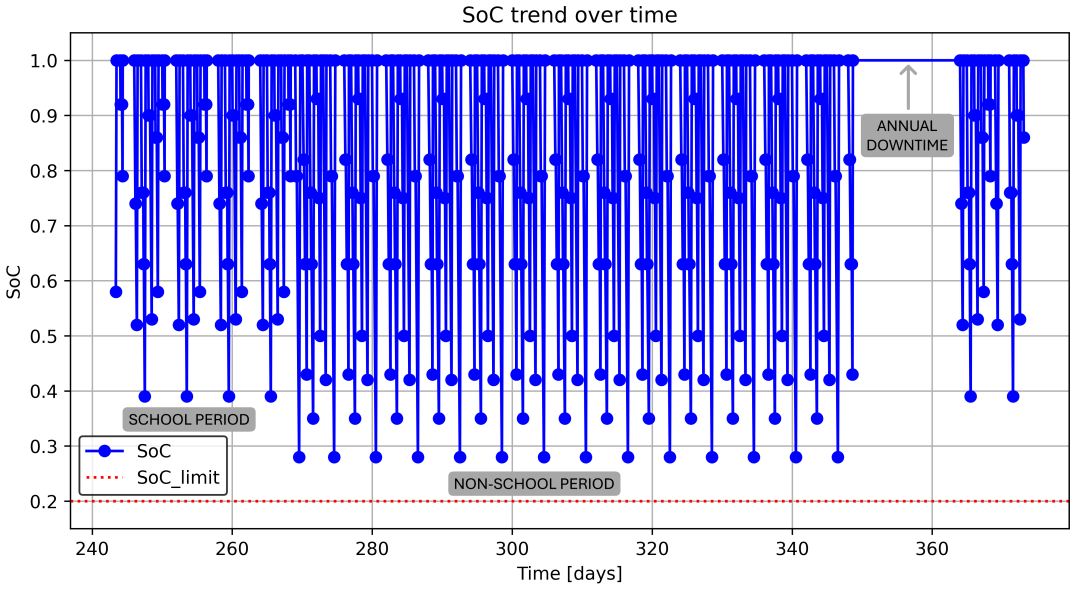


Figure 4.9: Excerpt of the SoC evolution over time for the Base scenario, showing the annual resting period and the transition between school and non-school scheduling.

As discussed in the previous section, each scenario is characterized by a specific SoC profile, which is cyclically repeated until the End of Life condition is reached. The SoC profiles associated with the analyzed scenarios exhibit significant differences, and this variability results in distinct battery degradation trends over time. For the 12-meter buses, the State of Health evolution is reported in Figure 4.10, while Figure 4.11 presents the corresponding results for the 9-meter buses.

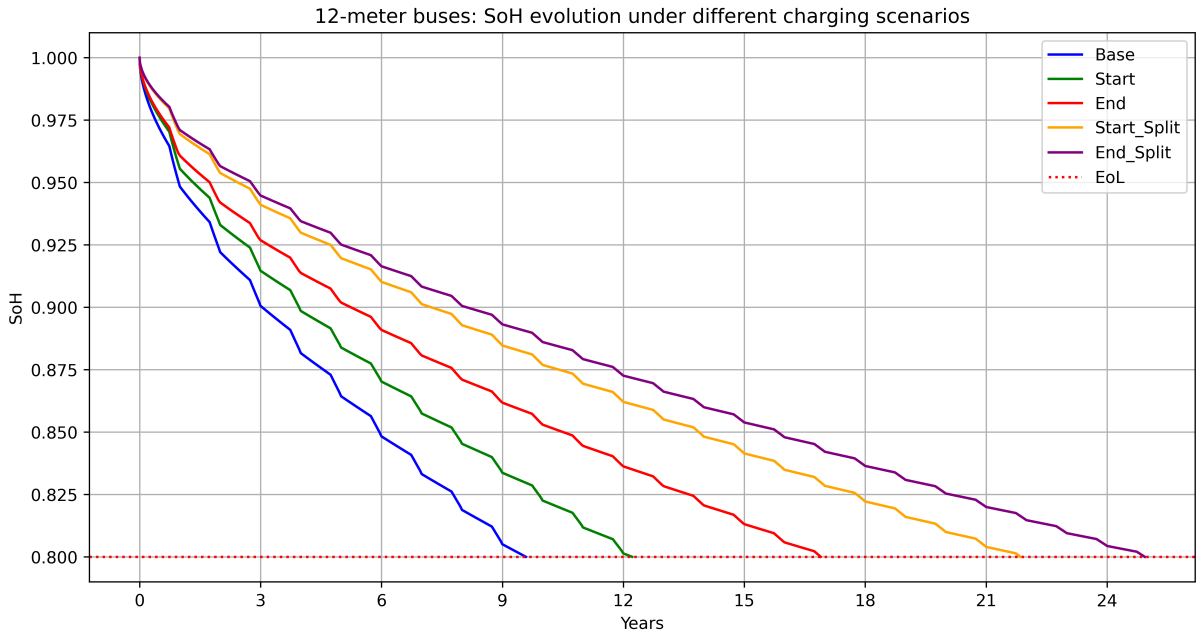


Figure 4.10: Evolution of battery SoH over time for the different charging scenarios for the 12-meter buses.

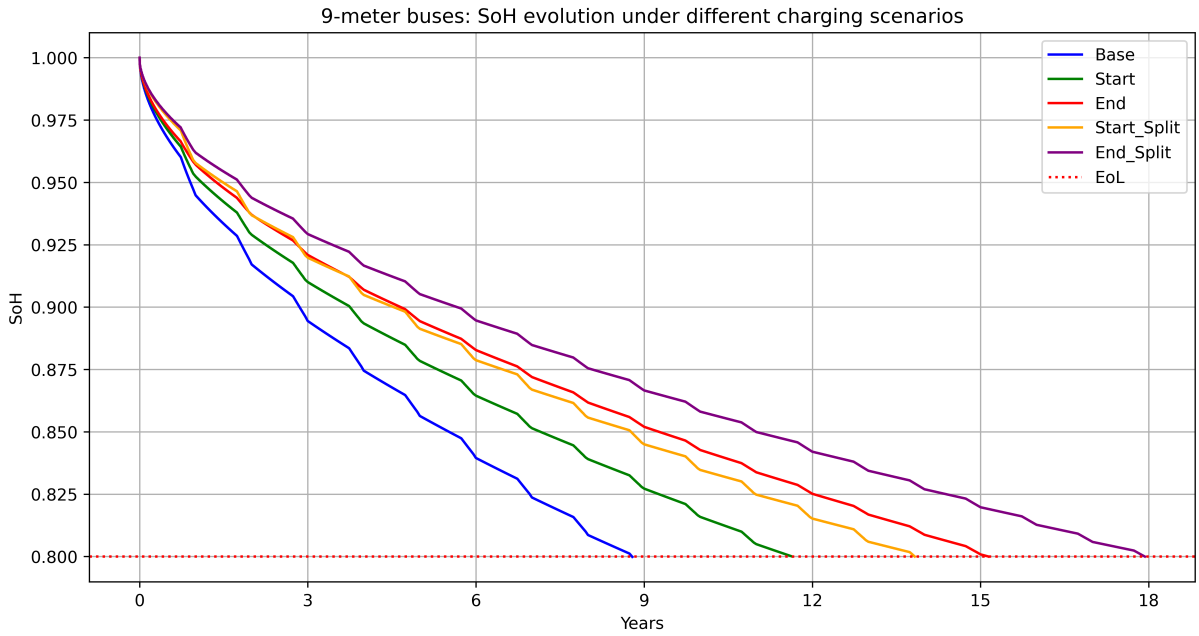


Figure 4.11: Evolution of battery SoH over time for the different charging scenarios for the 9-meter buses.

In both figures, the degradation curves are clearly non-linear and exhibit a certain degree of irregularity. This behavior is primarily attributable to the alternation between

the school period schedule and the non-school period schedule, which are characterized by different DoD and operating SoC ranges. Moreover, a major contribution arises from the different operating temperatures associated with the two periods, which, as discussed in Chapter 2 and demonstrated in Chapter 3, have a strong influence on battery aging mechanisms.

For both vehicle groups, the End-Split scenario is shown to be the most effective strategy in extending battery lifetime, allowing the highest values of useful life to be achieved. However, the relative performance of the remaining scenarios differs between the two bus categories. For the 12-meter buses, the Start-Split scenario results in a longer useful life compared to the End scenario, whereas for the 9-meter buses the opposite trend is observed, with the Start-Split scenario performing worse than the End scenario.

This difference can be explained by the distinct characteristics of the bus blocks assigned to the two vehicle groups. In particular, the bus blocks of the 9-meter buses, especially during the non-school period, are often characterized by higher DoD values and, in many cases, by a single driving shift per day. Under these conditions, the application of split charging strategies has a reduced impact on the overall SoC profile and, consequently, on battery degradation, compared to the 12-meter buses, which in this case operate more articulated daily schedules.

The results of the five scenarios, for both vehicle groups, are summarized in Table 4.2, which reports, for each case, the expected battery lifetime expressed in years and conservatively rounded down to the nearest integer.

Scenario	**12-meter buses**	**9-meter buses**
BASE SCENARIO	9	8
START SCENARIO	12	11
END SCENARIO	16	15
START-SPLIT SCENARIO	21	13
END-SPLIT SCENARIO	24	17

Table 4.2: Expected battery lifetime, expressed in years, under the different charging scenarios for 9-meter and 12-meter buses.

4.3. Application of the Charging Optimization Model

The bus blocks presented in Figure 4.5 and Figure 4.6 are also used as input data for the Charging Optimization Model, with the dual objective of, first, verifying the feasibility of the proposed charging plans and, second, assessing the differences in energy consumption across the various time bands, as well as determining the number of chargers required under each scenario. The model also computes and stores the duration of each charging event; this information is subsequently passed to the Battery Optimization Model via a .pkl file.

The optimization function implemented in this Python script, and described in detail in Chapter 3, can in some cases require relatively high computational effort. For certain scenarios, the solution time exceeds 80 minutes. Nevertheless, the model has demonstrated its robustness and effectiveness, as it was able to identify an optimal charging solution for all the analyzed scenarios.

The model has been applied to generate the charging schedules for the five scenarios under both school period and non-school period operating conditions. In the following sections, the results obtained for the school period schedules are presented and discussed. The corresponding non-school period schedules are not reported in detail, as they exhibit similar qualitative trends and do not provide additional insights. However, they remain relevant, since in some cases the required number of chargers differs between the school period and the non-school period for the same scenario. In particular, a charging configuration that requires a given number of chargers during the school period may require a higher number during the non-school period. For this reason, the non-school period results are reported in Appendix B.

The depot of Cremona is equipped with 150 kW chargers, each of which is provided with two plugs. When a single plug is in use, the charger can deliver its full rated power, while when both plugs are used simultaneously the available power is equally shared, resulting in a maximum of 75 kW per plug.

For all the charging schedules presented in the following figures, the same graphical convention is adopted. For each bus, a series of black rectangles highlights the periods of the day during which the vehicle is located at the depot and therefore the time windows in which charging operations can be performed. When a charging activity takes place, the corresponding time slots are colored according to the charger used, as indicated in the

legend. This representation makes it possible to visually identify the temporal allocation of each charger and to verify the absence of scheduling conflicts. If two vehicles are connected simultaneously to the same charger, the color of the corresponding charging slots is shown in a lighter shade. The specific plug of the charger used for each charging event is reported on the left side of the corresponding charging slots.

Figure 4.12 illustrates the scheduling of charging activities for all buses in the considered fleet under the Base scenario during the school period. In this scenario, charging activities are performed at the end of the operational day. Within the analyzed scheduling programme, buses return to the depot for overnight parking at different times, and therefore the charging demand is temporally distributed. As a result, the charging demand can be met using only two chargers.

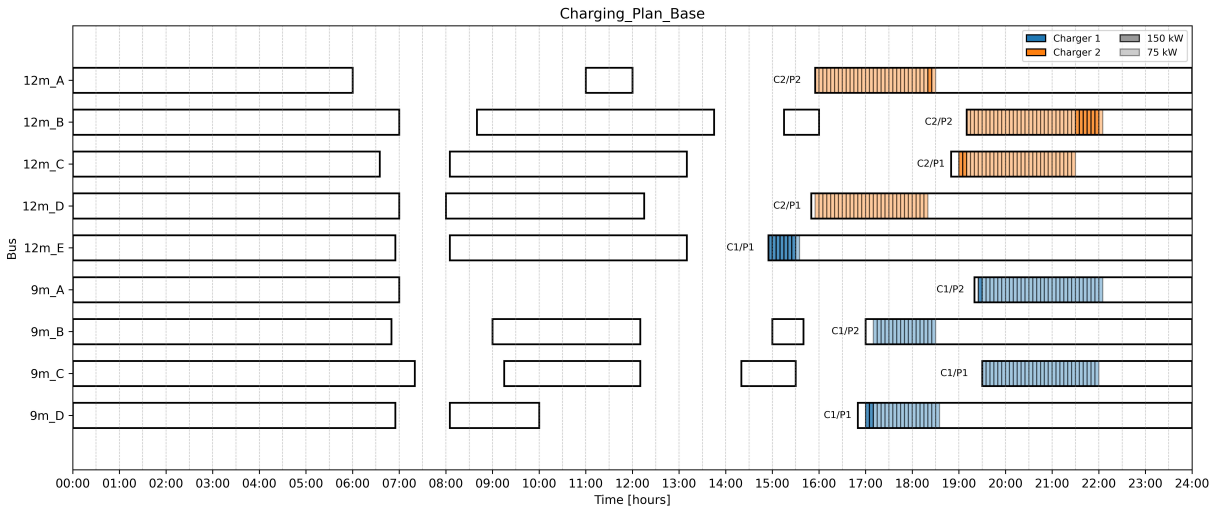


Figure 4.12: Gantt chart illustrating the optimized charging schedule of the fleet in the Base scenario under school period operation.

Figure 4.13 illustrates the scheduling of charging activities under the Start scenario during the school period. Compared to the Base scenario, this scenario is quite similar. The buses are recharged in the same period, immediately after completing their last shift of the day. However, the energy demand differs, as the buses must reach the SoC required for the following day, resulting in charging durations that are not identical to those in the Base scenario. In this case as well, the charging demand can be met using only two chargers.

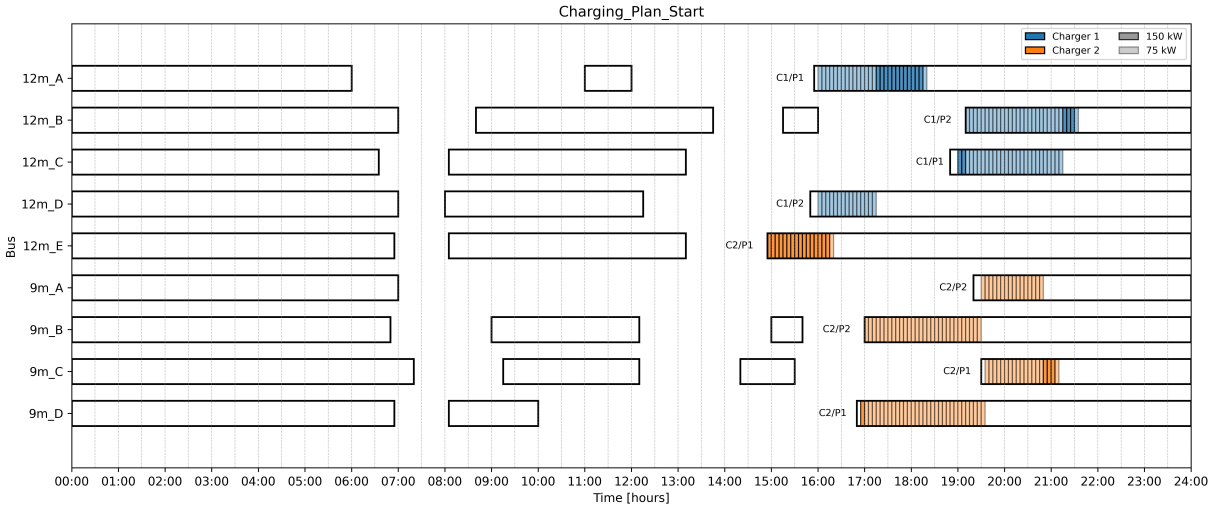


Figure 4.13: Gantt chart illustrating the optimized charging schedule of the fleet in the Start scenario under school period operation.

The situation is different in Figure 4.14, which shows the scheduling of charging activities under the End scenario during the school period. In this scenario, four chargers are required, as in the school period timetable all buses start their service around six or seven o'clock in the morning. Since charging activities must be performed immediately before the start of the operational day, all charging is concentrated in the morning, and in some time slots up to eight buses need to be recharged simultaneously.

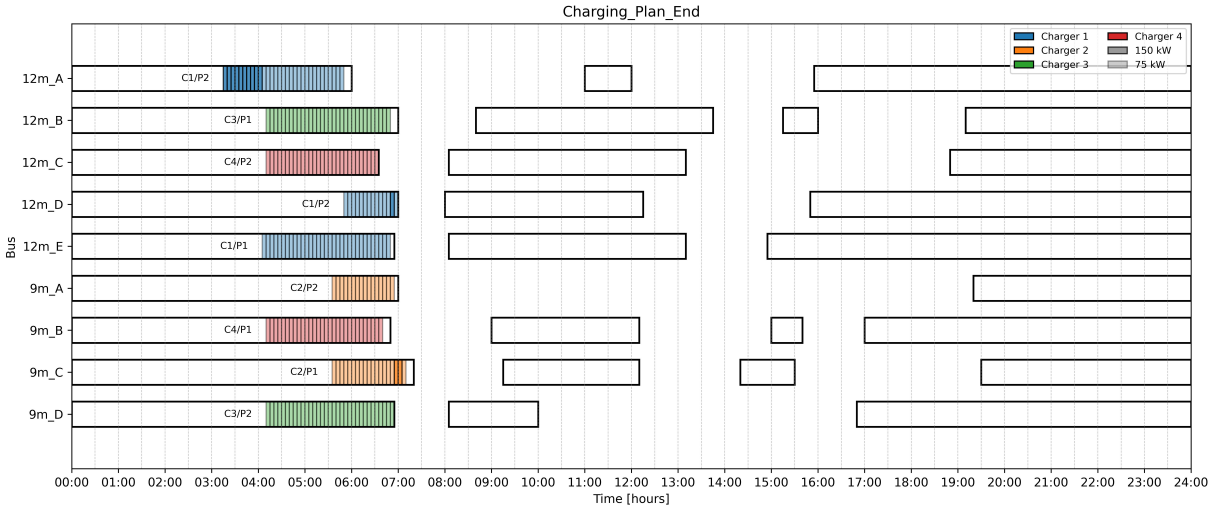


Figure 4.14: Gantt chart illustrating the optimized charging schedule of the fleet in the End scenario under school period operation.

Figure 4.15 illustrates the scheduling of charging activities under the Start-Split scenario during the school period. In this scenario, buses are recharged immediately after the end of each shift. Consequently, charging activities are no longer concentrated in the early morning or in the evening, but are distributed throughout the day. However, since many buses return to the depot at the same time in the morning, some charging events overlap, making it impossible to meet the demand with only two chargers. Therefore, three chargers are required in this scenario.

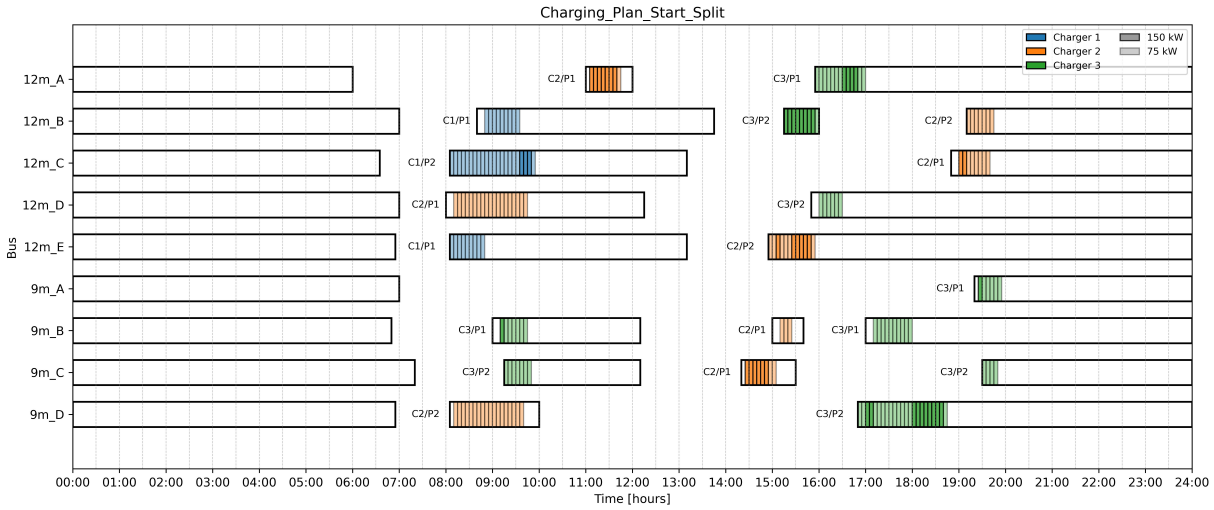


Figure 4.15: Gantt chart illustrating the optimized charging schedule of the fleet in the Start-Split scenario under school period operation.

Finally, Figure 4.16 shows the scheduling of charging activities under the End-Split scenario during the school period. As in the previous scenario, charging activities are distributed throughout the day. However, since this is an "end" scenario, charging is performed at the end of each resting period, immediately before the bus departs from the depot for the next shift. Three chargers are required in this scenario as well, due to the morning charging congestion already discussed for the End scenario.

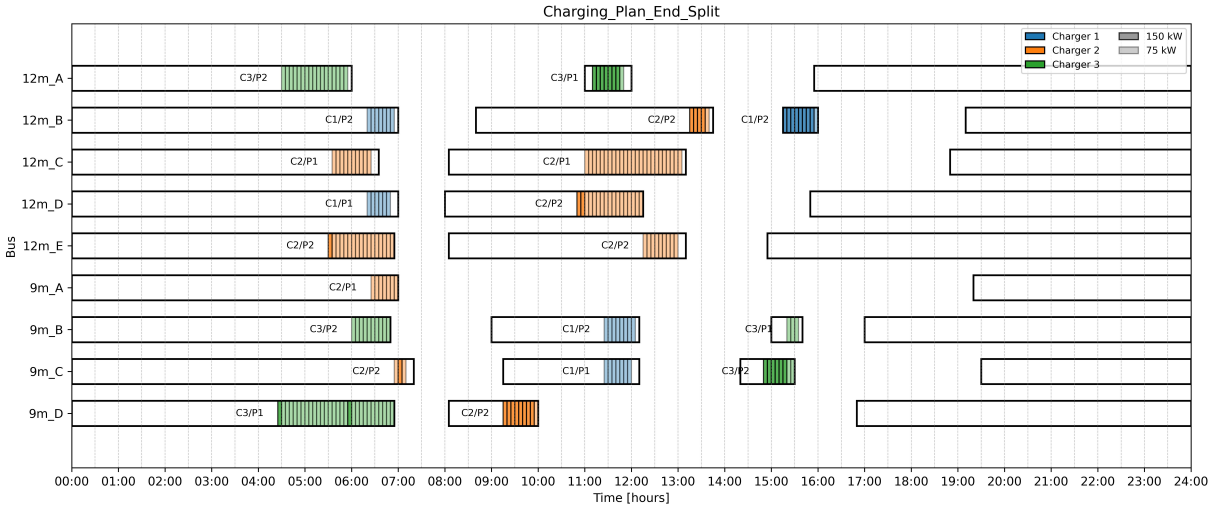


Figure 4.16: Gantt chart illustrating the optimized charging schedule of the fleet in the End-Split scenario under school period operation.

4.4. Application of the Economic Evaluation Model

The outputs of the Battery Optimization Model and the Charging Optimization Model are subsequently used as input to the Economic Evaluation Model. This final Python script, described in detail in the previous chapter, allows the computation of the Life Cycle Cost for each analyzed scenario. Each scenario is evaluated under three different bus lifetime assumptions, resulting in a total of fifteen Life Cycle Cost assessments.

With respect to energy expenditures, the model accounts for the fact that each bus operates under both a school period schedule and a non-school period schedule over the year, which are characterized by different energy demands and by charging activities distributed across different time bands. Furthermore, for each scenario, the number of chargers is assumed to be equal to the maximum between the number required to satisfy the energy demand and operational constraints during the school period and the number required during the non-school period. In this way, the charging infrastructure is dimensioned to ensure feasibility under the most demanding operating condition.

Regarding the charging infrastructure considered in this study, a purchase cost of 40 000 € per charger has been assumed [65], together with an annual maintenance cost equal to 5% of the investment cost and a useful lifetime of 24 years, in line with assumptions commonly adopted in the literature [66].

All the remaining economic assumptions adopted in the model have already been discussed in Chapter 3 and are not repeated here for the sake of brevity. The detailed results of all fifteen Life Cycle Cost computations are not fully reported in this thesis. As an illustrative example, Figure 4.17 presents the breakdown of the Life Cycle Cost for the Base scenario under the optimistic bus lifetime assumption.

In Figure 4.17, both capital expenditures and operational expenditures are reported for each year of operation. In addition, the residual value of the batteries is accounted for in the year in which a replacement occurs, while the residual value of the chargers is considered in the final year of the simulation. These values are then used to compute the annual cash flow and the cumulative LCC.

Year	OPEX ENERGY	OPEX CHARGERS	CAPEX CHARGERS	CAPEX BATTERIES	RESIDUAL BATTERY VALUE	RESIDUAL CHARGER VALUE	CF	DISCOUNTED CF	LCC	LCC ENERGY	LCC CHARGERS	LCC BATTERIES
2026	69028	6000	120000	0	0	0	-195028	-195028	195028	69028	126000	0
2027	69028	6000	0	0	0	0	-75028	-72842	267870	136045	131825	0
2028	69028	6000	0	0	0	0	-75028	-70721	338591	201110	137481	0
2029	69028	6000	0	0	0	0	-75028	-68661	407252	264280	142972	0
2030	69028	6000	0	0	0	0	-75028	-66661	473913	325611	148303	0
2031	69028	6000	0	0	0	0	-75028	-64720	538633	385155	153478	0
2032	69028	6000	0	0	0	0	-75028	-62835	601467	442964	158503	0
2033	69028	6000	0	0	0	0	-75028	-61004	662472	499090	163382	0
2034	69028	6000	0	138944	61751	0	-152221	-120165	782636	553581	168118	60937
2035	69028	6000	0	248115	109428	0	-213715	-163795	946431	606485	172717	167229
2036	69028	6000	0	0	0	0	-75028	-55828	1002258	657848	177181	167229
2037	69028	6000	0	0	0	0	-75028	-54202	1056460	707715	181516	167229
2038	69028	6000	0	0	0	0	-75028	-52623	1109083	756130	185724	167229
2039	69028	6000	0	0	0	0	-75028	-51090	1160173	803135	189810	167229
2040	69028	6000	0	0	0	0	-75028	-49602	1209775	848770	193776	167229
2041	69028	6000	0	0	0	0	-75028	-48157	1257933	893076	197628	167229
2042	69028	6000	0	138944	61751	0	-152221	-94859	1352792	936092	201367	215333
2043	69028	6000	0	0	0	0	-75028	-45393	1398185	977855	204997	215333
2044	69028	6000	0	248115	109428	0	-213715	-125535	1523720	1018402	208521	296797
2045	69028	6000	0	0	207463	20000	152435	86931	1436788	1057767	200537	178484

Figure 4.17: Breakdown of the LCC for the Base scenario under the optimistic bus lifetime assumption.

Once the LCCs have been computed, it becomes possible to compare the different scenarios across the considered time horizons. The first time horizon analyzed is 12 years, which corresponds to a pessimistic estimate of the useful life of electric buses. Under this assumption, after 12 years of operation the buses are considered to have reached their End of Life and are therefore replaced, regardless of any battery replacements that may have occurred during the period.

Table 4.3 reports the Life Cycle Cost for each scenario under this pessimistic lifetime assumption. For clarity, each LCC is decomposed into its three main components, namely energy, chargers, and batteries expenditures. It can be observed that, in some scenarios, the battery-related contribution to the LCC is negative. This indicates that the revenues obtained from the sale of dismissed batteries exceed the costs incurred for battery replacements over the considered time horizon. This result is explained by the modeling assumptions introduced in Chapter 3. In particular, at the beginning of the simulation each bus is assumed to be equipped with new batteries, whose initial cost, together with the purchase cost of the bus, is not included in the LCC computation, as it is identical for all scenarios. Neglecting these common costs is therefore consistent with standard practice and allows the comparison to focus exclusively on the cost differences induced by the adopted charging and battery management strategies.

Scenario	**Energy**	**Chargers**	**Batteries**	**Total LCC**
BASE SCENARIO	707 715 €	138 170 €	21 017 €	866 902 €
START SCENARIO	702 514 €	92 114 €	-80 627 €	714 001 €
END SCENARIO	609 541 €	184 227 €	-130 556 €	663 212 €
START-SPLIT SCENARIO	691 999 €	138 170 €	-134 007 €	696 162 €
END-SPLIT SCENARIO	650 921 €	138 170 €	-138 353 €	650 738 €

Table 4.3: Total LCC and the breakdown into energy, chargers, and battery costs for each charging scenario under the pessimistic bus lifetime assumption (12 years).

The data reported in Table 4.3 are used to generate the graphical representation shown in Figure 4.18, which enables a more intuitive comparison of the results across the different scenarios. The figure highlights that, for the analyzed fleet, moving from the Base scenario, in which no optimization strategies are applied, to any of the optimized scenarios, the Public Transport Operator can achieve savings of up to approximately 200 000 € over the life cycle of the fleet. However, it can also be observed that the differences among the four optimized scenarios are relatively small. Consequently, the choice of one charging strategy over another is not primarily driven by the extension of the battery lifetime guaranteed by each scenario, but rather by the costs associated with the charging infrastructure and, most importantly, by energy expenditures, whose contribution to the overall Life Cycle Cost has been shown to be predominant.

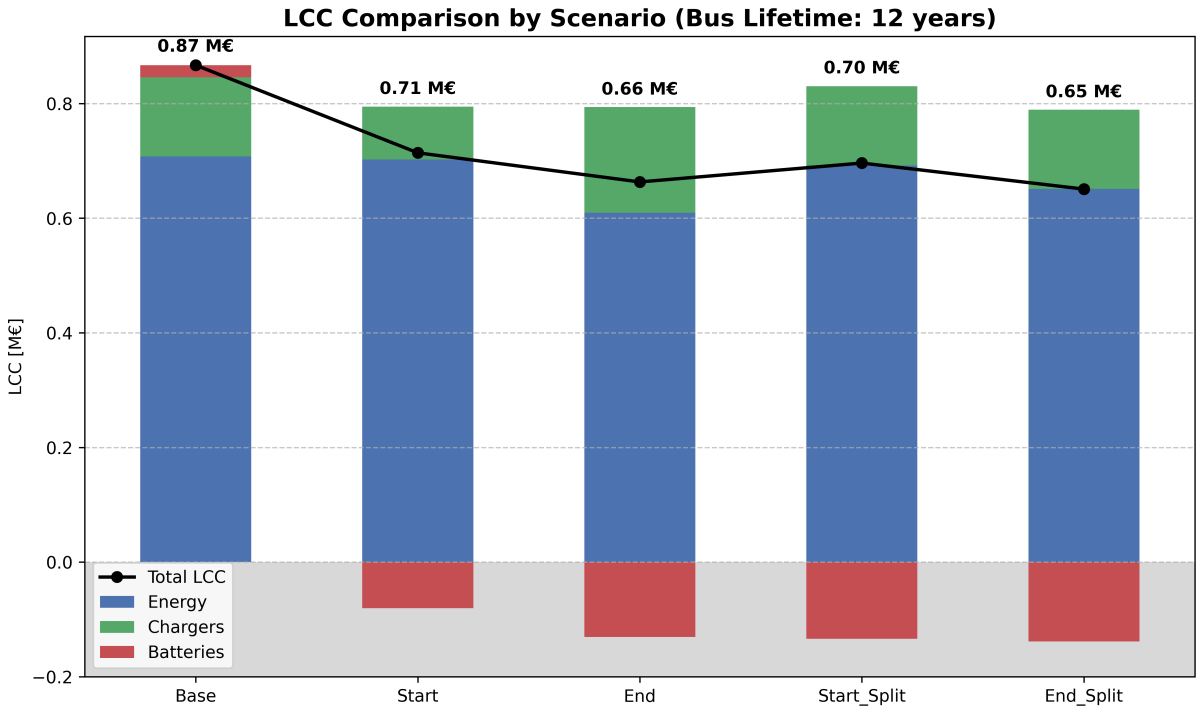


Figure 4.18: Graphical representation of the total LCC and its components for each charging scenario under the pessimistic bus lifetime assumption.

The second time horizon analyzed is 16 years, which corresponds to a moderate estimate of the useful life of electric buses. Under this assumption, the buses are dismissed after 16 years of operation. This time horizon represents a realistic and commonly adopted service life, in line with the fleet renewal policies currently applied by the operator. Table 4.4 reports the Life Cycle Cost for each scenario under this moderate lifetime assumption.

It can be observed that, for the Start scenario, the battery-related component of the LCC is no longer a revenue but becomes a cost. This change is a direct consequence of extending the analysis horizon from 12 to 16 years. In fact, under the Start scenario, as well as under the Base scenario, the useful battery lifetime for both 9-meter and 12-meter buses is shorter than 16 years, and battery replacements are therefore required within the vehicle lifetime.

Scenario	Energy	Chargers	Batteries	Total LCC
BASE SCENARIO	893 076 €	171 953 €	53 103 €	1 118 132 €
START SCENARIO	886 513 €	114 635 €	24 064 €	1 025 212 €
END SCENARIO	769 188 €	229 271 €	-72 362 €	926 097 €
START-SPLIT SCENARIO	873 244 €	171 953 €	-70 998 €	974 199 €
END-SPLIT SCENARIO	821 407 €	171 953 €	-116 707 €	876 653 €

Table 4.4: Total LCC and the breakdown into energy, chargers, and battery costs for each charging scenario under the moderate bus lifetime assumption (16 years).

The data reported in Table 4.4 are used to generate the graphical representation for the 16-year time horizon, shown in Figure 4.19. Also in this case, the difference between the Base scenario and the other scenarios is significant. Moreover, for this time horizon, the differences among the various optimization scenarios are no longer negligible. The Start scenario no longer represents a favorable solution, while the End scenario performs better than the Start-Split scenario. Among all the analyzed options, the End-Split scenario emerges as the best alternative.

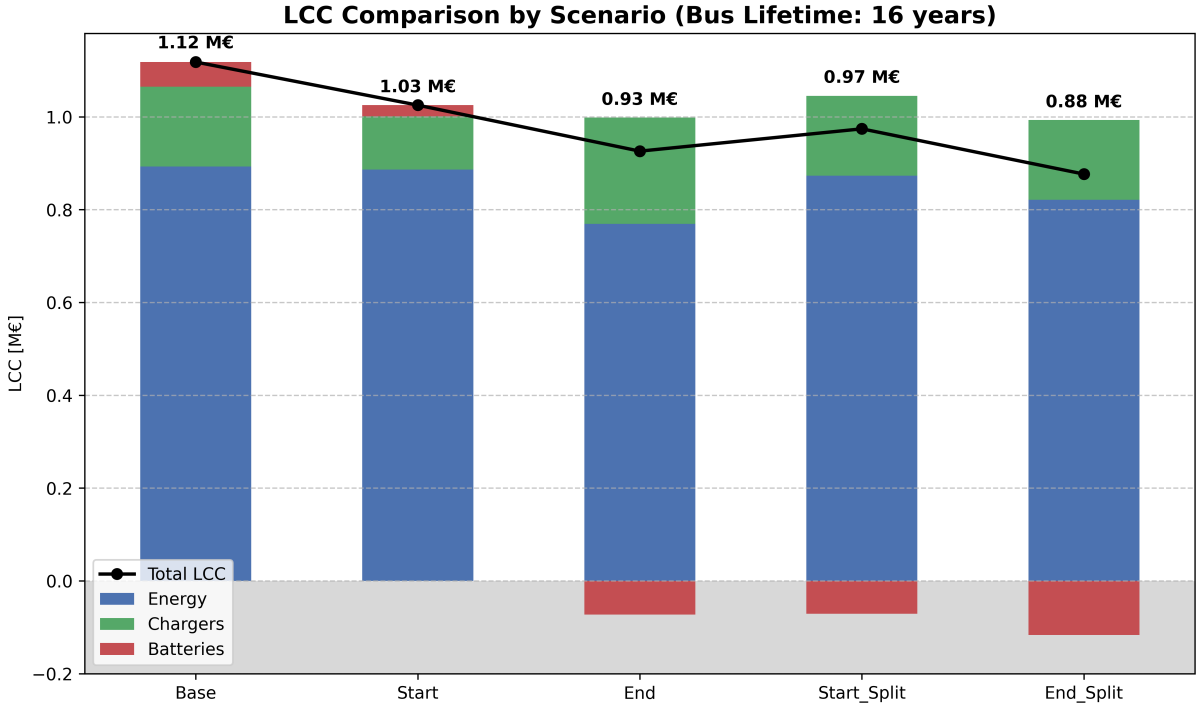


Figure 4.19: Graphical representation of the total LCC and its components for each charging scenario under the moderate bus lifetime assumption.

Finally, the last time horizon analyzed is 20 years, which corresponds to an optimistic estimate of the useful life of electric buses. Under this assumption, the buses are dismissed after 20 years of operation. Although this represents a relatively long service life, conventional diesel buses are often able to reach such an operational age. Therefore, it is reasonable to assume that electric buses may achieve comparable, or potentially even superior, levels of durability over time. Table 4.5 reports the Life Cycle Cost for each scenario under this optimistic lifetime assumption.

From Table 4.5, it can be observed that the battery-related component of the LCC becomes a cost also in the End scenario. As a result, for the first time, the Life Cycle Cost of this scenario exceeds that of the Start-Split scenario.

Scenario	**Energy**	**Chargers**	**Batteries**	**Total LCC**
BASE SCENARIO	1 057 767 €	200 537 €	178 484 €	1 436 788 €
START SCENARIO	1 049 993 €	133 691 €	49 562 €	1 233 246 €
END SCENARIO	911 033 €	267 383 €	17 830 €	1 196 246 €
START-SPLIT SCENARIO	986 985 €	200 537 €	-49 859 €	1 137 663 €
END-SPLIT SCENARIO	972 881 €	200 537 €	-62 510 €	1 110 908 €

Table 4.5: Total LCC and the breakdown into energy, chargers, and battery costs for each charging scenario under the optimistic bus lifetime assumption (20 years).

The data reported in Table 4.5 are used to generate the graphical comparison shown in Figure 4.20. As in the previous analyses, the most significant difference is observed between the Base scenario and the four optimized scenarios. However, some minor differences among the four optimized scenarios can also be observed. The End-Split scenario emerges as the overall best solution, performing slightly better than the Start-Split scenario and allowing the PTO to achieve savings of more than 300 000 € compared to the Base scenario.

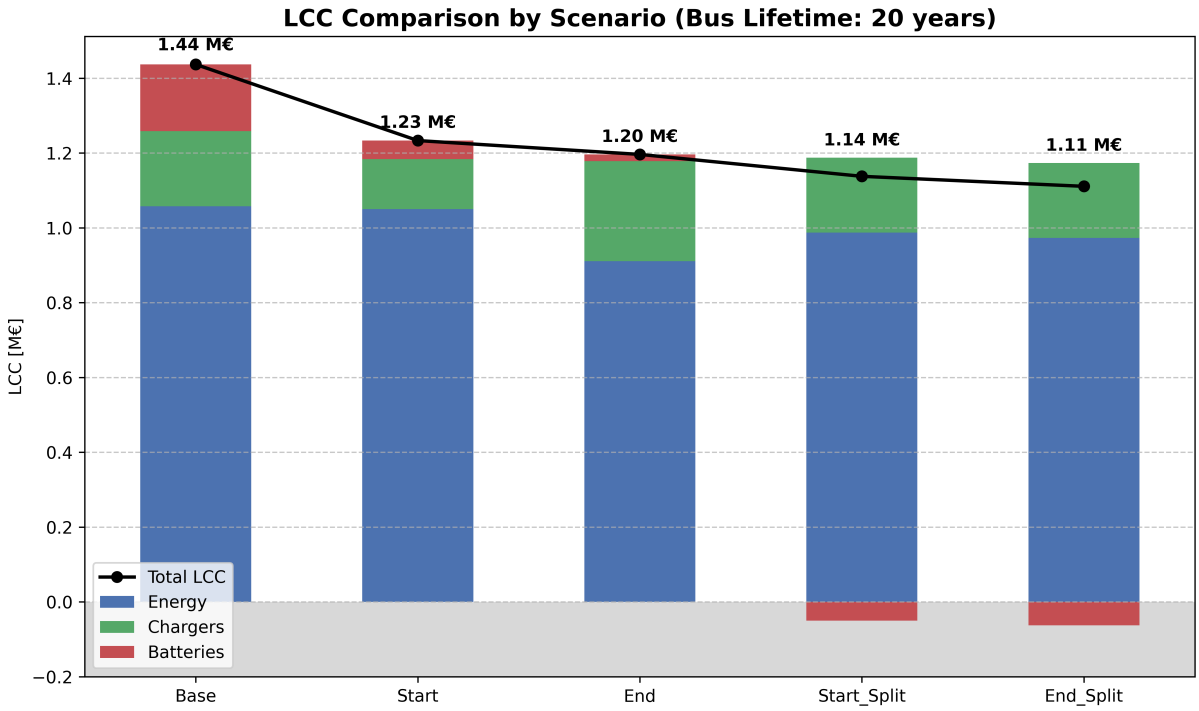


Figure 4.20: Graphical representation of the total LCC and its components for each charging scenario under the optimistic bus lifetime assumption.

By applying the developed models to the considered case study, it has been possible to demonstrate their capability to represent and simulate a real-life operational context, including its inherent complexity and variability.

Overall, the results highlight that the relationship between the extension of battery lifetime and the Life Cycle Cost of electric buses is not linear. Consequently, a scenario that maximizes battery lifespan should not be adopted a priori without considering its impact on the other cost components, particularly energy and charging infrastructure costs. The main conclusions and key insights emerging from this thesis, together with potential future developments and model extensions, are discussed in the final chapter.

5 | Conclusions and future developments

In this thesis, a methodological approach has been presented to make applicable to real-world situations the theoretical models which allow the computation of the State of Health of Li-ion batteries.

This has been made possible thanks to the creation of a Python environment in which the PTO can provide inputs corresponding to the technical characteristics of the adopted vehicles, as well as the characteristics of the service, the environment, and the procedures adopted in the company. This makes the model adaptable to the requirements of specific situations, providing a tailored estimation of the State of Health under different operational scenarios. Another important feature of this work is its easy upgradability. Indeed, if research advances make a new mathematical model available to better predict battery degradation, or if the user possesses a model that, based on his experience, better describes the behavior of his batteries, the underlying mathematical model of this tool can be easily substituted with the desired one, while the proposed methodological approach and simulation environment remain fully functional and consistent.

Notably, it has been demonstrated that extending the useful life of BEB batteries represents only a minor aspect within the broader framework of BEB cost optimization. While increasing battery longevity contributes to reducing the life cycle costs of the batteries, other factors, particularly the charging infrastructure and, above all, energy costs, have a much stronger influence on the overall economic benefits achievable by a Public Transport Operator when adopting a specific charging strategy. As a result, the evaluation of any charging strategy cannot be based solely on its potential to prolong battery life, but must instead consider the full set of cost components affected by operational and technical decisions.

It can be observed that energy costs can differ substantially according to the type of energy supply contract in place. For example, a contract that establishes time-of-use tariffs, with different prices for different periods of the day, may produce results very different from a flat-rate contract, in which the energy price is constant regardless of the time of consumption. Moreover, in some cases, the PTO may partially or fully self-produce the energy required to operate its electric fleet through owned power generation facilities, further modifying the economic impact of charging strategies.

An important component developed in this thesis is the charging optimization algorithm, which can be used to optimize the charging schedule of a BEB fleet in any operational context, regardless of the specific charging strategy adopted. This makes it a powerful tool that can also be applied beyond the scope of the present study.

5.1. Future developments

Future developments could focus on integrating the Python models presented in this thesis into a single optimization algorithm aimed at identifying the charging strategy that minimizes the overall Life Cycle Cost of the fleet. Such an extension would be an interesting advancement, but it requires substantial computational resources. Indeed, the optimization algorithm developed in this thesis, whose objective was to minimize the number of chargers required, which represents only one component of the fleet's LCC, has already proven to be computationally intensive, as described in Section 4.3. Consequently, an upgraded model that includes all LCC components would not be feasible to run on a standard personal laptop. However, its implementation on more powerful computing platforms or dedicated computational resources could enable comprehensive analyses and would represent a valuable and interesting contribution to this field of research.

Bibliography

[1] Council of the European Union. Inquinamento. URL https://www.consilium.europa.eu/it/topics/pollution/. Accessed: January 2026.

[2] Met Office. Effects of climate change. URL https://weather.metoffice.gov.uk/climate-change/effects-of-climate-change. Accessed: February 2026.

[3] Our World in Data. Greenhouse gas emissions, 2024. URL https://ourworldindata.org/greenhouse-gas-emissions. Accessed: February 2026.

[4] Sara Perinetto. Come il cambiamento climatico impatta sulle barriere coralline. URL https://www.renewablematter.eu/come-cambiamento-climatico-impatta-barriere-coralline. Accessed: January 2026.

[5] Our World in Data. Emissions by sector, 2024. URL https://ourworldindata.org/emissions-by-sector. Accessed: February 2026.

[6] Our World in Data. Electricity production by source: fossil, renewables, and nuclear, 2026. URL https://ourworldindata.org/grapher/electricity-fossil-renewables-nuclear-line. Accessed: February 2026.

[7] European Environment Agency. Europes environment 2025 - main report. Technical report, European Environment Agency, 2025.

[8] Giulio Guandalini. Energy and emissions in transportation systems. Lecture slides, Politecnico di Milano, 2024.

[9] Allianz Research. The chinese challenge to the european automotive industry. Technical report, Allianz Research, 2023.

[10] European Automobile Manufacturers' Association (ACEA). Automotive insights – charging ahead: accelerating the rollout of eu electric vehicle charging infrastructure. Technical report, European Automobile Manufacturers' Association (ACEA), 4 2024.

[11] European Automobile Manufacturers' Association (ACEA). Vehicles on european

roads. Technical report, European Automobile Manufacturers' Association (ACEA), 1 2025.

[12] European Alternative Fuels Observatory (EAFO). Vehicles and fleet overview for the european union (eu27), 2025. URL https://alternative-fuels-observatory.ec.europa.eu/transport-mode/road/european-union-eu27/vehicles-and-fleet. Accessed: January 2026.

[13] Mordor Intelligence. Europe electric bus market size share analysis - growth trends and forecast (2026 - 2031). Technical report, Mordor Intelligence, 2026. URL https://www.mordorintelligence.com/industry-reports/europe-electric-bus-market. Accessed: January 2026.

[14] Svetlana Ushak, Wenji Song, Paula E. Marín, Yanio Milian, Ding Zhao, Mario Grageda, Wenye Lin, Mingbiao Chen, and Ying Han. A review on phase change materials employed in li-ion batteries for thermal management systems. *Applied Materials Today*, 37:102021, 2024. ISSN 2352-9407. doi: https://doi.org/10.1016/j.apmt.2023.102021. URL https://www.sciencedirect.com/science/article/pii/S2352940723002901.

[15] International Energy Agency (IEA). Electric vehicle battery sales share by chemistry and region, 2022–2024, 2025. URL https://www.iea.org/data-and-statistics/charts/electric-vehicle-battery-sales-share-by-chemistry-and-region-2022-2024. Accessed: January 2026.

[16] Cosimo Palleschi. La corsa all'oro blu: perché il cobalto può definire gli equilibri del prossimo secolo, 11 2023. URL https://www.forbes.it/2023/11/13/cobalto-perche-oro-blu-definire-secolo-geopolitica/. Accessed: January 2026.

[17] Aniruddha Joshi, Dillip Kumar Mishra, Rajendra Singh, Jiangfeng Zhang, and Yi Ding. A comprehensive review of solid-state batteries. *Applied Energy*, 386:125546, 2025. ISSN 0306-2619. doi: https://doi.org/10.1016/j.apenergy.2025.125546. URL https://www.sciencedirect.com/science/article/pii/S0306261925002764.

[18] A. F. Burke and J. Zhao. Advanced battery technologies: Bus, heavy-duty vocational truck, and construction machinery applications. Technical report, UC Davis, National Center for Sustainable Transportation, 2025. URL https://escholarship.org/uc/item/5zx1k22k.

[19] Eduardo Redondo-Iglesias, Pascal Venet, and Serge Pelissier. Modelling lithium-ion battery ageing in electric vehicle applications—calendar and cycling ageing combina-

tion effects. *Batteries*, 6(1), 2020. ISSN 2313-0105. doi: 10.3390/batteries6010014. URL https://www.mdpi.com/2313-0105/6/1/14.

[20] Eduardo Redondo-Iglesias, Pascal Venet, and Serge Pelissier. Calendar and cycling ageing combination of batteries in electric vehicles. *Microelectronics Reliability*, 88-90:1212–1215, 2018. ISSN 0026-2714. doi: https://doi.org/10.1016/j.microrel.2018.06.113. URL https://www.sciencedirect.com/science/article/pii/S0026271418305377. 29th European Symposium on Reliability of Electron Devices, Failure Physics and Analysis (ESREF 2018).

[21] Jia Guo, Yaqi Li, Kjeld Pedersen, and Daniel-Ioan Stroe. Lithium-ion battery operation, degradation, and aging mechanism in electric vehicles: An overview. *Energies*, 14(17), 2021. ISSN 1996-1073. doi: 10.3390/en14175220. URL https://www.mdpi.com/1996-1073/14/17/5220.

[22] Gulsah Yarimca and Erdal Cetkin. Review of cell level battery (calendar and cycling) aging models: Electric vehicles. *Batteries*, 10(11), 2024. ISSN 2313-0105. doi: 10.3390/batteries10110374. URL https://www.mdpi.com/2313-0105/10/11/374.

[23] Yang Gao, Jiuchun Jiang, Caiping Zhang, Weige Zhang, and Yan Jiang. Aging mechanisms under different state-of-charge ranges and the multi-indicators system of state-of-health for lithium-ion battery with li(nimnco)o2 cathode. *Journal of Power Sources*, 400:641–651, 2018. ISSN 0378-7753. doi: https://doi.org/10.1016/j.jpowsour.2018.07.018. URL https://www.sciencedirect.com/science/article/pii/S0378775318307262.

[24] Joris de Hoog, Jean-Marc Timmermans, Daniel Ioan-Stroe, Maciej Swierczynski, Joris Jaguemont, Shovon Goutam, Noshin Omar, Joeri Van Mierlo, and Peter Van Den Bossche. Combined cycling and calendar capacity fade modeling of a nickel-manganese-cobalt oxide cell with real-life profile validation. *Applied Energy*, 200:47–61, 2017. ISSN 0306-2619. doi: https://doi.org/10.1016/j.apenergy.2017.05.018. URL https://www.sciencedirect.com/science/article/pii/S0306261917305251.

[25] Evelina Wikner and Torbjörn Thiringer. Extending battery lifetime by avoiding high soc. *Applied Sciences*, 8(10), 2018. ISSN 2076-3417. doi: 10.3390/app8101825. URL https://www.mdpi.com/2076-3417/8/10/1825.

[26] Samuel Pelletier, Ola Jabali, Gilbert Laporte, and Marco Veneroni. Battery degradation and behaviour for electric vehicles: Review and numerical analyses of several models. *Transportation Research Part B: Methodological*, 103:158–187, 2017. ISSN 0191-2615. doi: https://doi.org/10.1016/j.trb.2017.01.020. URL

https://www.sciencedirect.com/science/article/pii/S0191261516303794. Green Urban Transportation.

[27] Noshin Omar, Mohamed Abdel Monem, Yousef Firouz, Justin Salminen, Jelle Smekens, Omar Hegazy, Hamid Gaulous, Grietus Mulder, Peter Van den Bossche, Thierry Coosemans, and Joeri Van Mierlo. Lithium iron phosphate based battery – assessment of the aging parameters and development of cycle life model. *Applied Energy*, 113:1575–1585, 2014. ISSN 0306-2619. doi: https://doi.org/10.1016/j.apenergy.2013.09.003. URL https://www.sciencedirect.com/science/article/pii/S0306261913007393.

[28] M. Maures, Y. Zhang, C. Martin, J.-Y. Delétage, J.-M. Vinassa, and O. Briat. Impact of temperature on calendar ageing of lithium-ion battery using incremental capacity analysis. *Microelectronics Reliability*, 100-101:113364, 2019. ISSN 0026-2714. doi: https://doi.org/10.1016/j.microrel.2019.06.056. URL https://www.sciencedirect.com/science/article/pii/S0026271419304731. 30th European Symposium on Reliability of Electron Devices, Failure Physics and Analysis.

[29] Xuning Feng, Minggao Ouyang, Xiang Liu, Languang Lu, Yong Xia, and Xiangming He. Thermal runaway mechanism of lithium ion battery for electric vehicles: A review. *Energy Storage Materials*, 10:246–267, 2018. ISSN 2405-8297. doi: https://doi.org/10.1016/j.ensm.2017.05.013. URL https://www.sciencedirect.com/science/article/pii/S2405829716303464.

[30] Binay Paudyal, Ashutosh Timilsina, Abinash Khanal, and Saugat Ghimire. Comparative analysis of cell balancing topologies in battery management system. 05 2019.

[31] Sonu Kumar, S. Koteswara Rao, Arvind R. Singh, and Raj Naidoo. Switched-resistor passive balancing of li-ion battery pack and estimation of power limits for battery management system. *International Journal of Energy Research*, 2023(1):5547603, 2023. doi: https://doi.org/10.1155/2023/5547603. URL https://onlinelibrary.wiley.com/doi/abs/10.1155/2023/5547603.

[32] Anupama R Itagi, Rakhee Kallimani, Krishna Pai, Sridhar Iyer, and Onel L. A. Lopez. Cell balancing for the transportation sector: Techniques, challenges, and future research directions, 2024. URL https://arxiv.org/abs/2404.13890.

[33] Thiruvonasundari Duraisamy and Deepa Kaliyaperumal. Adaptive passive balancing in battery management system for e-mobility. *International Journal of Energy*

Research, 45(7):10752–10764, 2021. doi: https://doi.org/10.1002/er.6560. URL https://onlinelibrary.wiley.com/doi/abs/10.1002/er.6560.

[34] Alessandro Santiago, Leo Allen Tayo, Janine Giron, Mark Arnel Domingo, and Lew Tria. Evaluation of cell balancing methods for high capacity electric vehicle lithium-ion battery packs. In *2024 IEEE Transportation Electrification Conference and Expo, Asia-Pacific (ITEC Asia-Pacific)*, pages 664–668, 2024. doi: 10.1109/ITECAsia-Pacific63159.2024.10738638.

[35] Kristaps Vitols. Research and development of battery packs and their balancing methods for personal mobility vehicles. Master's thesis, RIGA TECHNICAL UNIVERSITY, 05 2022.

[36] Johannes Schmalstieg, Stefan Käbitz, Madeleine Ecker, and Dirk Uwe Sauer. A holistic aging model for li(nimnco)o2 based 18650 lithium-ion batteries. *Journal of Power Sources*, 257:325–334, 2014. ISSN 0378-7753. doi: https://doi.org/10.1016/j.jpowsour.2014.02.012. URL https://www.sciencedirect.com/science/article/pii/S0378775314001876.

[37] Long Lam and Pavol Bauer. Practical capacity fading model for li-ion battery cells in electric vehicles. *IEEE Transactions on Power Electronics*, 28(12):5910–5918, 2013. doi: 10.1109/TPEL.2012.2235083.

[38] Maciej Swierczynski, Daniel-Ioan Stroe, Ana-Irina Stan, Remus Teodorescu, and Søren Knudsen Kær. Lifetime estimation of the nanophosphate $LiFePO_4$/C battery chemistry used in fully electric vehicles. *IEEE Transactions on Industry Applications*, 51(4):3453–3461, 2015. doi: 10.1109/TIA.2015.2405500.

[39] E. Sarasketa-Zabala, I. Gandiaga, L.M. Rodriguez-Martinez, and I. Villarreal. Calendar ageing analysis of a lifepo4/graphite cell with dynamic model validations: Towards realistic lifetime predictions. *Journal of Power Sources*, 272:45–57, 2014. ISSN 0378-7753. doi: https://doi.org/10.1016/j.jpowsour.2014.08.051. URL https://www.sciencedirect.com/science/article/pii/S0378775314013068.

[40] E. Sarasketa-Zabala, I. Gandiaga, E. Martinez-Laserna, L.M. Rodriguez-Martinez, and I. Villarreal. Cycle ageing analysis of a lifepo4/graphite cell with dynamic model validations: Towards realistic lifetime predictions. *Journal of Power Sources*, 275:573–587, 2015. ISSN 0378-7753. doi: https://doi.org/10.1016/j.jpowsour.2014.10.153. URL https://www.sciencedirect.com/science/article/pii/S0378775314017728.

[41] Madeleine Ecker, Nerea Nieto, Stefan Käbitz, Johannes Schmalstieg, Holger Blanke,

Alexander Warnecke, and Dirk Uwe Sauer. Calendar and cycle life study of li(nimnco)o2-based 18650 lithium-ion batteries. *Journal of Power Sources*, 248:839–851, 2014. ISSN 0378-7753. doi: https://doi.org/10.1016/j.jpowsour.2013.09.143. URL https://www.sciencedirect.com/science/article/pii/S0378775313016510.

[42] Foroogh Behnia, Beth-Anne Schuelke-Leech, and Mitra Mirhassani. Optimizing sustainable urban mobility: A comprehensive review of electric bus scheduling strategies and future directions. *Sustainable Cities and Society*, 108:105497, 2024. ISSN 2210-6707. doi: https://doi.org/10.1016/j.scs.2024.105497. URL https://www.sciencedirect.com/science/article/pii/S221067072400324X.

[43] Yi He, Zhaocai Liu, and Ziqi Song. Integrated charging infrastructure planning and charging scheduling for battery electric bus systems. *Transportation Research Part D: Transport and Environment*, 111:103437, 2022. ISSN 1361-9209. doi: https://doi.org/10.1016/j.trd.2022.103437. URL https://www.sciencedirect.com/science/article/pii/S1361920922002632.

[44] Yi He, Zhaocai Liu, and Ziqi Song. Joint optimization of electric bus charging infrastructure, vehicle scheduling, and charging management. *Transportation Research Part D: Transport and Environment*, 117:103653, 2023. ISSN 1361-9209. doi: https://doi.org/10.1016/j.trd.2023.103653. URL https://www.sciencedirect.com/science/article/pii/S1361920923000500.

[45] Yongxing Wang, Feixiong Liao, Jun Bi, and Chaoru Lu. Optimal battery electric bus system planning considering heterogeneous vehicles, opportunity charging, and battery degradation. *Renewable Energy*, 237:121596, 2024. ISSN 0960-1481. doi: https://doi.org/10.1016/j.renene.2024.121596. URL https://www.sciencedirect.com/science/article/pii/S0960148124016641.

[46] Yiming Bie, Jinhua Ji, Xiangyu Wang, and Xiaobo Qu. Optimization of electric bus scheduling considering stochastic volatilities in trip travel time and energy consumption. *Computer-Aided Civil and Infrastructure Engineering*, 36(12): 1530–1548, 2021. doi: https://doi.org/10.1111/mice.12684. URL https://onlinelibrary.wiley.com/doi/abs/10.1111/mice.12684.

[47] Aniruddha Jana, Gregory M. Shaver, and R. Edwin García. Physical, on the fly, capacity degradation prediction of linimncoo2-graphite cells. *Journal of Power Sources*, 422:185–195, 2019. ISSN 0378-7753. doi: https://doi.org/10.1016/j.jpowsour.2019.

02.073. URL https://www.sciencedirect.com/science/article/pii/S0378775319301983.

[48] Samuel Pelletier, Ola Jabali, and Gilbert Laporte. Charge scheduling for electric freight vehicles. *Transportation Research Part B: Methodological*, 115:246–269, 2018. ISSN 0191-2615. doi: https://doi.org/10.1016/j.trb.2018.07.010. URL https://www.sciencedirect.com/science/article/pii/S0191261517308871.

[49] Sekyung Han, Soohee Han, and Hirohisa Aki. A practical battery wear model for electric vehicle charging applications. *Applied Energy*, 113:1100–1108, 2014. ISSN 0306-2619. doi: https://doi.org/10.1016/j.apenergy.2013.08.062. URL https://www.sciencedirect.com/science/article/pii/S030626191300706X.

[50] Benedikt Lunz, Zexiong Yan, Jochen Bernhard Gerschler, and Dirk Uwe Sauer. Influence of plug-in hybrid electric vehicle charging strategies on charging and battery degradation costs. *Energy Policy*, 46:511–519, 2012. ISSN 0301-4215. doi: https://doi.org/10.1016/j.enpol.2012.04.017. URL https://www.sciencedirect.com/science/article/pii/S0301421512003175.

[51] Adnane Houbbadi, Rochdi Trigui, Serge Pelissier, Eduardo Redondo-Iglesias, and Tanguy Bouton. Optimal scheduling to manage an electric bus fleet overnight charging. *Energies*, 12(14), 2019. ISSN 1996-1073. doi: 10.3390/en12142727. URL https://www.mdpi.com/1996-1073/12/14/2727.

[52] Olly Bartrum. Electricity market, 09 2022. URL https://www.instituteforgovernment.org.uk/article/explainer/electricity-market. Accessed: January 2026.

[53] European Union Agency for the Cooperation of Energy Regulators (ACER). Bidding zone review. URL https://www.acer.europa.eu/electricity/market-rules/capacity-allocation-and-congestion-management/bidding-zone-review. Accessed: January 2026.

[54] Daniel Felix Ahelegbey, Roberto Casarin, Emmanuel Senyo Fianu, and Luigi Grossi. Structural changes in contagion channels: the impact of covid-19 on the italian electricity market. *SSRN Electronic Journal*, 01 2021. doi: 10.2139/ssrn.3988660.

[55] GME – Gestore dei Mercati Energetici. Pun index gme – day-ahead market (mgp) results, 2026. URL https://www.mercatoelettrico.org/en-us/Home/Results/Electricity/MGP/Results/PUN. Accessed: January 2026.

[56] Senergie. Crisi energetica in europa: cause e possibili scenari. URL https://ww

w.senergie.it/crisi-energetica-in-europa-cause-e-possibili-scenari/. Accessed: January 2026.

[57] Autorità di Regolazione per Energia Reti e Ambiente (ARERA). Atlante per il consumatore: la bolletta elettrica — cosa si paga. URL https://www.arera.it/atlante-per-il-consumatore/elettricita/la-bolletta/cosa-si-paga. Accessed: January 2026.

[58] Forsee Power. Zen 42 high-energy battery, 2024. URL https://www.forseepower.com/lithium-ion-battery/high-energy-batteries/zen-42/. Accessed: January 2026.

[59] Google Developers. Or-tools | google for developers, . URL https://developers.google.com/optimization/. Accessed: January 2026.

[60] Gaizka Saldaña, José Ignacio San Martín, Inmaculada Zamora, Francisco Javier Asensio, Oier Oñederra, and Mikel González. Empirical electrical and degradation model for electric vehicle batteries. *IEEE Access*, 8:155576–155589, 2020. doi: 10.1109/ACCESS.2020.3019477.

[61] Google Developers. Cp-sat solver | or-tools, . URL https://developers.google.com/optimization/cp/cp_solver. Accessed: January 2026.

[62] Roger Brereton. Does extended electric bus life call for more durable components?, 7 2025. URL https://www.route-one.net/opinion/does-extended-electric-bus-life-call-for-more-durable-components/. Accessed: January 2026.

[63] Amadeus Bach, Stefan J. Reichelstein, Simona Onori, and Jihan Zhuang. Fair market valuation of electric vehicle batteries in second life applications, 8 2024. URL https://www.gsb.stanford.edu/faculty-research/working-papers/fair-market-valuation-electric-vehicle-batteries-second-life. Accessed: January 2026.

[64] BloombergNEF. Lithium-ion battery pack prices see largest drop since 2017, falling to $115 per kilowatt-hour, 12 2024. URL https://about.bnef.com/insights/commodities/lithium-ion-battery-pack-prices-see-largest-drop-since-2017-falling-to-115-per-kilowatt-hour-bloombergnef/. Accessed: January 2026.

[65] Evedis. X-charge c6eu 150 kw fast charger. URL https://evedis.eu/nl_BE/shop/x-charge-c6eu-150kw-348. Accessed: February 2026.

[66] Zicheng Bi, Robert De Kleine, and Gregory A. Keoleian. Integrated life cycle assessment and life cycle cost model for comparing plug-in versus wireless charging

for an electric bus system. *Journal of Industrial Ecology*, 21(2):344–355, 2017. doi: https://doi.org/10.1111/jiec.12419. URL https://onlinelibrary.wiley.com/doi/abs/10.1111/jiec.12419.

A | Appendix – Python functions

A.1. run_alternating_turns

```
def run_alternating_turns(DoD_turns_S, h_rest_S, h_charge_S,
    day_breaks_S, dur_turns_S, DoD_BASE_S, soc_rest_vals_S, soc_start_S,
    DoD_turns_NS, h_rest_NS, h_charge_NS, day_breaks_NS, dur_turns_NS,
    DoD_BASE_NS, soc_rest_vals_NS, soc_start_NS, plot_soc=False,
    soc_rest_mode="start"):

    S = preprocess_sequence(DoD_turns_S, h_rest_S, h_charge_S,
        day_breaks_S, dur_turns_S, DoD_BASE_S, soc_rest_vals_S,
        soc_start_S, T_rest_S)
    NS = preprocess_sequence(DoD_turns_NS, h_rest_NS, h_charge_NS,
        day_breaks_NS, dur_turns_NS, DoD_BASE_NS, soc_rest_vals_NS,
        soc_start_NS, T_rest_NS)

    # state variables
    SoH = 1.0
    Q_eq = 0.0
    t_eq = 0.0
    turn_idx = 0
    day = 1
    year_day_counter = 1
    balance_counter = 1
    balance= False
    current = S
    SoH_list = [SoH]

    def is_end_of_day(i):
        return (i in day_breaks_set) or (i == n_turns - 1)

    SOC=[]
    TIME=[]

    if isinstance(soc_start_S, (list, np.ndarray)):
        SOC.append(round(soc_start_S[0], 2))
```

```
    else:
        SOC.append(round(soc_start_S, 2))
    TIME.append(0)

    while SoH > SoH_end:
        # switch sequences
        if year_day_counter == 270 and turn_idx>10:
            current = NS
            turn_idx=0
            Q_old = Q_eq
            Q_eq = ((1 - SoH - gamma * S["alpha_turns"][next_i] * t_eq
                **0.75) / (gamma * NS["beta_turns"][0]))**2
            t_eq = ((1 - gamma * S["beta_turns"][next_i] * np.sqrt(Q_old
                ) - SoH) / (gamma * NS["alpha_turns"][0]))**(4.0/3.0)
        if year_day_counter == 0 and turn_idx>10:
            current = S
            turn_idx=0
            Q_old = Q_eq
            Q_eq = ((1 - SoH - gamma * NS["alpha_turns"][next_i] * t_eq
                **0.75) / (gamma * S["beta_turns"][0]))**2
            t_eq = ((1 - gamma * NS["beta_turns"][next_i] * np.sqrt(
                Q_old) - SoH) / (gamma * S["alpha_turns"][0]))**(4.0/3.0)

        # load current sequence variables
        DoD_turns = current["DoD_turns"]
        DoD_BASE = current["DoD_BASE"]
        soc_rest_vals = current["soc_rest_vals"]
        soc_start = current["soc_start"]
        t_charge = current["t_charge"]
        t_rest = current["t_rest"]
        t_turn = current["t_turn"]
        n_turns = current["n_turns"]
        alpha_bal = current["alpha_bal"]
        day_breaks_set = current["day_breaks_set"]
        alpha_turns = current["alpha_turns"]
        beta_turns = current["beta_turns"]
        Q_turns = current["Q_turns"]
        T_rest = current["T_rest"]

        i = turn_idx % n_turns
        next_i = (i + 1) % n_turns
        TIME.append(round(TIME[-1] + t_turn[turn_idx % len(t_turn)], 8))
        TIME.append(round(TIME[-1] + t_rest[turn_idx % len(t_rest)], 8))

```

```
66          # battery balancing
67          if DoD_turns[i] > 0 and balance_counter == 15 and is_end_of_day(
                i):
68              balance= True
69              balance_counter = 0
70              soc_mean_bal = 1 - DoD_turns[i] / 2.0
71              V_mean_bal = 3.32 + 0.78 * soc_mean_bal
72              beta_bal = 7.348e-3 * (V_mean_bal - 3.667)**2 + 7.6e-4 +
                    4.081e-3 * DoD_turns[i]
73              Q_eq = ((1 - SoH - gamma * alpha_turns[i] * t_eq**0.75) / (
                    gamma * beta_bal))**2
74              alpha = alpha_turns[i]
75              beta = beta_bal
76              SOC.append(round(SOC[-1]-DoD_BASE[i], 2))
77              if soc_rest_mode == "start":
78                  SOC.append(1.00)
79                  TIME.append(round(TIME[-1]+t_charge[turn_idx % len(
                        t_charge)], 8))
80                  TIME[-2]=round(TIME[-3]+t_charge[turn_idx % len(t_charge
                        )], 8)
81              else:
82                  SOC.append(round(float(soc_rest_vals[(turn_idx) % len(
                        soc_rest_vals)]), 2))
83                  TIME.append(round(TIME[-1]+t_charge[turn_idx % len(
                        t_charge)], 8))
84              SOC.append(1.00)
85          else:
86              beta = beta_turns[i]
87              # multiple conditional updates for SoH and SOC
88              if soc_rest_mode == "start" and DoD_turns[i] > 0 and
                    balance_counter == 14 and (i+1) in day_breaks_set:
89                  t_eq = ((1 - SoH - gamma * beta_turns[i] * np.sqrt(Q_eq)
                        ) / (gamma * alpha_bal))**(4.0/3.0)
90                  alpha=alpha_bal
91              elif soc_rest_mode == "start" and DoD_turns[i] > 0 and
                    year_day_counter == 269 and (i+1) in day_breaks_set:
92                  t_eq = ((1 - SoH - gamma * beta_turns[i] * np.sqrt(Q_eq)
                        ) / (gamma * NS["alpha_turns"][0]))**(4.0/3.0)
93                  alpha=NS["alpha_turns"][0]
94              else:
95                  alpha = alpha_turns[i]
96
97              if isinstance(soc_start, (list, np.ndarray)) and balance==
                    True and (SOC[-1] - DoD_BASE[i])> soc_start[next_i]:
```

```
98                  SOC_mean= SOC[-1] - DoD_turns[i] / 2.0
99                  V_ab = 3.32 + 0.78 * SOC_mean
100                 beta = 7.348e-3 * (V_ab - 3.667)**2 + 7.6e-4 + 4.081e-3
                        * DoD_turns[i]
101                 V_rest_ab = 3.32 + 0.78 * (SOC[-1] - DoD_turns[i])
102                 alpha = (7.534 * V_rest_ab - 23.75) * 1e6 * np.exp(-6976
                        / T_rest)
103                 Q_old=Q_eq
104                 Q_eq = ((1 - SoH - gamma * alpha_turns[i] * t_eq**0.75)
                        / (gamma * beta))**2
105                 t_eq = ((1 - SoH - gamma * beta_turns[i] * np.sqrt(Q_old
                        )) / (gamma * alpha))**(4.0/3.0)
106                 SOC.append(SOC[-1]-DoD_BASE[i])
107                 SOC.append(SOC[-1])
108                 TIME[-1]=round(TIME[-1] + t_charge[turn_idx % len(
                        t_charge)], 8)
109             else:
110                 balance=False
111                 SOC.append(round(SOC[-1]-DoD_BASE[i], 2))
112                 SOC.append(round(SOC[-1], 2))
113                 # plot SOC update
114                 if DoD_turns[i]!=0 and plot_soc==True:
115                     if soc_rest_mode == "start":
116                         if year_day_counter == 268:
117                             SOC[-1]=(round(float(NS["soc_start"][0]), 2)
                                    )
118                         elif year_day_counter >= 349:
119                             SOC[-1]=(round(float(S["soc_start"][0]), 2))
120                         else:
121                             SOC[-1]=round(float(soc_rest_vals[(turn_idx)
                                    % len(soc_rest_vals)]), 2)
122                         TIME.append(round(TIME[-1] + t_charge[turn_idx %
                                len(t_charge)], 8))
123                         TIME[-2] = round(TIME[-3] + t_charge[turn_idx %
                                len(t_charge)], 8)
124                     else:
125                         TIME.append(round(TIME[-1]+t_charge[turn_idx %
                                len(t_charge)], 8))
126                     if year_day_counter == 268:
127                         SOC.append(round(float(NS["soc_start"][0]), 2))
128                     elif year_day_counter >= 349:
129                         SOC.append(round(float(S["soc_start"][0]), 2))
130                     else:
```

```
                        SOC.append(round(float(soc_start[(turn_idx+1) %
                            len(soc_start)]), 2))

        t = t_rest[turn_idx % len(t_rest)]
        t_f = t_eq + t
        Q_f = Q_eq + Q_turns[i]
        SoH = 1 - gamma * beta * np.sqrt(Q_f) - gamma * alpha * (t_f)
            **0.75

        if is_end_of_day(i):
            day += 1
            year_day_counter += 1
            balance_counter += 1
            SoH_list.append(SoH)
            # rest days
            if (day > 0) and (year_day_counter % 6 == 0) and
                year_day_counter != 270:
                t_f += 1
                SoH = 1 - gamma * beta * np.sqrt(Q_f) - gamma * alpha *
                    (t_f)**0.75
                SoH_list.append(SoH)
                if soc_rest_mode == "start":
                    TIME[-1]=round((TIME[-1]+1),0)
                else:
                    TIME[-2]=round((TIME[-2]+1),8)
                    TIME[-1]=round((TIME[-2]+t_charge[turn_idx % len(
                        t_charge)]),0)
                day += 1
                year_day_counter += 1
            # annual downtime
            if year_day_counter >= 350 and DoD_turns[i]!=0:
                for k in range(15):
                    t_f += 1.0
                    SoH = 1 - gamma * beta * np.sqrt(Q_f) - gamma *
                        alpha * (t_f)**0.75
                    SoH_list.append(SoH)
                    if soc_rest_mode == "start":
                        TIME[-1]=(TIME[-1]+1)
                    elif k==0:
                        TIME[-2]=(TIME[-2]+15)
                        TIME[-1]=(TIME[-2]+t_charge[turn_idx % len(
                            t_charge)])
                    day += 1
                year_day_counter = 0
```

```
168                 balance_counter=0
169
170         turn_idx += 1
171         Q_eq = ((1 - SoH - gamma * alpha * t_f**0.75) / (gamma *
                beta_turns[next_i]))**2
172         t_eq = ((1 - gamma * beta * np.sqrt(Q_f) - SoH) / (gamma *
                alpha_turns[next_i]))**(4.0/3.0)
173
174     # plot first 50 SOC points if requested
175     SOC_50 = SOC[:50]
176     TIME_50 = TIME[:50]
177     if plot_soc == True:
178         plt.figure(figsize=(10,5))
179         plt.plot(TIME_50, SOC_50, marker='o', linestyle='-', label='SoC'
                , color='blue', zorder=3)
180         plt.xlabel("Time [days]")
181         plt.ylabel("SoC")
182         plt.axhline(0.20, color='red', linestyle=':', label='SoC_limit',
                 zorder=2)
183         plt.ylim(bottom=0.15, top=1.05)
184         plt.title("SoC trend over time")
185         plt.grid(True, zorder=0)
186         plt.legend(loc='upper left', bbox_to_anchor=(0, 0.97), frameon=
                True, facecolor='white', edgecolor='black')
187         plt.show()
188
189     return SoH_list
```

A.2. charging_optimization

```python
def charging_optimization(bus_blocks, charging_strategy="start", title="Charging_Plan", detail=False, save=False):

    # Slot definition
    slot_minutes = 5
    slots_per_day = 24 * 60 // slot_minutes
    slot_h = slot_minutes / 60.0

    # Charger parameters
    num_charger_upper = 5
    plugs_per_charger = 2
    Power = 150
    scale = 100
    slot_energy_single = int(round(Power * slot_h * scale))
    slot_energy_double = int(round(Power/2 * slot_h * scale))

    # Helper function to convert slot to time
    def slot_to_time(slot):
        s = slot % slots_per_day
        minutes = s * slot_minutes
        hh = minutes // 60
        mm = minutes % 60
        return f"{int(hh):02d}:{int(mm):02d}"

    # Prepare charging blocks
    blocks = []
    for b, blist in bus_blocks.items():
        for i, (start, end, energy_kwh) in enumerate(blist):
            s = time_to_slot(start, slot_minutes)
            e = time_to_slot(end, slot_minutes)
            if e <= s: e += slots_per_day
            blocks.append({"bus": b, "block_idx": i, "start_slot": s, "end_slot": e - 1, "energy_kwh": energy_kwh})

    block_id_map = {idx: blk for idx, blk in enumerate(blocks)}
    block_ids = list(block_id_map.keys())

    # Model
    model = cp_model.CpModel()
    charger_range = range(num_charger_upper)
    plug_range = range(plugs_per_charger)

```

```
    # Variables
    assign, cover, s_var, L_var = {}, {}, {}, {}
    x, y, z1, z2, w1, w2, e_units = {}, {}, {}, {}, {}, {}, {}

    # Model constraints
    for bid in block_ids:
        blk = block_id_map[bid]
        start, end = blk["start_slot"], blk["end_slot"]
        max_len = end - start + 1
        L_var[bid] = model.NewIntVar(0, max_len, f"L_{bid}")

        if charging_strategy == "start":
            allowed_starts = [start, min(start+2, end)]
            s_var[bid] = model.NewIntVar(min(allowed_starts), max(
                allowed_starts), f"s_{bid}")
        elif charging_strategy == "end":
            s_var[bid] = model.NewIntVar(start, end, f"s_{bid}")
            end_var = model.NewIntVar(end-2, end, f"end_{bid}")
            model.Add(end_var == s_var[bid] + L_var[bid] - 1)

        for t in range(start, end+1):
            cover[(bid,t)] = model.NewBoolVar(f"cover_b{bid}_t{t}")
        for c in charger_range:
            for p in plug_range:
                assign[(bid,c,p)] = model.NewBoolVar(f"assign_b{bid}_c{c
                    }_p{p}")

        model.Add(sum(cover[(bid,t)] for t in range(start, end+1)) ==
            L_var[bid])
        M = 10000
        for t in range(start, end+1):
            model.Add(s_var[bid] <= t + M * (1 - cover[(bid,t)]))
            model.Add(t <= s_var[bid] + L_var[bid] - 1 + M * (1 - cover
                [(bid,t)]))

        model.Add(sum(assign[(bid,c,p)] for c in charger_range for p in
            plug_range) == 1)

    # x linking assign & cover
    for bid in block_ids:
        blk = block_id_map[bid]
        for c in charger_range:
            for p in plug_range:
                for t in range(blk["start_slot"], blk["end_slot"]+1):
```

```
                    x[(bid,c,p,t)] = model.NewBoolVar(f"x_b{bid}_c{c}_p{
                        p}_t{t}")
                    model.Add(x[(bid,c,p,t)] <= assign[(bid,c,p)])
                    model.Add(x[(bid,c,p,t)] <= cover[(bid,t)])
                    model.Add(x[(bid,c,p,t)] >= assign[(bid,c,p)] +
                        cover[(bid,t)] - 1)

    # y and z variables
    relevant_slots = sorted({t for bid in block_ids for t in range(
        block_id_map[bid]["start_slot"], block_id_map[bid]["end_slot"]+1)
        })
    for c in charger_range:
        for t in relevant_slots:
            y[(c,t)] = model.NewIntVar(0, plugs_per_charger, f"y_c{c}_t{
                t}")
            z1[(c,t)] = model.NewBoolVar(f"z1_c{c}_t{t}")
            z2[(c,t)] = model.NewBoolVar(f"z2_c{c}_t{t}")
            model.Add(y[(c,t)] == z1[(c,t)] + 2 * z2[(c,t)])
            model.Add(y[(c,t)] == sum(x[(bid,c,p,t)] for bid in
                block_ids for p in plug_range if t >= block_id_map[bid]["
                start_slot"] and t <= block_id_map[bid]["end_slot"]))

    # No plug double occupancy
    for c in charger_range:
        for p in plug_range:
            for t in relevant_slots:
                model.Add(sum(x[(bid,c,p,t)] for bid in block_ids if t
                    >= block_id_map[bid]["start_slot"] and t <=
                    block_id_map[bid]["end_slot"]) <= 1)

    # Energy assignment and constraints
    is_last = {}
    for bid in block_ids:
        blk = block_id_map[bid]
        last_slot_expr = s_var[bid] + L_var[bid] - 1
        for t in range(blk["start_slot"], blk["end_slot"]+1):
            is_last[(bid,t)] = model.NewBoolVar(f"is_last_b{bid}_t{t}")
            model.Add(last_slot_expr == t).OnlyEnforceIf(is_last[(bid,t)
                ])
            model.Add(last_slot_expr != t).OnlyEnforceIf(is_last[(bid,t)
                ].Not())

    for bid in block_ids:
        blk = block_id_map[bid]
```

```
113         for c in charger_range:
114             for p in plug_range:
115                 for t in range(blk["start_slot"], blk["end_slot"]+1):
116                     w1[(bid,c,p,t)] = model.NewBoolVar(f"w1_b{bid}_c{c}
                            _p{p}_t{t}")
117                     w2[(bid,c,p,t)] = model.NewBoolVar(f"w2_b{bid}_c{c}
                            _p{p}_t{t}")
118                     model.Add(w1[(bid,c,p,t)] <= x[(bid,c,p,t)])
119                     model.Add(w1[(bid,c,p,t)] <= z1[(c,t)])
120                     model.Add(w1[(bid,c,p,t)] >= x[(bid,c,p,t)] + z1[(c,
                            t)] - 1)
121                     model.Add(w2[(bid,c,p,t)] <= x[(bid,c,p,t)])
122                     model.Add(w2[(bid,c,p,t)] <= z2[(c,t)])
123                     model.Add(w2[(bid,c,p,t)] >= x[(bid,c,p,t)] + z2[(c,
                            t)] - 1)
124                     e_units[(bid,c,p,t)] = model.NewIntVar(0,
                            slot_energy_single, f"e_b{bid}_c{c}_p{p}_t{t}")
125                     model.Add(e_units[(bid,c,p,t)] == slot_energy_single
                             * w1[(bid,c,p,t)] + slot_energy_double * w2[(bid
                            ,c,p,t)]).OnlyEnforceIf(is_last[(bid,t)].Not())
126                     model.Add(e_units[(bid,c,p,t)] <= slot_energy_single
                             * w1[(bid,c,p,t)] + slot_energy_double * w2[(bid
                            ,c,p,t)]).OnlyEnforceIf(is_last[(bid,t)])
127
128     # Total energy constraint per block
129     for bid in block_ids:
130         blk = block_id_map[bid]
131         required_units = int(round(blk["energy_kwh"] * scale))
132         total_energy_expr = sum(e_units[(bid,c,p,t)] for c in
               charger_range for p in plug_range for t in range(blk["
               start_slot"], blk["end_slot"]+1))
133         if required_units > 0:
134             model.Add(total_energy_expr == required_units)
135             model.Add(L_var[bid] >= 1)
136         else:
137             model.Add(total_energy_expr == 0)
138             model.Add(L_var[bid] == 0)
139
140     # Charger usage indicator
141     charger_usage = {}
142     for c in charger_range:
143         charger_usage[c] = model.NewBoolVar(f"Charger_used_{c}")
144         for bid in block_ids:
145             for p in plug_range:
```

```
146                 model.Add(charger_usage[c] >= assign[(bid,c,p)])
147
148     # Objective: minimize chargers and maximize total charging
149     MAX_SLOTS = slots_per_day * num_charger_upper
150     weight_charger = MAX_SLOTS
151     weight_slots = 1
152     model.Minimize(weight_charger * sum(charger_usage[c] for c in
            charger_range) - weight_slots * sum(L_var[bid] for bid in
            block_ids))
153
154     # Symmetry breaking
155     for c in range(num_charger_upper - 1):
156         model.Add(charger_usage[c] >= charger_usage[c+1])
157
158     # Solve
159     solver = cp_model.CpSolver()
160     solver.parameters.max_time_in_seconds = 9000
161     solver.parameters.num_search_workers = 8
162     solver.parameters.random_seed = 1234
163     start_time = time.time()
164     res = solver.Solve(model)
165     end_time = time.time()
166     print(f"Solver␣elapsed␣time:␣{end_time␣-␣start_time:.2f}␣s")
167
168     if res == cp_model.OPTIMAL or res == cp_model.FEASIBLE:
169         charger_used = [c for c in charger_range if solver.Value(
                charger_usage[c]) == 1]
170         print(f"Solution␣status:␣{solver.StatusName(res)}")
171         print(f"Minimum␣number␣of␣chargers␣required:␣{len(charger_used)}
                ␣\n")
172
173         charge_durations = [solver.Value(L_var[bid]) * slot_minutes for
                bid in block_ids]
174         print("Charging␣durations␣(minutes)␣in␣order:", charge_durations
                , "\n")
175
176         results_rows = []
177         for bid in block_ids:
178             blk = block_id_map[bid]
179             b = blk["bus"]
180             for t in range(blk["start_slot"], blk["end_slot"]+1):
181                 for c in charger_range:
182                     for p in plug_range:
183                         if solver.Value(x[(bid,c,p,t)]) == 1:
```

```
184                             e = solver.Value(e_units[(bid,c,p,t)])
185                             results_rows.append({"bus": b, "block": blk[
                                    'block_idx'], "slot": t, "charger": c+1,
                                    "plug": p+1, "energy_kwh": e/scale})
186
187         df = pd.DataFrame(results_rows)
188
189         if detail:
190             for bid in block_ids:
191                 blk = block_id_map[bid]
192                 b = blk["bus"]
193                 block_rows = [r for r in results_rows if r['bus']==b and
                        r['block']==blk['block_idx']]
194                 total_energy = sum(r['energy_kwh'] for r in block_rows)
195                 print(f"Bus {b} - Block {blk['block_idx']} (window {
                        slot_to_time(blk['start_slot'])} - {slot_to_time(blk
                        ['end_slot']+1)})")
196                 for r in block_rows:
197                     t = r['slot']; c = r['charger']; p = r['plug'];
                            power = r['energy_kwh']/slot_h
198                     print(f" -> Slot {t} ({slot_to_time(t)}), Charger {c
                            }, Plug {p}, Power ~{power:.2f} kW, Energy {r['
                            energy_kwh']:.4f} kWh")
199                 print(f" ===> Total energy charged in block: {
                        total_energy:.4f} kWh\n")
200
201         df["timeband"] = df["slot"].apply(slot_to_timeband)
202         energy_by_timeband = df.groupby("timeband")["energy_kwh"].sum().
                reindex(["F1","F2","F3"], fill_value=0)
203
204         print("\nTotal energy used per timeband:")
205         for tb, energy in energy_by_timeband.items():
206             print(f" {tb}: {energy:.2f} kWh")
207
208         plot_charging_plan(results_rows, blocks, slot_minutes=
                slot_minutes, slot_h=slot_h, title=title, detail=detail, save
                =save)
209         num_charger_used = len(charger_used)
210         return charge_durations, energy_by_timeband, num_charger_used
211
212     else:
213         print("No feasible solution found.")
214         return None
```

A.3. calculate_LCC_scenario

```
def calculate_LCC_scenario(scenario, df_results, num_chargers, SoH_12m, SoH_9m, energy_by_timeband_S, energy_by_timeband_NS, bus_lifetime):

    # Common parameters for all scenarios
    discount_rate = 0.03
    charger_cost = 40000
    charger_opex = 0.05 # 5% of the charger cost
    num_buses_12m = 5
    num_buses_9m = 4
    cap_12m = 420  # kWh, battery capacity of a 12 m bus
    cap_9m = 294   # kWh, battery capacity of a 9 m bus
    battery_value_12m = battery_cost_per_kWh * num_buses_12m * cap_12m
    battery_value_9m  = battery_cost_per_kWh * num_buses_9m * cap_9m
    charger_lifetime = 24  # expected lifetime of a charger in years

    # Time horizon for the LCC analysis (years)
    years = range(2026, 2026+bus_lifetime)

    # Annual energy cost
    annual_energy_cost = (
        energy_by_timeband_S["F1"] * average_prices_S["F1 [euro/kWh]"] +
        energy_by_timeband_S["F2"] * average_prices_S["F2 [euro/kWh]"] +
        energy_by_timeband_S["F3"] * average_prices_S["F3 [euro/kWh]"]
    ) * 225 + (
        energy_by_timeband_NS["F1"] * average_prices_NS["F1 [euro/kWh]"]
            +
        energy_by_timeband_NS["F2"] * average_prices_NS["F2 [euro/kWh]"]
            +
        energy_by_timeband_NS["F3"] * average_prices_NS["F3 [euro/kWh]"]
    ) * 67

    # Create DataFrame
    df = pd.DataFrame({'Year': years})
    df['OPEX ENERGY'] = annual_energy_cost
    df['OPEX CHARGERS'] = num_chargers * charger_cost * charger_opex
    df['CAPEX CHARGERS'] = 0.0
    df['CAPEX BATTERIES'] = 0.0
    df['RESIDUAL BATTERY VALUE'] = 0.0
    df['RESIDUAL CHARGER VALUE'] = 0.0

    # Battery lifespan
```

```
    lifespan_12m = int(np.floor(df_results.loc[df_results['Scenario'] ==
        scenario, 'Bus 12 m'].iloc[0] / 365))
    lifespan_9m  = int(np.floor(df_results.loc[df_results['Scenario'] ==
        scenario, 'Bus 9 m'].iloc[0] / 365))

    # Charger CAPEX and residual value
    df.loc[0, 'CAPEX CHARGERS'] = num_chargers * charger_cost
    df.loc[len(df)-1, 'RESIDUAL CHARGER VALUE'] = charger_cost *
       num_chargers * (charger_lifetime - len(df)) / charger_lifetime

    # Helper function for battery replacements
    def apply_replacements(lifespan, battery_cost, num_buses,
       bus_capacity, soh_array):
        num_replacements = (len(df) - 1) // lifespan
        replacement_years = [(i + 1) * lifespan for i in range(
           num_replacements)]
        last_year = 0
        for year in replacement_years:
            delta_years = year - last_year
            day_index = min(delta_years * 365, len(soh_array) - 1)
            current_SoH = soh_array[day_index]
            residual_value = used_battery_value(current_SoH) * num_buses
                * bus_capacity
            df.loc[year, 'CAPEX BATTERIES'] += battery_cost
            df.loc[year, 'RESIDUAL BATTERY VALUE'] += residual_value
            last_year = year
        return replacement_years

    # Apply replacements for 12m and 9m buses
    replacement_years_12m = apply_replacements(lifespan_12m,
       battery_value_12m, num_buses_12m, cap_12m, SoH_12m)
    replacement_years_9m  = apply_replacements(lifespan_9m,
       battery_value_9m, num_buses_9m, cap_9m, SoH_9m)

    # Final battery value for 12m and 9m buses
    df.loc[len(df)-1, 'RESIDUAL BATTERY VALUE'] += (
        final_battery_value(SoH_12m, replacement_years_12m,
           num_buses_12m, cap_12m) +
        final_battery_value(SoH_9m, replacement_years_9m, num_buses_9m,
           cap_9m)
    )

    # Calculate cash flow (CF), discounted CF, and LCC
```

```
72      df['CF'] = -(df['OPEX ENERGY'] + df['OPEX CHARGERS'] + df['CAPEX
            CHARGERS'] + df['CAPEX BATTERIES']) \
73                  + (df['RESIDUAL BATTERY VALUE'] + df['RESIDUAL CHARGER
                        VALUE'])
74
75      df['DISCOUNTED CF'] = df['CF'] / (1 + discount_rate) ** (df.index)
76      df['LCC'] = -df['DISCOUNTED CF'].cumsum()
77
78      # Discounted LCC by component
79      df['LCC ENERGY'] = (df['OPEX ENERGY'] / (1 + discount_rate) ** df.
            index).cumsum()
80      df['LCC CHARGERS'] = ((df['OPEX CHARGERS'] + df['CAPEX CHARGERS'] -
            df['RESIDUAL CHARGER VALUE']) / (1 + discount_rate) ** df.index).
            cumsum()
81      df['LCC BATTERIES'] = ((df['CAPEX BATTERIES'] - df['RESIDUAL BATTERY
            VALUE']) / (1 + discount_rate) ** df.index).cumsum()
82
83      pd.options.display.float_format = '{:.0f}'.format
84
85      return df
```

B | Appendix – Charging schedules under non-school period operation

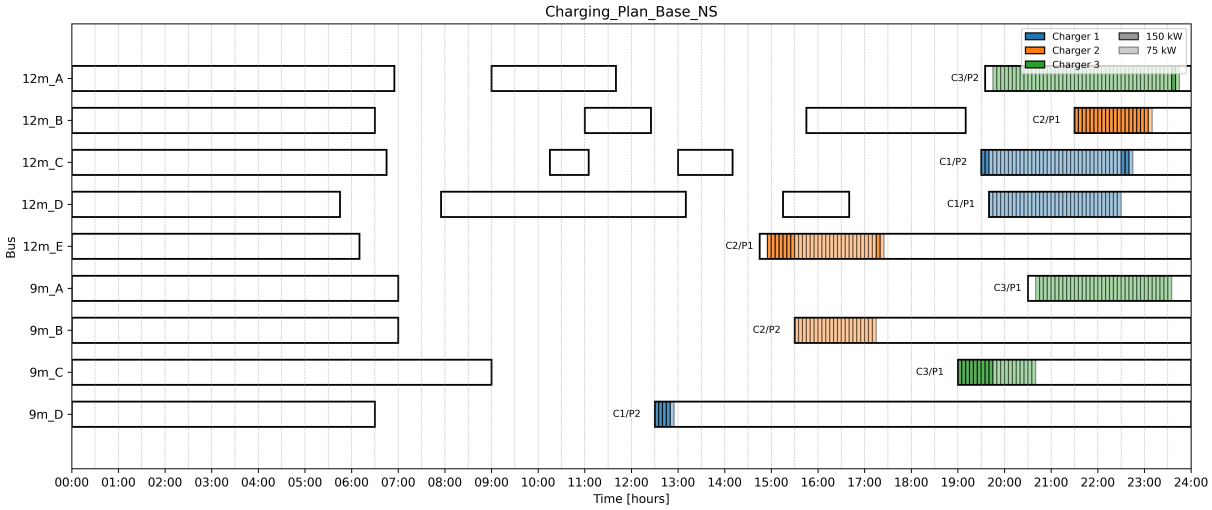


Figure B.1: Gantt chart illustrating the optimized charging schedule of the fleet in the Base scenario under non-school period operation.

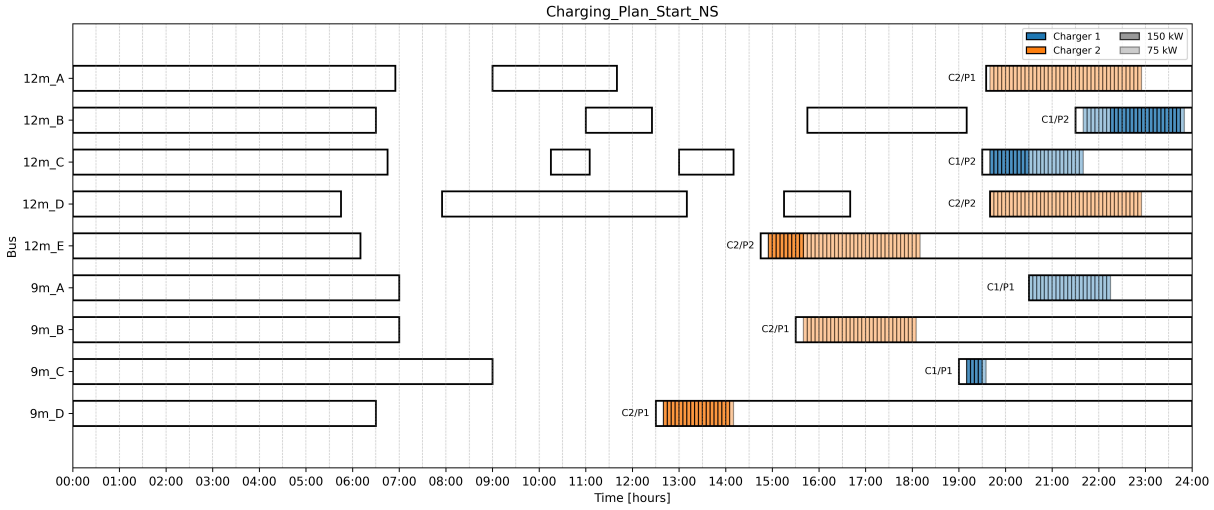


Figure B.2: Gantt chart illustrating the optimized charging schedule of the fleet in the Start scenario under non-school period operation.

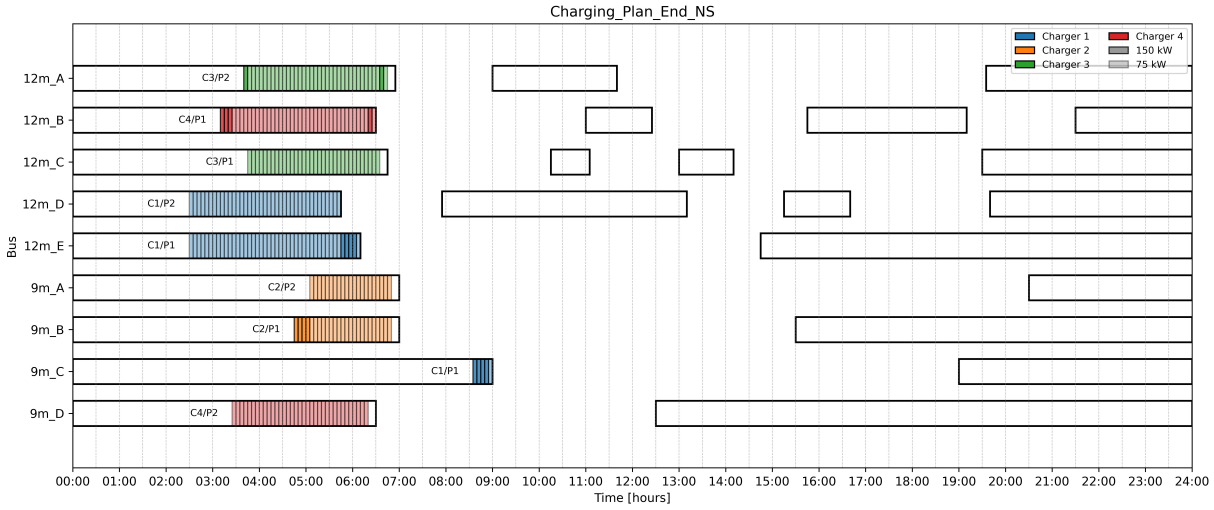


Figure B.3: Gantt chart illustrating the optimized charging schedule of the fleet in the End scenario under non-school period operation.

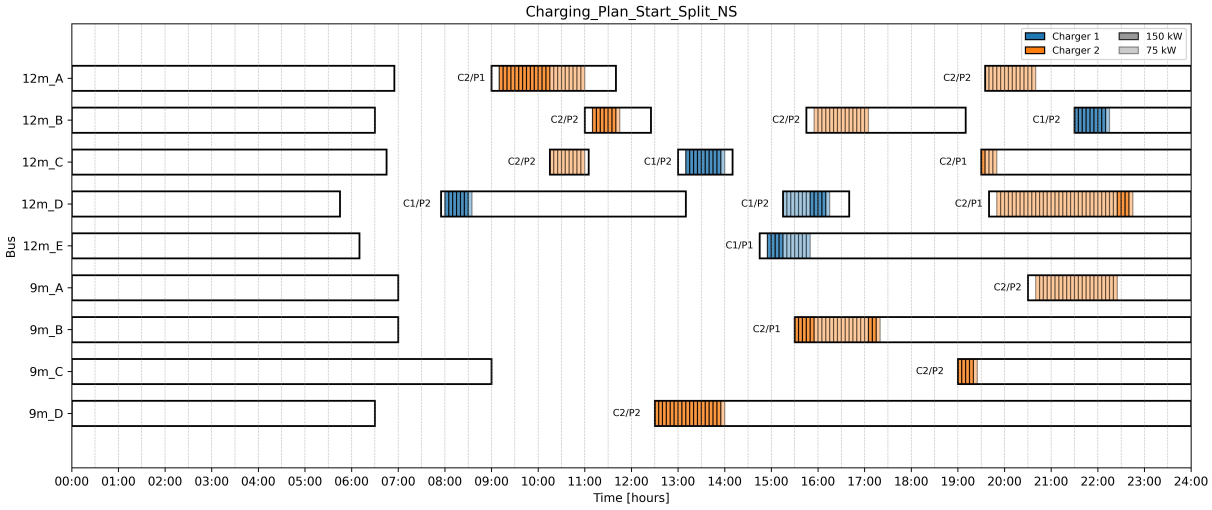


Figure B.4: Gantt chart illustrating the optimized charging schedule of the fleet in the Start-Split scenario under non-school period operation.

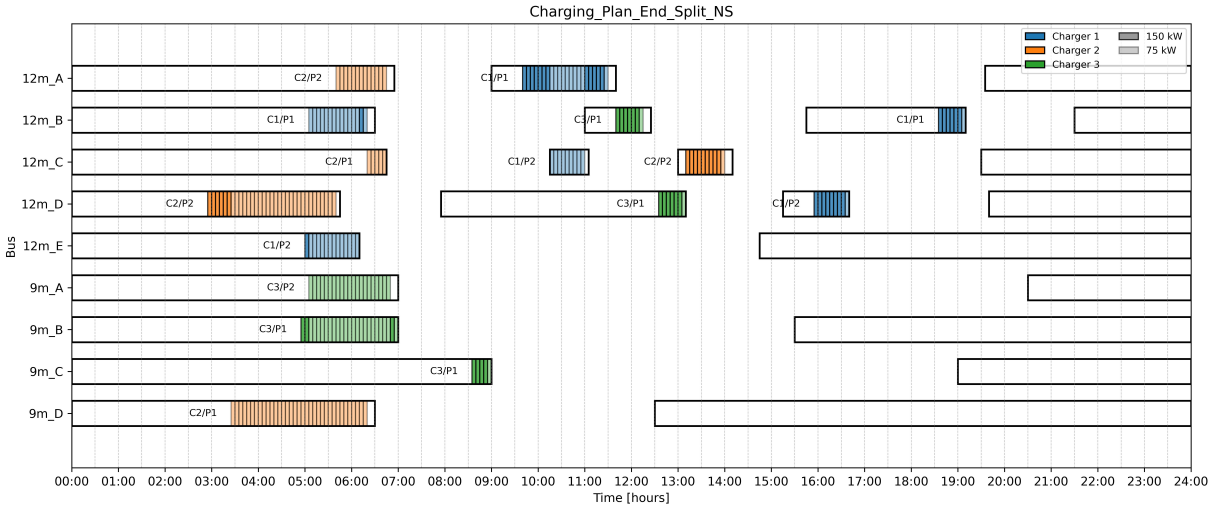


Figure B.5: Gantt chart illustrating the optimized charging schedule of the fleet in the End-Split scenario under non-school period operation.

List of Figures

1.1 Global mean surface temperature anomaly relative to the pre-industrial period (1850–1900), estimated from multiple independent datasets [2]. . . 1
1.2 Greenhouse gas emissions from all sources, expressed in tonnes of CO_2 eq [3]. 2
1.3 Global greenhouse gas emissions by sector, expressed in tonnes of CO_2 eq [5]. 3
1.4 Share of electricity generation from fossil fuels, renewables, and nuclear sources in the EU [6]. 4
1.5 Share of newly registered alternative fuelled buses as a percentage of total registrations in the EU [12] 7

2.1 Schematic illustration of Li-ion working principle in charging and discharging modes [14]. 11
2.2 EV battery market share by chemistry and region [15]. 14
2.3 Factors affecting aging, chemical and physical mechanisms, and the effects they cause [22]. 17
2.4 relationship between the number of achievable cycles and DOD [26]. 19
2.5 Evolution of remaining capacity versus cycle life at different current rate [27]. 20
2.6 Illustration of early charge and early discharge termination events [33] . . . 22
2.7 Fixed shunt resistor passive balancing [32]. 23
2.8 Switched shunt resistor passive balancing [32]. 24
2.9 Open circuit voltage over State of Charge [41]. 29
2.10 Electric bus schedule and battery SOC profile [44]. 31
2.11 Battery State of Charge variation curve [46]. 33
2.12 Optimal charging schedules compared with three typical charging strategies [51]. 35
2.13 Battery capacity loss after 10 years of operation [51]. 35
2.14 Merit order illustration [52]. 37

2.15 Evolution of the Italian electricity market bidding zone configuration, showing the transition from six to seven zones [54]. 39
2.16 Typical daily fluctuation of the Italian PUN [55]. 40
2.17 Typical monthly trend of the Italian PUN [55]. 40
2.18 Historical trend of the Italian PUN, 2004-2025 [55]. 41

3.1 Workflow of the models implemented in this thesis. 46
3.2 ZEN 42 battery pack [58]. 49
3.3 Capacity degradation curves due to cycling aging, as predicted by the calibrated aging model, for different mean SoC values under an 80% DoD cycling condition. 51
3.4 Capacity degradation curves due to cycling aging, as predicted by the calibrated aging model, for different mean SoC values under an 60% DoD cycling condition. 52
3.5 Capacity degradation curves due to cycling aging, as predicted by the calibrated aging model, for different mean SoC values under an 40% DoD cycling condition. 52
3.6 Capacity degradation curves due to calendar aging, as predicted by the calibrated aging model, for different storage temperatures at a fixed storage SoC of 80%. 54
3.7 Capacity degradation curves due to calendar aging, as predicted by the calibrated aging model, for different storage SoC values at a fixed storage temperature of 25 °C. 54
3.8 Initial part of the Python function implementing the mathematical simulation of battery aging. 61
3.9 Python utility function for discretizing time into uniform simulation slots. . 65
3.10 Initial part of the Python function implementing the charging optimization algorithm. 66
3.11 Excerpt of the Python function defining the two-level objective function of the charging optimization algorithm. 67
3.12 Example of detailed scheduling and power allocation of a single charging block from the charging optimization algorithm. 69
3.13 Initial part of the Python function used to compute the LCC for each scenario. 73

4.1 Iveco E-Way electric bus of the Autoguidovie S.p.A. fleet. 75
4.2 Interurban and suburban bus routes in the Cremona area. 76
4.3 Urban bus routes within the city of Crema. 77
4.4 Example of daily profile data provided by Iveco's monitoring system. . . . 78

4.5 Bus blocks corresponding to the school period, showing the SoC [%] required for each shift. . . . 79
4.6 Bus blocks corresponding to the non-school period, showing the SoC [%] required for each shift. . . . 80
4.7 Excerpt of the SoC evolution over time for the Start scenario. . . . 82
4.8 Excerpt of the SoC evolution over time for the End-Split scenario, showing a periodic cell-balancing event. . . . 83
4.9 Excerpt of the SoC evolution over time for the Base scenario, showing the annual resting period and the transition between school and non-school scheduling. . . . 84
4.10 Evolution of battery SoH over time for the different charging scenarios for the 12-meter buses. . . . 85
4.11 Evolution of battery SoH over time for the different charging scenarios for the 9-meter buses. . . . 85
4.12 Gantt chart illustrating the optimized charging schedule of the fleet in the Base scenario under school period operation. . . . 88
4.13 Gantt chart illustrating the optimized charging schedule of the fleet in the Start scenario under school period operation. . . . 89
4.14 Gantt chart illustrating the optimized charging schedule of the fleet in the End scenario under school period operation. . . . 89
4.15 Gantt chart illustrating the optimized charging schedule of the fleet in the Start-Split scenario under school period operation. . . . 90
4.16 Gantt chart illustrating the optimized charging schedule of the fleet in the End-Split scenario under school period operation. . . . 91
4.17 Breakdown of the LCC for the Base scenario under the optimistic bus lifetime assumption. . . . 92
4.18 Graphical representation of the total LCC and its components for each charging scenario under the pessimistic bus lifetime assumption. . . . 94
4.19 Graphical representation of the total LCC and its components for each charging scenario under the moderate bus lifetime assumption. . . . 95
4.20 Graphical representation of the total LCC and its components for each charging scenario under the optimistic bus lifetime assumption. . . . 97

B.1 Gantt chart illustrating the optimized charging schedule of the fleet in the Base scenario under non-school period operation. . . . 127
B.2 Gantt chart illustrating the optimized charging schedule of the fleet in the Start scenario under non-school period operation. . . . 128

B.3 Gantt chart illustrating the optimized charging schedule of the fleet in the End scenario under non-school period operation. 128
B.4 Gantt chart illustrating the optimized charging schedule of the fleet in the Start-Split scenario under non-school period operation. 129
B.5 Gantt chart illustrating the optimized charging schedule of the fleet in the End-Split scenario under non-school period operation. 129

List of Tables

1.1 Local pollutants, their impacts, and contributions from industry and transport [8] 5

2.1 Effect of stress factors on aging for cell chemistries for both aging modes. (●●●●: highest impact,●●●: high impact,●●: medium impact,●: low impact) [22]. 21

3.1 Overview of the charging strategy scenarios and enabled optimization features. 61
3.2 Battery residual value as a function of SoH, expressed in $/kWh and as a percentage of the initial value. 72

4.1 Technical characteristics of the E-Way bus models considered in this study. 77
4.2 Expected battery lifetime, expressed in years, under the different charging scenarios for 9-meter and 12-meter buses. 86
4.3 Total LCC and the breakdown into energy, chargers, and battery costs for each charging scenario under the pessimistic bus lifetime assumption (12 years). 93
4.4 Total LCC and the breakdown into energy, chargers, and battery costs for each charging scenario under the moderate bus lifetime assumption (16 years). 95
4.5 Total LCC and the breakdown into energy, chargers, and battery costs for each charging scenario under the optimistic bus lifetime assumption (20 years). 96

Acknowledgements

Con questo lavoro porto a termine il mio percorso di studi presso il Politecnico di Milano e desidero ringraziare tutte le persone che mi sono state vicine durante questo progetto e, più in generale, in questi anni universitari.
Prima di tutto, ci tengo a ringraziare i miei genitori, per aver sempre creduto in me e per avermi sostenuto lungo tutto questo percorso.
Grazie mamma, per esserci sempre, per ascoltarmi e per permettermi di contare in ogni momento sul tuo aiuto e sui tuoi consigli. Grazie anche per aver letto tutta la mia tesi (più volte) durante la sua stesura.
Grazie papà, per avermi insegnato a non fare le cose "tanto per farle", ma a capirle davvero, mettendoci passione; tu mi hai aiutato a vedere le cose in modo critico, spronandomi a non accontentarmi quando posso fare meglio, sei sempre stato sincero nei tuoi giudizi, non limitandoti ad una critica fine a se stessa, ma indirizzando il mio ragionamento verso la ricerca della soluzione migliore.
Grazie a Giulia, per essere stata una parte importante di questo percorso, per avermi fatto scoprire aspetti di me che non conoscevo e per avermi motivato a dare il meglio di me. Grazie per la strada percorsa insieme.
Voglio ringraziare anche il resto della mia famiglia: i miei nonni, i miei zii, le mie cuginette, mia sorella Elisa e mio fratello Davide, per aver sempre fatto il tifo per me, sostenendomi con affetto e gioia in ogni momento.
Grazie ai miei coinquilini, Edoardo e Lorenzo, per aver reso più leggero il mio percorso universitario, per le risate e per tutti i bei momenti che abbiamo condiviso.
Ci tengo a ringraziare anche Fabio Borghetti e Stefano Rossi, per aver reso possibile questo lavoro, e Paolo Rapinesi per il sostegno, la disponibilità e la fiducia. Ringrazio inoltre i ragazzi di Autoguidovie, in particolare Giovanni, Edoardo e Luca, per aver condiviso la loro competenza e per avermi fornito preziosi suggerimenti e consigli durante la stesura della tesi.
Infine, grazie a Cecco e a tutti i ragazzi e le ragazze con cui mi sono allenato in questi anni: l'atletica è stata per me una valvola di sfogo, che mi ha permesso di liberare la mente quando ne avevo bisogno, e voi siete stati altrettanto importanti. Grazie di cuore.